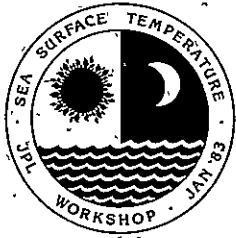




Satellite-Derived Sea Surface Temperature: Workshop-I

January 27-28, 1983
Pasadena, California



(NASA-CR-173450)	SATELLITE-DERIVED SEA	N84-21955
SURFACE TEMPERATURE: WORKSHOP I (Jet		THRU
Propulsion Lab.)	156 p HC A08/MF A01	N84-21969
	CSCL 05B	Unclas
		G3/43 13028

May 1, 1983



National Aeronautics and Space Administration

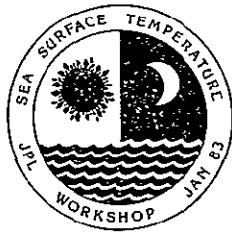
Jet Propulsion Laboratory
California Institute of Technology
Pasadena, California

1. Report No. 83-34		2. Government Accession No.		3. Recipient's Catalog No.	
4. Title and Subtitle Satellite-Derived Sea Surface Temperature Workshop-I; January 27-28, 1983, Pasadena, California				5. Report Date 1 May 1983	
				6. Performing Organization Code	
7. Author(s) Coordinated by E. Njoku (JPL)				8. Performing Organization Report No.	
9. Performing Organization Name and Address JET PROPULSION LABORATORY California Institute of Technology 4800 Oak Grove Drive Pasadena, California 91109				10. Work Unit No.	
				11. Contract or Grant No. NAS7-918	
				13. Type of Report and Period Covered JPL PUBLICATION	
12. Sponsoring Agency Name and Address NATIONAL AERONAUTICS AND SPACE ADMINISTRATION Washington, D.C. 20546				14. Sponsoring Agency Code	
15. Supplementary Notes (RTOP or Customer Code BP-161-40-03-04-00).					
16. Abstract Satellite measurements of sea surface temperature are now possible using a variety of sensors. The present accuracies of these methods are in the range of 0.5 to 2.0°C. This makes them potentially useful for synoptic studies of ocean currents and for global monitoring of climatological anomalies. To improve confidence in the satellite data, objective evaluations of sensor accuracies are necessary, and the conditions under which these accuracies degrade need to be understood. A workshop was held at the Jet Propulsion Laboratory (JPL), January 27 and 28, 1983, under sponsorship of the National Aeronautics and Space Administration, to begin joint evaluation of the measurement accuracies of four currently-operating satellite sensors. The sensor studied in this first workshop was the Scanning Multichannel Microwave Radiometer (SMMR) on the Nimbus-7 satellite. Sea surface temperatures, derived from November 1979 SMMR data, were compared globally against ship measurements and climatology, using facilities of the JPL Pilot Ocean Data System. The workshop included presentations by investigators responsible for generating the satellite and in situ data sets. A feature of the workshop was the discussion of methods for improved data analysis and plans for additional workshops to incorporate data from other sensors. This report summarizes the background to the workshop, describes its proceedings, and presents conclusions and recommendations arising from the discussions.					
17. Key Words (Selected by Author(s)) Meteorology and Climatology Dynamic Oceanography Spacecraft Instrumentation			18. Distribution Statement Unclassified-Unlimited		
19. Security Classif. (of this report) Unclassified		20. Security Classif. (of this page) Unclassified		21. No. of Pages 104	22. Price

JPL PUBLICATION 83-34

Satellite-Derived Sea Surface Temperature: Workshop-I

January 27-28, 1983
Pasadena, California



May 1 1983

NASA

National Aeronautics and Space Administration

Jet Propulsion Laboratory
California Institute of Technology
Pasadena California

ABSTRACT

Satellite measurements of sea surface temperature are now possible using a variety of sensors. The present accuracies of these methods are in the range of 0.5 to 2.0°C. This makes them potentially useful for synoptic studies of ocean currents and for global monitoring of climatological anomalies. To improve confidence in the satellite data, objective evaluations of sensor accuracies are necessary, and the conditions under which these accuracies degrade need to be understood.

A workshop was held at the Jet Propulsion Laboratory (JPL), January 27 and 28, 1983, under sponsorship of the National Aeronautics and Space Administration, to begin joint evaluation of the measurement accuracies of four currently-operating satellite sensors. The sensor studied in this first workshop was the Scanning Multichannel Microwave Radiometer (SMMR) on the Nimbus-7 satellite. Sea surface temperatures, derived from November 1979 SMMR data, were compared globally against ship measurements and climatology, using facilities of the JPL Pilot Ocean Data System. The workshop included presentations by investigators responsible for generating the satellite and in situ data sets. A feature of the workshop was the discussion of methods for improved data analysis and plans for additional workshops to incorporate data from other sensors. This report summarizes the background to the workshop, describes its proceedings, and presents conclusions and recommendations arising from the discussions.

PRECEDING PAGE BLANK NOT FILMED

FOREWORD

This report documents the proceedings of a Satellite-Derived Sea Surface Temperature (SST) Workshop, held at the Jet Propulsion Laboratory (JPL), Pasadena, California, January 27 and 28, 1983. The workshop was the first of a series designed to compare directly SST measurements from existing satellite sensors, thereby evaluating their global accuracies and enabling informed decisions to be made concerning future sensor development. Motivation for the comparisons arose from reports of approximately 1°C accuracy in SST measurement by four different satellite sensors, and from the need of oceanographers and climate scientists to understand conditions under which better or worse performance could be expected from each sensor type. The workshop was convened under sponsorship of the Oceanic Processes Branch, Environmental Observation Division of the National Aeronautics and Space Administration, NASA TASK RE-4, NASA RTOP, No. BP-161-40-03-40-00.

A planning meeting was held at the NASA Goddard Space Flight Center, April 16, 1982, at which the principal workshop participants met to discuss approaches to the proposed satellite and in situ data comparisons. Subsequent workshop organization took place at JPL to facilitate archival and processing of the satellite and in situ data sets on the JPL Pilot Ocean Data System.

A substantial level of effort is necessary to acquire, assimilate, and analyze several months of satellite data of divergent sampling densities, spatial resolutions, and formats. The first workshop, therefore, was limited to analysis of a single month (November 1979) and to evaluation of approaches developed to compare the satellite data sets with each other and with climatology, ship, and buoy observations. Three versions of SST retrievals from the Nimbus-7 Scanning Multichannel Microwave Radiometer (SMMR) were examined and compared with ship data and climatology. In addition, the workshop provided an opportunity for open discussion by investigators of their data sets and algorithms, and for planning future evaluations in subsequent workshops. The next workshop will be held at the Jet Propulsion Laboratory, June 22-24, 1983.

Sections of this report were contributed mainly by individual workshop participants except Section VII, which combines contributions from several participants. The report was reviewed by all contributors, however, and the recommendations are the outcome of collective discussions by all participants.

ACKNOWLEDGEMENTS

Many individuals contributed to the accomplishments of Workshop-I and to the preparation of this report. SMMR sea surface temperature data were provided by T. Wilhelm, A. Milman, and C. Prabhakara. P. McClain, J. Susskind, and J. Bates, respectively, provided summaries for the AVHRR, HIRS/MSU, and VAS. Ship and buoy SST data were collected and organized by S. Pazan. D. Chelton led the development and discussion of data analysis techniques. Software implementation and data processing on the JPL Pilot Ocean Data System were accomplished by J. Hilland and the PODS staff. Evaluation of the SST comparisons was led by R. Bernstein. The workshop and publication of this report were coordinated at JPL by E. Njoku. Editorial assistance was provided by C. Edwards. In addition, valuable contributions to data evaluation and discussions were made by several workshop participants. A list of the workshop attendance is provided in Appendix H.

NASA Headquarters program management for the workshop was provided initially by K. Carder and continued by W. Esaias.

GLOSSARY

AVHRR	Advanced Very High Resolution Radiometer
CTD	Conductivity, Temperature, Density, Measuring Instrument
EPOCS	Equatorial Pacific Ocean Climate Study
FGGE	First GARP Global Experiment
FNOC	Fleet Numerical Oceanography Center
GARP	Global Atmospheric Research Project
GOES-East	Geostationary Operational Environmental Satellite-East
HIRS/MSU	High-Resolution Infrared Sounder/Microwave Sounding Unit
MBT	Mechanical Bathythermograph
McIDAS	Man-computer Interactive Data Access System
MCSST	Multi-Channel Sea Surface Temperature
NCAR	National Center for Atmospheric Research
NCC	National Climatic Center
NDBO	National Data Buoy Office
NESDIS	National Environmental Satellite, Data, and Information Service
NOAA	National Oceanic and Atmospheric Administration
NODC	National Oceanographic Data Center
PMEL	Pacific Marine Environmental Laboratory
PODS	Pilot Ocean Data System
PODSGRAF	PODS Graphics Display System
PEG	Pacific Environmental Group
SMMR	Scanning Multichannel Microwave Radiometer
SIO	Scripps Institution of Oceanography
SSEC	Space Science and Engineering Center
SST	Sea Surface Temperature

GLOSSARY

STD	Salinity, Temperature, Density, Measuring Instrument
TIROS	Television Infrared Observational Satellite
VAS	Visible-Infrared Spin-Scan Radiometer Atmospheric Sounder
XBT	Expendable Bathythermograph

CONTENTS

I. INTRODUCTION 1-1
(E. Njoku)

II. WORKSHOP-I ANALYSIS TECHNIQUES 2-1
(D. Chelton)

III. WORKSHOP-I PROCESSING SYSTEM 3-1
(J. Hilland)

IV. IN SITU DATA 4-1
(S. Pazan)

V. SATELLITE DATA 5-1
(E. Njoku)

VI. COMPARISON OF SATELLITE AND IN SITU DATA 6-1
(R. Bernstein)

VII. CONCLUSIONS AND RECOMMENDATIONS 7-1

REFERENCES 8-1

APPENDICES

A. SEA SURFACE TEMPERATURES FROM THE NIMBUS-7 SMMR
(A. Milman and T. Wilheit) A-1

B. A STATISTICAL METHOD TO SENSE SEA SURFACE TEMPERATURE
FROM THE NIMBUS-7 SMMR
(C. Prabhakara and I. Wang) B-1

C. NOAA SATELLITE-DERIVED OPERATIONAL SEA SURFACE
TEMPERATURE PRODUCTS
(P. McClain) C-1

D. MEASUREMENT OF SEA SURFACE TEMPERATURE FROM HIRS2/MSU
(J. Susskind) D-1

E. USE OF VAS MULTISPECTRAL DATA FOR SEA SURFACE
TEMPERATURE DETERMINATION
(J. Bates) E-1

F. PILOT OCEAN DATA SYSTEM FILE FORMAT SPECIFICATIONS
(J. Hilland) F-1

PRECEDING PAGE BLANK NOT FILMED

CONTENTS (Continued)

G.	THREE-WAY PARTITIONING OF SEA SURFACE TEMPERATURE MEASUREMENT ERROR -- (D. Chelton)	G-1
H.	SEA SURFACE TEMPERATURE WORKSHOP-I PARTICIPANTS	H-1

SECTION I
INTRODUCTION

E. Njoku

A. BACKGROUND

Satellites now play an increasing role in systematic monitoring of the global oceans. Measurements of sea surface temperature (SST) are of primary importance in understanding heat storage and transport within the ocean and across the ocean-atmosphere boundary. In some regions, local changes in SST of only 1 to 2°C can have major effects on global climate and weather patterns. In contributing to the study of such phenomena, repetitive, global SST measurements, as provided by satellites, can be of great value. The satellite measurements provide a data base complementary to the (sometimes) accurate but sparsely-distributed point measurements available from ships and buoys.

The demands placed on satellite sensors are stringent. Accuracies of better than 1°C are required and are often desired to a few tenths of a degree. Furthermore, measurement accuracies must be stable spatially and temporally in order for satellite data to be used with confidence in models of air-sea interaction and climate. Significant improvements in accuracy have been made since the first satellite sensors were launched. There now exists a need to evaluate objectively the performance of the latest generation of sensors under a sufficient variety of environmental conditions to indicate present accuracies, deficiencies, and potential for improvement. The utility of the data for operational and scientific purposes needs also to be examined. The Satellite-Derived Sea Surface Temperature Workshops were initiated to address these issues.

Infrared sensors, using visible channels for cloud detection, were the first to measure SST remotely from space. Successive improvements to these sensors since the early 1970s have led to current implementation of the five-channel Advanced Very High Resolution Radiometer (AVHRR) on the polar-orbiting NOAA-7 satellite. Measurements at high spatial resolution are available from this sensor (approximately 8 km resolution on a 50 km spacing for global coverage), but SST cannot be obtained reliably with clouds in the field of view, and careful corrections for atmospheric water vapor and aerosols must be made in cloud-free areas.

During the same period, infrared and microwave sounding instruments were being developed, leading to the High-Resolution Infrared Sounder (HIRS) and Microwave Sounding Unit (MSU) presently operating on NOAA-7. The increased number of infrared and microwave sounding channels available with the HIRS/MSU permits an alternative scheme for correcting atmospheric effects and in particular enables SST retrievals to be made under broken cloud, but not completely overcast, conditions. The spatial resolution of the retrievals is presently about 125 km.

Visible and infrared multi-channel sensors have also been developed for use on geostationary satellites. The most advanced of these is the Visible-Infrared Spin-Scan Radiometer Atmospheric Sounder (VAS) currently operating on the GOES-East satellite. Because geostationary satellites view the Earth from a fixed perspective, SST retrievals can be obtained over the same ocean region much more frequently than with the polar-orbiting satellites (approximately every hour instead of every 12 hours to 3 days). Presently, however, similar restrictions due to cloud cover exist for the VAS as with the AVHRR. Spatial resolution for VAS retrievals is about 14 km, and the useful portion of the Earth's surface visible from geostationary orbit is limited to a circle of radius approximately 45° latitude, centered on the equator at longitude 75° W.

These techniques all take advantage of the uniform emissivity of the ocean at infrared wavelengths, but even window channels in the infrared suffer from substantial atmospheric attenuation and scattering by water vapor, aerosols, and clouds. By contrast, window channels in the microwave region are much less affected by atmospheric attenuation, and atmospheric corrections can be made in nearly all non-raining conditions. The microwave emissivity of the ocean, however, exhibits substantial variability due to wind-induced roughness, and multiple channels are required for correction in order to derive accurate SST measurements. The first and only satellite instrument to exploit this approach is the Scanning Multichannel Microwave Radiometer (SMMR) launched on the Seasat and Nimbus-7 polar orbiting satellites. Only the Nimbus-7 SMMR is currently operational. Spatial resolution using this sensor is approximately 150 km.

Further descriptions of the four sensors (AVHRR, HIRS/MSU, VAS, and SMMR) and their respective SST retrieval techniques are provided in Appendices A through E.

B. SEA SURFACE TEMPERATURE WORKSHOP

By early 1982 it was evident that sufficiently high quality SST retrievals were available from each of the AVHRR, HIRS/MSU, VAS, and SMMR to suggest that global satellite measurements of about 1° C accuracy might be possible. Figures 1-1, 1-2, and 1-3 show global contour maps of SST derived from the NOAA-7 AVHRR, TIROS-N HIRS/MSU, and Seasat SMMR, respectively. Evaluation of each sensor was performed independently, using different analysis methods, and in most cases under limited regional and environmental conditions. Thus, some skepticism remains concerning the SST accuracies (particularly in sub-optimal environmental conditions), and the relative merits and complementary possibilities of the sensors remains undemonstrated.

A workshop approach was devised to address these issues by comparing the four satellite-derived SST products over the same months and geographic regions, using the same in situ data for verification, and using consistent methods of analysis. At an initial planning meeting held at the NASA Goddard Space Flight Center, investigators were identified to be responsible for generation of each satellite data set. (In cases where alternative approaches exist for SST retrieval from the same sensor there may be several investigators). Subsequently, other participants were added to the core group to coordinate acquisition of in situ SST data and to assist in specification and

implementation of data analysis methods on the Pilot Ocean Data System (PODS). The PODS is a computer-based archival and processing system for oceanographic data, located at the Jet Propulsion Laboratory. The present core participants in the workshop are listed in Table 1-1.

It was agreed that the satellite data comparisons should be global, with emphasis on regions of common sampling. The most limited spatial coverage is available from the VAS on GOES-East, which is stationed above the equator at longitude 75°W and primarily views regions in the north-west Atlantic and south-east Pacific Oceans. Also, in situ ship data are most abundant in the north Atlantic and Pacific Oceans. Three months of data were selected for initial study. November 1979 was chosen because it was the month for which FGGE buoy SST data were available in the southern oceans. However, only HIRS/MSU and SMMR satellite data were available for this month (the TIROS-N four-channel AVHRR data were also available). December 1981 was selected because it was the first month for which the operational five-channel AVHRR data were available. Finally, July 1982 was chosen because VAS data had by then become available, and July was seasonally comparable with the early Seasat SMMR period in 1978.

Ironically, at the time these decisions were being made (April 1982), El Chichon volcano in southern Mexico had recently erupted, ejecting a cloud of particulates into the atmosphere just north of the equator and causing marked degradation in the operational AVHRR SST retrievals. On the one hand,

Table 1-1. Key Workshop Participants and Responsibilities

Area of Responsibility	Key Workshop Participants
Satellite Data:	
AVHRR:	P. McClain (NOAA/NESDIS), R. Bernstein (SIO)
HIRS/MSU:	J. Susskind (GSFC)/M. Chahine (JPL)
SMMR:	T. Wilheit (GSFC)/A. Milman (SASC), C. Prabhakara (GSFC), E. Njoku (JPL)
VAS:	W. Smith/J. Bates (U. Wisconsin)
In Situ Data:	S. Pazan (JPL/SIO), R. Bernstein (SIO)
Analysis Methods:	D. Chelton (JPL), T. Barnett (SIO)
Data Processing (PODS):	J. Hilland (JPL)
Organizer/Chairman:	E. Njoku (JPL)
Program Manager:	W. Esaias (NASA/Hq)

this afforded a unique opportunity to evaluate the various SST sensors in the presence of atmospheric aerosol contamination, which by July 1982 had become extensive. However, the possibility arose that unless a month other than July 1982 were chosen for study, very little uncontaminated VAS data would be available for comparison in optimal as well as sub-optimal conditions. For this reason the month of March 1982 (the first in which VAS data were available and just prior to the El Chichon eruption) was added to the workshop list.

The procedure for the comparisons was for each investigator to provide JPL with a tape containing all SST retrievals for a given month, earth-located at the original retrieval points (i.e., without gridding, smoothing, or other processing). The SST data sets were then archived on the PODS computer and intercompared by two basic methods: (1) collocating individual retrievals and in situ data using a time-distance window of appropriate size, and (2) forming monthly averaged fields by binning data into fixed latitude-longitude cells. A variety of display methods and statistics were developed to analyze the results. These methods are described in Sections II and III of this report.

The in situ SST measurements were obtained from a variety of sources. The bulk of the data came from Fleet Numerical Oceanography Center (FNOC) ship reports, with higher quality data coming from expendable bathythermographs (XBTs), buoys, and research vessels. These data are discussed in Section IV. Because the in situ data are themselves of uncertain accuracy, they were treated not as "truth" but as an additional data set to be evaluated with the satellite data. To maintain the integrity of the comparisons, investigators were requested not to "tune" their retrieval algorithms using in situ data for the month under study. Use of climatology and in situ data from prior months were considered acceptable for initial development of the algorithms. All subsequent algorithm tuning was to be closely monitored at the workshop in order to evaluate temporal stability of the algorithms and sensor calibrations.

C. WORKSHOP-I

As planning for the workshops progressed, it became evident that acquisition of several months of satellite data and processing the data to the SST level were major tasks for investigators (except for the operational AVHRR SST product). Also, development of software to assimilate and process the SST data at JPL required significant resources. Therefore, it was decided to hold the workshops in stages. The first workshop, reported here, analyzed data for the month of November 1979. Three satellite SST data sets were examined, all derived from the Nimbus-7 SMMR. The first, labelled SMMR-A, was the early Nimbus Project release version. The second, SMMR-D, was an update to this version, with some small but significant improvements to the retrieval algorithm. These data sets are described in Appendix A. The third data set, SMMR-C, was derived using a quite different retrieval approach and is described in Appendix B. These SMMR data sets were originally referred to as SMMR-I, SMMR-II, and SMMR-III, respectively. They have been renamed in this report to conform with the file code conventions listed in Table 3-1 and to avoid confusion in future workshops. Although no data from the five-channel AVHRR, HIRS/MSU, or VAS were studied in this workshop, descriptions of the sensors and retrieval techniques are provided for reference in Appendices C, D and E, respectively.

For most participants the two-day workshop was too short to study the data products in depth. However, preliminary evaluations are reported in Sections IV, V, and VI, and firmer conclusions will be drawn on further study. Workshop-I also provided an opportunity for participants to review the software and analysis approaches used to compare data sets and to discuss improvements for subsequent workshops. An important section of this report deals with the conclusions and recommendations that arose from these discussions (Section VII).

Present plans include two additional workshops. The next workshop, to be held June 22-24, 1983, will analyze data from December 1981 and will include data from the SMMR, AVHRR, and HIRS/MSU. The final workshop will be held in early 1984 and will include data from all sensors for the months of March and July 1982.

1-9

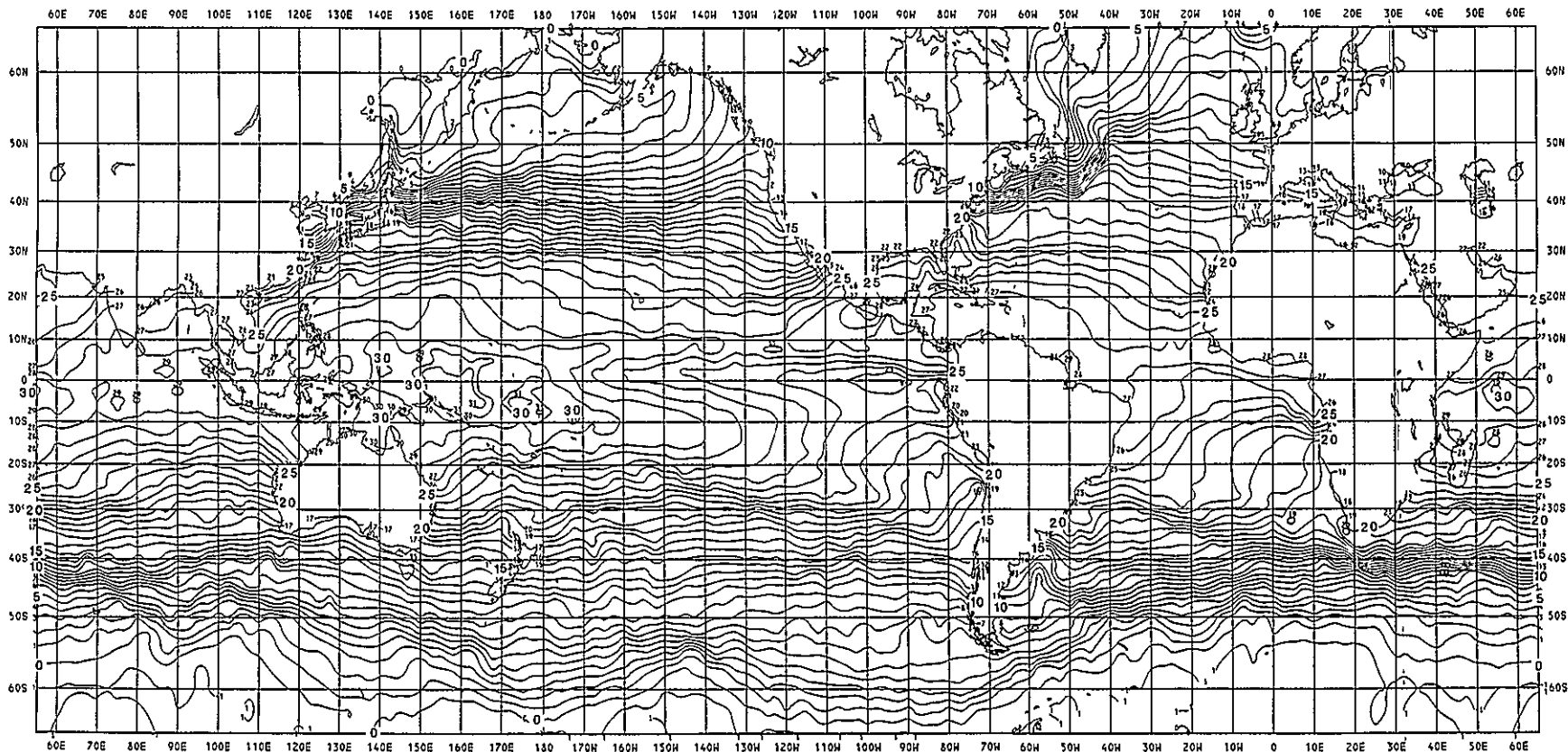
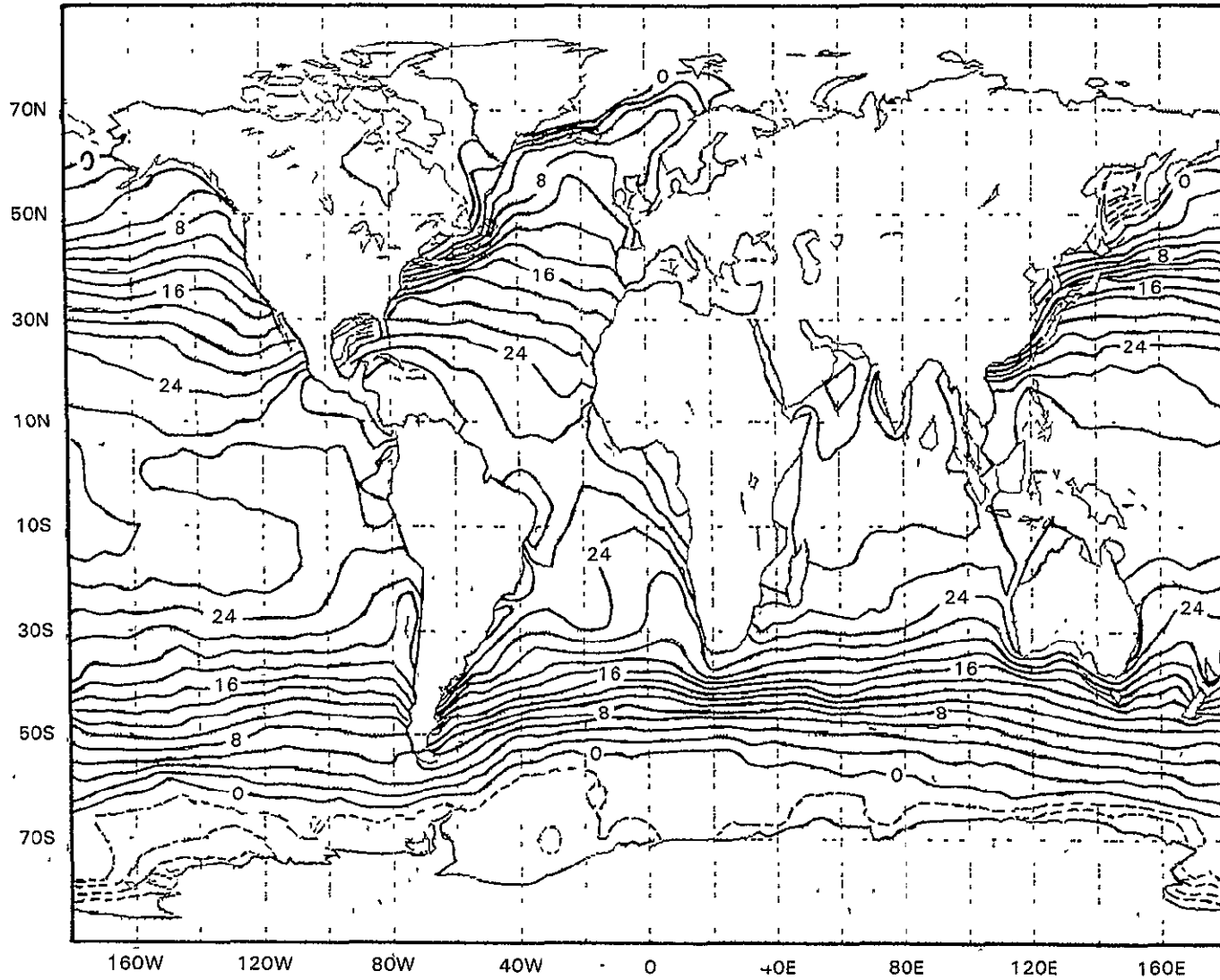


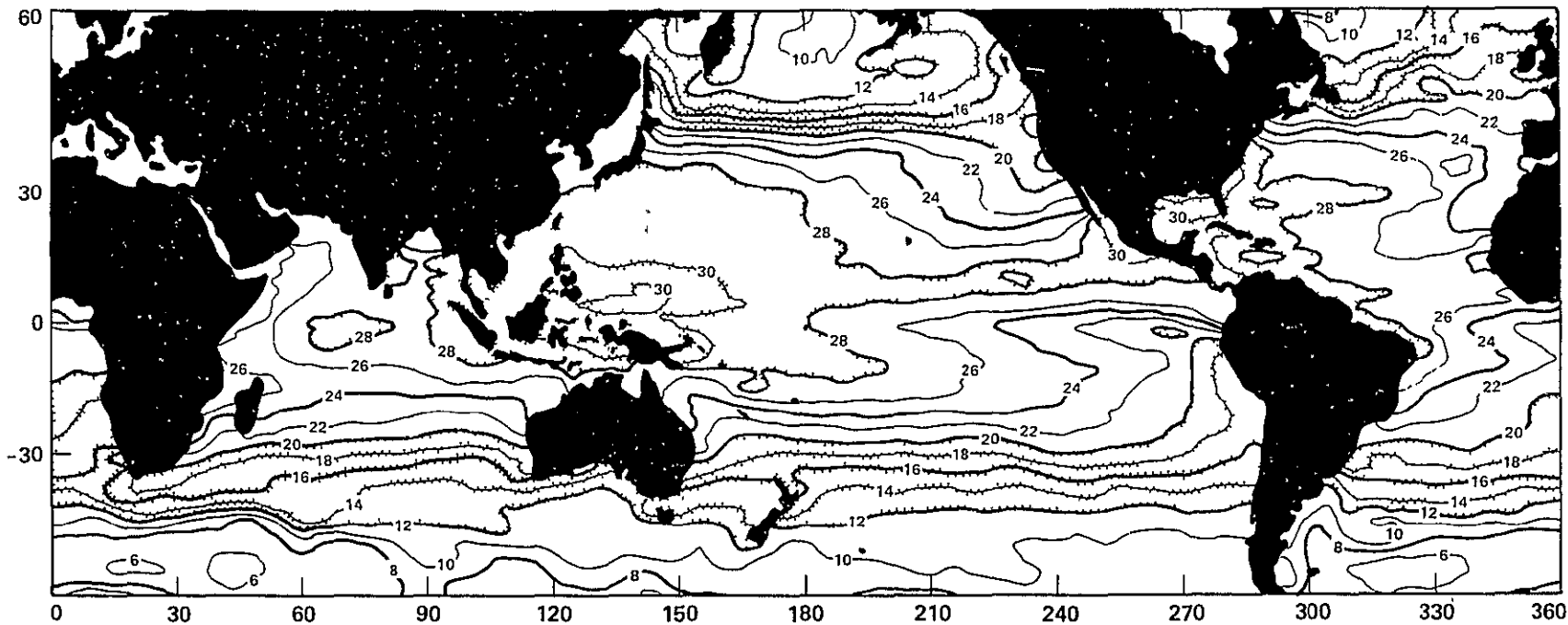
Figure 1-1. Global MCSST contour map of sea surface temperature derived from NOAA-7 AVHRR, December 1981 (Source: Ref. 1)



ORIGINAL PAGE IS
OF POOR QUALITY

Figure 1-2. Global surface temperature contour map derived from TIROS-N HIRS/MSU, January 1979 (Source: Ref. 2)

1-8



ORIGINAL PAGE IS
OF POOR QUALITY

Figure 1-3. Global sea surface temperature contour map derived from Seasat SMMR, August 1978 (Source: Ref. 3)

SECTION II

WORKSHOP-I ANALYSIS TECHNIQUES

D. Chelton

A. BACKGROUND

On August 18, 1982, a meeting was held at Scripps Institution of Oceanography (SIO) in La Jolla, California, to discuss appropriate analysis techniques for the sea surface temperature (SST) intercomparison. The discussion panel consisted of E. Njoku, D. Chelton, T. Barnett, R. Bernstein and S. Pazan. A concern of the panel was that the purpose of the SST workshops not be misinterpreted. The goal is not to rate various techniques but rather to identify and examine any systematic differences between the various measurement techniques. This in turn might reveal areas for needed improvement in the SST retrieval algorithms or, at the very least, a clearer understanding of the limitations of each sensor. In this regard the relative maturity of the satellite sensors should be considered, infrared sensors having undergone a decade of development whereas microwave techniques are relatively new.

One of the conclusions of the La Jolla meeting was that the first SST workshop should be intended primarily as a "shake-down" of the data comparison procedures. This would then pave the way for future workshops to proceed more smoothly. In this vein, one of the important eventual outcomes of Workshop-I was the discussion session on the afternoon of the second day when recommendations were made for modifications and improvements of the analysis techniques established at the La Jolla meeting. These recommendations are summarized in Section VII of this report.

This section (Section II) discusses the analysis techniques used in Workshop-I. The term "sensor" will be used throughout to describe any of the various SST measurement techniques, e.g., "sensor" can refer to satellite measurements, ship measurements, buoy measurements or even climatological values. The SST data sets are described in subsequent sections of the report.

B. METHODS OF ANALYSIS

The methods of analysis used can be divided into two broad categories: (1) "spot" comparisons to examine the level of noise in individual measurements; and (2) temporal and spatial average comparisons. The second method smooths out much of any random noise that may be present in individual measurements.

Specifically, the analysis and graphics capabilities developed by the Pilot Ocean Data System (PODS) for Workshop-I consisted of the following spot and temporal and spatial average comparisons:

1. Spot Comparisons

- (1) Global maps of raw data locations. Any desired plot symbol can be plotted at the latitude and longitude coordinates of

raw data locations within any specified geographical region over any specified time period. Data locations are superimposed on maps of coastal boundaries.

- (2) Development of an efficient algorithm to identify matches between measurements by any two sensors within any desired time and space windows (12-hour time and 300-km radial distance separations were used for Workshop-I). The performance of this algorithm was approximately two orders of magnitude more efficient than a previous "brute force" method available in PODS.
- (3) Histograms of raw observations of SST by any sensor. User can specify temperature bin size for histograms and geographical region for data.
- (4) Scatter plots of SST measurements by one sensor versus measurements by another sensor, together with linear regression information. The user is allowed to specify desired time and space separation of "spot hits" and geographical region for data comparison.

2. Temporal and Spatial Average Comparisons

- (1) PODS can generate binned average SST over any desired temporal averaging period and any desired spatial average. For Workshop-I, monthly averages (November 1979) over 2° latitude and longitude regions were used.
- (2) Contour maps of 2° lat-lon binned SST by any sensor in any specified geographical region and with any desired contour interval. Data contours are superimposed on a map of coastal boundaries. Software allows for smoothing of data by simple zonal (longitudinal) running mean filters.
- (3) Scatter plots of 2° lat-lon binned SST by one sensor versus another sensor together with linear regression information. This is the same capability as for the spot comparisons described above. User can specify any desired geographical regions.
- (4) Contour maps of difference in 2° lat-lon binned SST measured by two different sensors in any specified geographical region and with any desired contour interval. Data contours are superimposed on a map of coastal boundaries. Software allows for smoothing of data by simple zonal running mean filters.
- (5) Scatter plots of the difference in 2° lat-lon binned SST measured by two different sensors versus the number of samples in the 2° lat-lon bin by either of the sensors. User can specify geographical region for data comparison.

- (6) Histograms of the distribution of 2° lat-lon binned SST by any sensor. This is the same capability as for the spot comparisons described above. User can specify temperature bin size for histograms and geographical region for analysis.

3

C. WORKSHOP MATERIALS

For presentation in Workshop-I, the following data products were generated using the above capabilities for each sensor, and distributed to the workshop participants:

- (1) Global map of raw observation locations (1 plot).
- (2) Atlantic and Pacific Ocean contour maps of unfiltered 2° lat-lon binned SST (2 plots).
- (3) Atlantic and Pacific Ocean contour maps of 2° lat-lon binned SST smoothed by a 6° lon by 2° lat running mean filter (2 plots).
- (4) Histogram of global distributions of 2° lat-lon binned SST with 1°C bin intervals (1 plot).
- (5) Histograms of raw SST data with 1°C temperature bin intervals by 20° latitudinal bands. The bands chosen were 60°S to 40°S, 40°S to 20°S, 20°S to equator, equator to 20°N, 20°N to 40°N, 40°N to 60°N (6 plots).
- (6) Contour maps of satellite minus Fleet Numerical Oceanography Center (FNOC) ship 2° lat-lon binned SST in northwest Pacific, northeast Pacific and north Atlantic, filtered by a 6° lon by 2° lat running mean filter (3 plots).
- (7) Scatter plots of satellite versus FNOC ship 2° lat-lon binned SST globally and by 20° latitudinal bands. See 5 above. (7 plots).
- (8) Scatter plot of global satellite minus FNOC ship 2° lat-lon binned SST versus number of FNOC ship samples in each 2° bin (1 plot).
- (9) Scatter plots of raw satellite versus raw FNOC ship SST globally and by 20° latitudinal bands. See 5 above. (7 plots).
- (10) Contour maps of sensor minus Reynolds climatology 2° lat-lon binned SST smoothed with a 6° lon by 2° lat running mean filter for the northwest Pacific, northeast Pacific, southwest Pacific, southeast Pacific, north Atlantic, south Atlantic and Indian Oceans (7 plots).
- (11) Scatter plots of 2° lat-lon binned sensor SST versus Reynolds climatology globally and by 20° latitudinal band (7 plots).

If data were supplied globally, the total number of plots per sensor was 44. Some of the data sets delivered to JPL were not global; consequently, fewer than 44 plots were generated for these sensors.

This selection of data products for the workshop was motivated by an initial assumption that the comparison between 2° lat-lon binned satellite and ship SST would provide the most useful information. The purpose of the global and 20° latitudinal banded scatter plots and histograms was to determine any geographical dependence of systematic differences. For example, it may turn out that satellite and ship SSTs agree very closely at middle and high latitudes but disagree in tropical regions. Information such as this may lead investigators to suspect potential problems with satellite SST retrieval in regions of high water vapor content or heavy cloud cover. As another example, large discrepancies between satellite and ship at high latitudes may be an indication of problems with ice contamination.

Unfortunately, the quality of the ship SST values (both in raw form and in 2° lat-lon binned averages) proved to be disappointing. Evidence for this comes from the scatter plots of 2° lat-lon binned satellite minus ship SST versus the number of ship SST per 2° lat-lon bin as shown in Figure 2-1. Approximately 20 ship samples are required per month before the difference between satellite and ship stabilizes, reflecting a large amount of noise in individual ship samples. Scatter plots of 2° lat-lon binned SST difference versus number of satellite observations per 2° lat-lon bin did not show such a simple dependence of the difference on satellite sampling errors. Additional evidence supporting the hypothesis that ship observations are of poor quality are the scatter plots of raw FNOC ship versus other raw FNOC ship SST within 6 hours and 100 km as shown in Figure 2-2. Based on this conclusion, comparisons between 2° lat-lon binned sensor and the Reynolds climatology as described in (10) and (11) above were added to the set of products given to Workshop-I attendees.

Discussions and conclusions drawn from the above set of statistical and graphical data are given in later sections. Section III summarizes the data-editing procedures, file-naming convention and analysis flow chart implemented by PODS at JPL.

ORIGINAL PAGE IS
OF POOR QUALITY

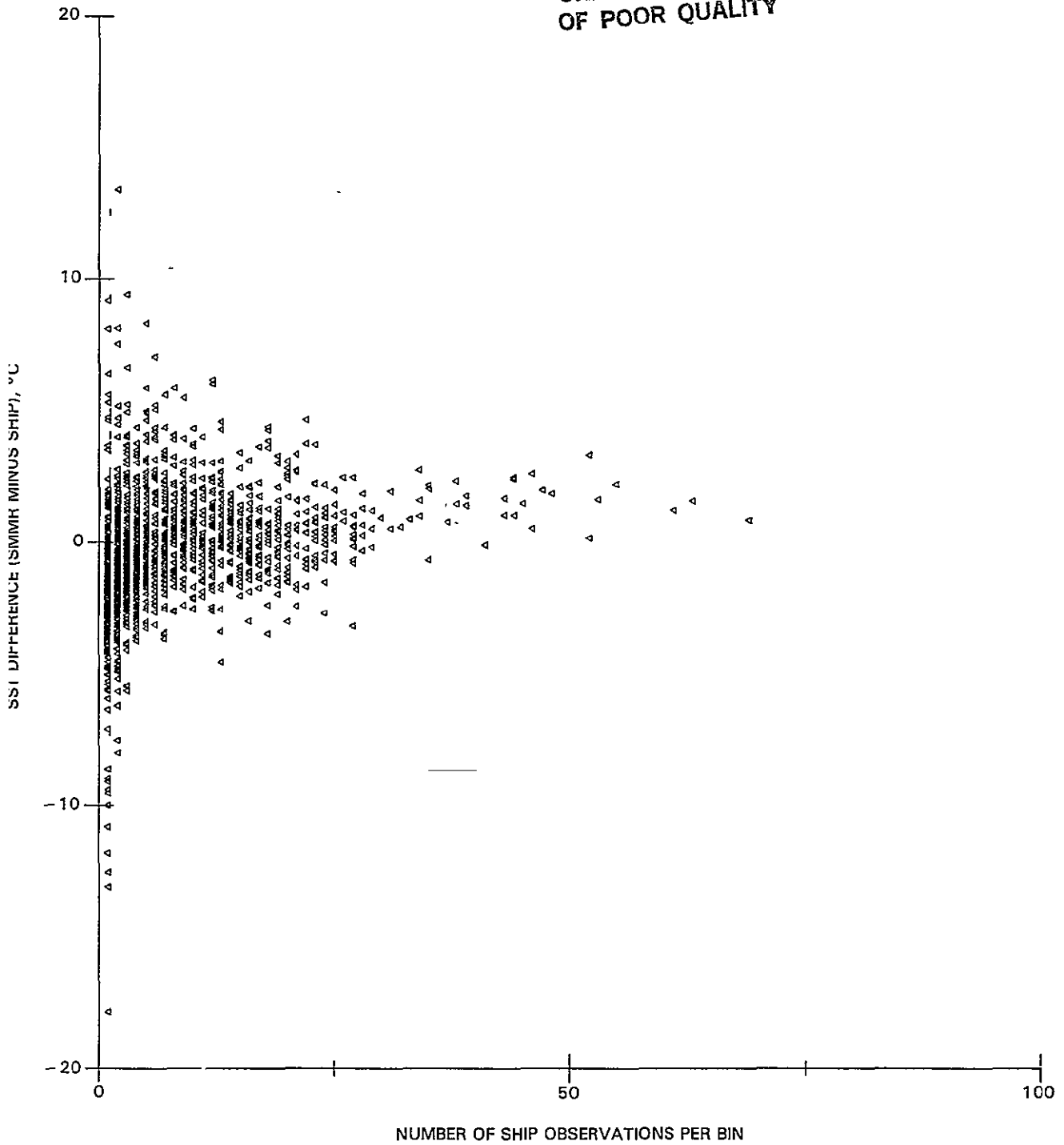


Figure 2-1. Scatterplot of SST difference, SMMR-A minus FNOC ship, in each 2° lat-lon bin versus number of ship observations in each bin

ORIGINAL PAGE IS
OF POOR QUALITY

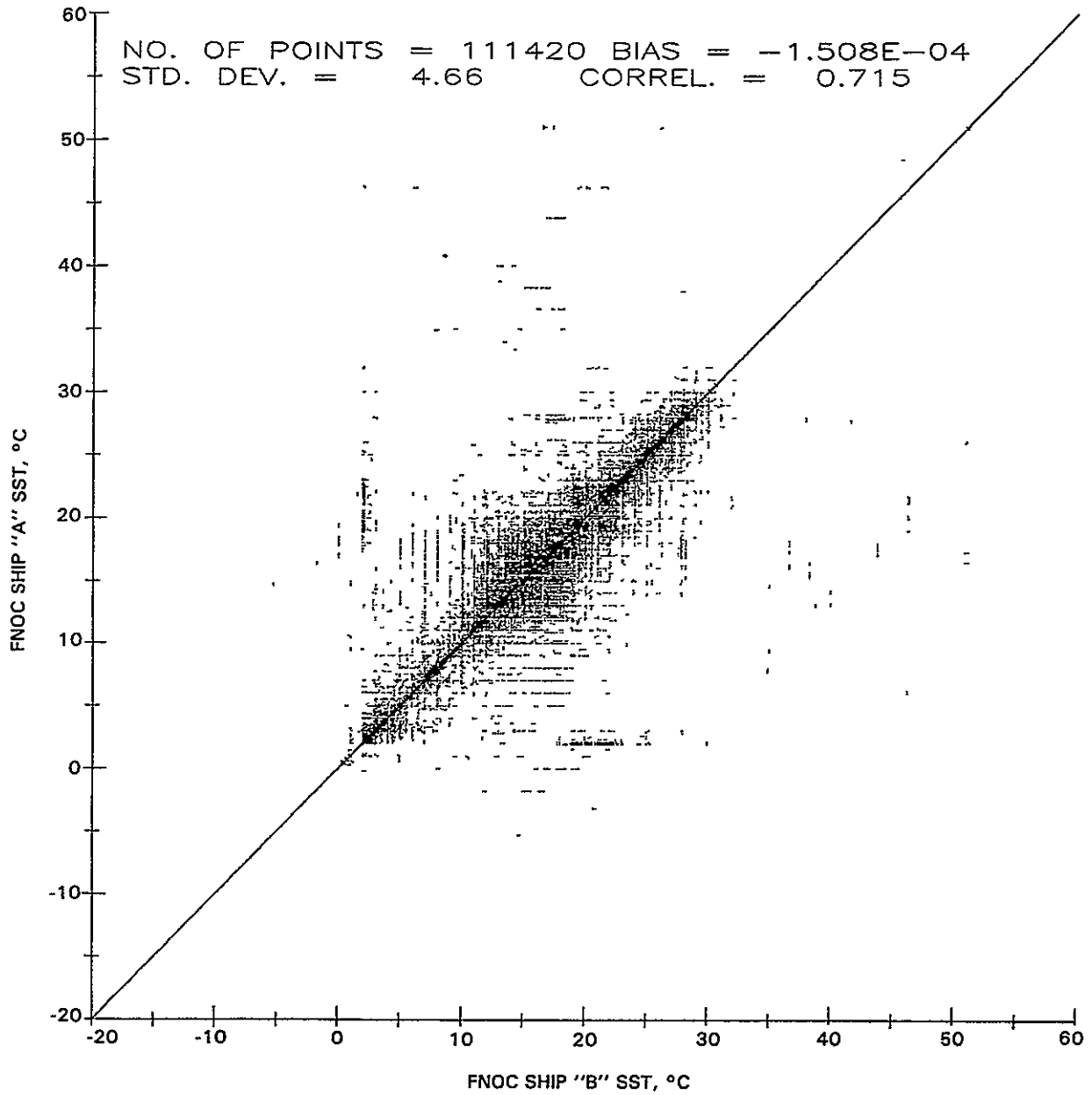


Figure 2-2. Scatterplot of FNOC ship SST observations versus other FNOC ship observations within 6 h and 100 km

SECTION III

WORKSHOP-I PROCESSING SYSTEM

J. Hilland

To implement the analysis techniques described in Section II and to provide end-to-end processing, a system was designed with the following capabilities:

- (1) Receive and catalog data from many sources.
- (2) Organize the data on mass storage for rapid access.
- (3) Edit for reasonableness.
- (4) Create new data sets by sorting on parameter, averaging and merging.
- (5) Provide statistical analysis and display tools.
- (6) Distribute data on demand.

Consideration was given to developing a flexible system that could meet immediate workshop needs and respond to future requirements. The following discussion will present system architecture and data set details implemented during Workshop-I.

Data was transmitted to the Jet Propulsion Laboratory (JPL) on magnetic tape in a format adopted by the principal investigators. Tape contents were then transferred to a disk file for rapid access. Disk files were processed for display by PODSGRAF and Surface-II. PODSGRAF is a JPL-designed system for creating plots of oceanographic data in the form of maps, time series, space series, histograms and scatter diagrams. In addition, basic statistics can be computed and displayed on the plots. Surface-II was developed by the Kansas Geological Survey for the presentation of spatially distributed data and was used to generate contour maps of sea surface temperature. All data analysis was performed on a Digital VAX 11/780.

To control the flow and cataloging of information, a VAX-compatible filename consisting of a prefix and suffix was given to each disk data set. This name was also used to label plots. The filename prefix described the file contents and the suffix described the processing level. Table 3-1 presents the syntax used for filenames. Only satellite data with prefixes SA, SD, and SC (SMMR-A, -D, and -C respectively) and in situ data with prefixes TB, TG, and TH, were analyzed in Workshop-I. File contents described by the prefix included sensor(s), day/twilight/night, and study period. A two-character code was used to identify each sensor and, depending on the processing level, one or two sensors may be identified in the prefix. Day/twilight/night was coded in the filename to assist Nimbus SMMR processing. A day value was defined as the spacecraft and surface point both illuminated by the sun, twilight data

Table 3-1. Filename Conventions

Data Sources	Code
<u>Nimbus/SMMR</u>	
Nimbus Project PARM-LO	SA
E. Njoku	SB
C. Prabhakara	SC
T. Wilheit/A. Milman	SD
<u>NOAA/AVHRR</u>	
NOAA SST (Global Observations at 50 km Spacing)	AA
R. Bernstein	AB
NOAA SST (Weekly Analyzed Field on 50 km Grid)	AC
NOAA SST (Daily Analyzed Field on 100 km Grid)	AD
<u>NOAA/HIRS</u>	
J. Susskind	HA
<u>GOES/VAS</u>	
J. Bates/W. Smith	VA
<u>IN SITU</u>	
Gemnil SST	TA
McLain Ships	TB
NDBO Buoys	TC
FGGE Buoys Level I	TD
FGGE Buoys Level II	TE
TransPac XBT	TF
R. Reynolds, Climatology	TG
S. Pazan, FNOG Ships	TH
Day/Twilight/Night	Code
Day	A
Twilight	B
Night	C
Twilight/Night	D
Day/Twilight	E
Day/Night	F
Day/Twilight/Night	G
Data Span	Code
November 1979	1
December 1981	2
March 1982	3
July 1982	4

were collected when the spacecraft was illuminated by the sun and the surface point was not, and night values were collected when the spacecraft was in the Earth's shadow and the surface point was not illuminated. This code will always be G for sensors other than Nimbus SMMR. The study period was identified by a two-digit integer (01 for November 1979) and will be increased sequentially to reflect new periods of interest. Filename suffixes indicated the processing level (type) of the contents. Each file type is described in Table 3-2.

To reduce access time and storage requirements most disk data were stored in a packed binary format. Detailed format specifications for each file type are contained in Appendix F. It can be seen from the format specifications that some parameters were repeated in different file types. In general, time,

Table 3-2. Processing Levels Defined in Filename^a

Code	Definition
RAW	As received from source
BIN	Binned on N deg x M deg cells over some period
MRG	Merged Sat/Sat, Sat/Ships for matching cells or time/space window
DIF	Differenced (Sensor A - Sensor B) Sat/Sat, Sat/Ship
S2M	Surface-II binary matrix format
GRD	Gridded output from Surface-II
RFM	Formatted spot data
MFM	Formatted merged spot data

^aExample Filename

Filenames were constructed in the following manner:

SensorASensorBDay/Twilight/NightDay/Twilight/NightDataSpan.
ProcessingLevel

SAC01.RAW = Nimbus Project SMMR PARM-10, Night, November 1979, Raw

SATHDG01.MRG = Nimbus Project (twilight/night) merged with FNOOC
ships (day/twilight/night) for November 1979.

latitude, longitude and sea surface temperature were common to all processing levels so that a single file could be input to the display routines from any point in the processing stream.

Data flow is illustrated by a system block diagram depicted in Figure 3-1. In this diagram rectangles represent processors and circles indicate files. Information was transferred from magnetic tape and stored on disk in the .RAW format. Contents of the .RAW files were time, latitude, longitude, sea surface temperature, and a status flag. Records were stored time sequentially and the status flag was used to segregate data based on the definitions given to this flag by each investigator. Once the data were on disk, several paths could be followed to analyze and display the information. The following steps are intended to delineate the analysis tools and not the order in which each path was followed. Clearly, the workshop requirements determined path priorities. Data included:

- (1) Edited and/or sorted by time, latitude, longitude, SST or status flag in EDITRAW and SORTRAW processors.
- (2) Converted by the FORMATRAW processor to .RFM format for input to SURFACE-II gridding routine. Surface-II interpolated the irregularly spaced SST values to a regular grid and stored the information in a matrix in the .S2M format. Note, in Figure 3-1, .S2M was the only format used for input to Surface-II contouring routines.
- (3) Averaged over arbitrary periods and latitude-longitude cells. For Workshop-I monthly averages were computed for $2^{\circ} \times 2^{\circ}$ cells. Averaging was done in the BINNER processor and written to disk in the .BIN format. This operation was given highest priority.
- (4) .BIN files were converted to .S2M form by CNVBINS2M and input to Surface-II for contouring. Alternatively, matrix subtraction could be performed on binned temperature files or matching cells merged in DIFF. Operations in DIFF were performed on matching cells that contained temperatures, and formed temperature, time and distance differences or placed matching cells in the same record. .DIF files were converted to Surface-II format by CNVDIFS2M for the purpose of making difference maps. This was a primary processing step. Contour maps of differenced fields can be distinguished from maps of absolute temperature by the "DIFF" label in the title. .MRG files were also output by DIFF and were reformatted by FORMATMRG to .MFM form for input to Surface-II.
- (5) .RAW satellite and in situ observations were matched within an arbitrary space-time window (initially 300 km radius, +12 h) by SPOTMERGE and edited in SPOTEDIT to smaller distance and time tolerances. Matching points were stored in .MRG format.
- (6) .S2M files were reformatted to .GRD for input to DIFF.

Data in the .RAW, .BIN, .DIF, .MRG and .GRD formats were input to PODSGRAF, as illustrated by Figure 3-2, where:

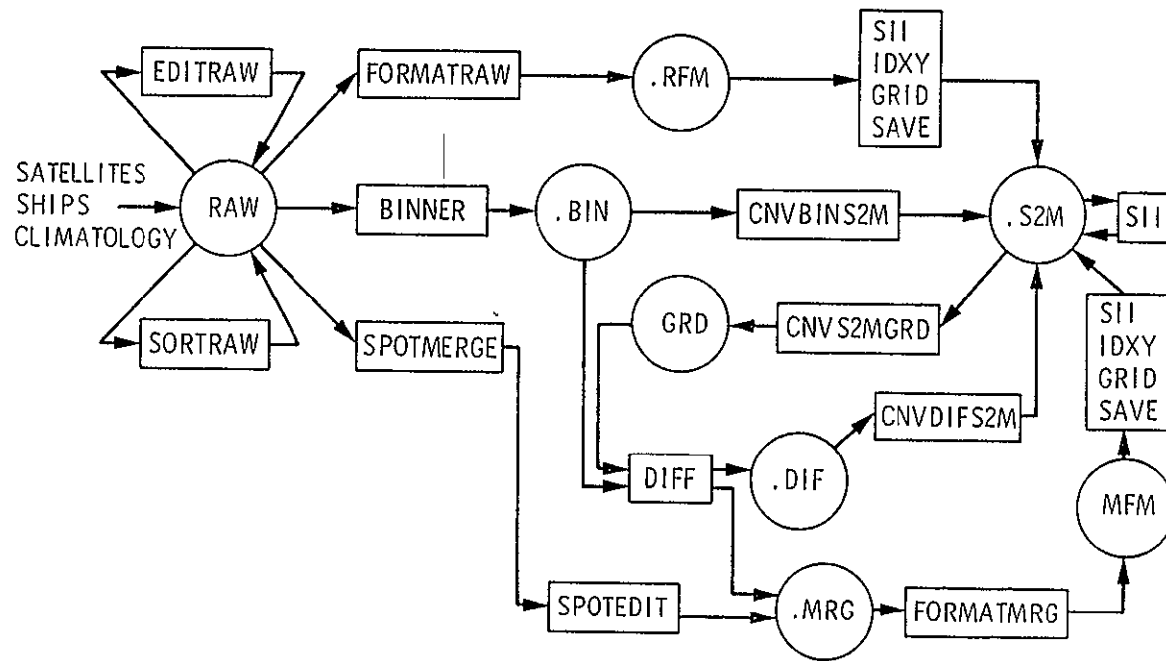
- (1) Contents of the file could be edited prior to computing statistics or plotting. Points were eliminated from processing by setting minimum and maximum bounds for any/all parameters, using the edit function.
- (2) Statistical information in the form of means, standard deviations, number of observations, range, mode and regression statistics were computed and displayed on plots.
- (3) Graphical presentation of the data was made in the form of histograms, scatter diagrams, data location maps, time and space series. It is important to distinguish between the file types plotted on the histograms and scatter diagrams as indicated by the filename suffix in the title. For .MRG illustrations, merged fields can be distinguished from merged spot observations by the "SPOT" label in the title.
- (4) Output from PODSGRAF was plotted on a Benson-Varian Model VA4211 electrostatic plotter or Digital VT100/graphics terminal.

Prior to generating the products, data were, in general, edited for extreme temperatures, land points and day/twilight/night. These operations were performed on the .RAW information in separate steps whereas the edit function in PODSGRAF was used to control the region and temperature range. Editing eliminated only the most gross points from computation and display; however, the values were not physically removed from storage. Hence, the complete range of temperatures could be manipulated at any time. Details of the editing done to each data set are presented in Table 3-3. This list does not include screening performed by principal investigators. Table 3-3 shows that editing was performed at the lowest processing levels; thus it follows that products formed from the .RAW and .BIN information, such as spot merged, bin merged and differenced fields were constrained by this editing.

Workshop-I served not only as a forum for comparing sensors but also as a test for the analysis tools. Recommendations made during the closing session will be translated into modifications to the processing system to be used for Workshop-II. Details of the recommendations are presented in Section VII.

Table 3-3. Data File Editing Steps

Data Set	Data Source	Editing Description
SAD01.RAW	Nimbus Project	None
SCG01.RAW	Nimbus (C. Prabhakara)	None
SDD01.RAW	Nimbus (Wilheit/Milman)	Twilight/Night only
TBG01.RAW	FNOG Ships (McLain)	None
TGG01.RAW	Reynolds Climatology	Eliminated interpolated points
THG01.RAW	FNOG Ships (Pazan)	Eliminated land points
SAD01.BIN		Binned SSTs in range 0-35°C inclusive
SCG01.BIN		Binned SSTs in range 0-35°C inclusive
SDD01.BIN		Binned SSTs in range 0-35°C inclusive
TBG01.BIN		Binned SSTs in range 0-35°C inclusive
TGG01.BIN		None
THG01.BIN		Binned SSTs in range 0-35°C inclusive



ORIGINAL PAGE IS
OF POOR QUALITY

Figure 3-1. Sea Surface Temperature Workshop-I Data Processing System



EDIT (MIN/MAX)

- TIME
- LAT
- LONG
- GEOPHYSICAL PARAMETER

DISPLAY

- PARAMETER VS TIME
- PARAMETER VS LAT/LONG
- HISTOGRAMS
- SCATTERPLOT
- MAPS LOCATIONS, VALUES, CONTOURS

Figure 3-2. POD'SGRAF Oceanographic Data Display System

SECTION IV

IN SITU DATA

S. Pazan

A. SOURCES OF THE DATA AND DATA PROCESSING TECHNIQUES

1. Reynolds Climatology

The initial version of this one degree, monthly climatology was produced by the National Climatic Center (NCC) for the U.S. Navy from surface marine weather reports (marine deck) and from the surface part of the National Oceanographic Data Center (NODC) Nansen cast, CTD, and XBT files.¹ The surface marine weather reports comprise approximately 40 million reports from 1854 to 1976. The actual ending date varies from 1970 to 1976, depending on the region. The NODC data set had approximately 600,000 reports in its Nansen cast and STD/CTD file and more than 600,000 XBT reports in 1976. In accord with this, Reynolds (Ref.4) estimates that the NODC data set is approximately 4% of the size of the NCC marine report set. According to Reynolds, the 5° x 5° monthly sea surface temperature climatology (Ref.5) produced from this data set is too coarse to resolve many important sub-grid ocean features, such as coastal upwelling or western boundary currents. Therefore, Reynolds has processed this surface marine summary by simple objective techniques into a one-degree monthly climatology. Data were processed between 40S and 60N because data distribution maps showed that most two-degree quadrangles had at least ten observations in those limits. Only data with four or more observations per one-degree quadrangle were used. Because of the presence of grid scale noise, it was necessary to apply a filter to the data. "A nonlinear filter based on computation of medians was used. Since medians were used rather than weighted means, extreme points could be systematically eliminated from the final product." (Ref.4) Finally, to eliminate a residue of grid scale noise, a five-point binomial filter was used.

2. McLain Summaries

Doug McLain of the Pacific Environmental Group (PEG) at Fleet Numerical Oceanography Center (FNOG) in Monterey, California, has been summarizing radioed marine ship reports by month for NOAA for the last several years. We have obtained his marine summary tapes for the period 1974 to the present. Not having unlimited computing resources, McLain and Roger Bauer (of Compass Systems, San Diego) have used a simple ad hoc editing technique which seems most effective.

The technique edits data that varies by more than a threshold value from the climatological mean, the threshold being determined from climatology as

¹XBT, MBT, CTD, and Nansen Casts are collectively referred to as "casts" in this text.

follows. Roger Bauer set up 12 monthly means for each 1° square using the marine deck (see Reynolds' climatology, above). McLain's processing takes six differences of the climatological field: two north-south differences; two east-west differences; and two time differences, of the previous month and the next month, respectively. These six numbers form an "index of variability" for each month and 1° x 1° square. The tolerance limit is somewhat arbitrarily set at 1.3 times this "index of variability." If any of the first 10 observations in a month and 1° square differs by more than the tolerance limit from the mean for that month and 1° square, it is discarded. After 10 good observations have been obtained in this way, the edit is continued with respect to the mean of the observations in that month, rather than the climatological mean. This allows the signal of large, nonstationary events to come through. The mean monthly sea surface temperature only is archived, not the standard deviation, and no edited marine reports are archived.

3. Fleet Numerical Oceanography Center Radio Reports

Fleet Numerical Oceanography Center (FNOG) archives the radioed marine weather reports, which are used in the McLain analysis (see above), and sends them to Tim Barnett at Scripps Institution of Oceanography (SIO), where Steve Pazan acquires them for JPL/PODS. These radio reports are edited and then summarized into 1° bins at JPL. The ship data were organized into PODS-type raw data files, and summaries were done using the same PODS software used on the SMMR files. The principal difference between this data set and the McLain analysis is in the editing. FNOG radio reports are indexed by ship name/date-time group, and the speed of the ship as calculated from the position and date-time group of its last reported position is calculated. If this speed exceeds 35 knots, this report is rejected. All sea surface temperatures that exceed 35°C are also rejected. The resulting data set retains two major flaws, which will be corrected by the next workshop. First, in the absence of any test against climatology, the analyzed fields have spikes in them, (erroneously large or small values of sea surface temperature in an isolated location). There were from 6 to 10 of these in the western Pacific during November of 1979. Second, there was no edit to delete data points on land. To eliminate the first problem, the McLain/Bauer technique will be used with the Reynolds Climatology. To rectify the second problem, a land editing subroutine developed by Dudley Chelton will be used.

B. DATA TYPES, SPATIAL/TEMPORAL COVERAGE, AND DATA QUALITY

1. Marine Weather Report Data for Ships

The surface marine weather reports are bucket and engine intake temperatures. The latter form the majority of the data used in the climatology and are the sole basis of the McLain and Pazan analyses. Intake temperatures are approximately accurate to only the nearest °C at best and there are intake temperature biases of up to several tenths of a degree C, depending on season and ship position (Refs. 6 and 7). The intake temperatures form the greatest part of the weather report data set, particularly after World War II. Bucket temperatures were the earliest sea surface temperature data to be systematically archived; at best, they can be as

accurate as a Nansen cast temperature. Bucket temperatures and intake temperatures are biased by a fraction of a degree relative to one another, as is apparent from examining average temperatures from 1930, when bucket temperatures predominated, to 1950, when intake temperatures predominated.

2. Ship Data Coverage for Climatology

Figures 4-1 and 4-2 are contour maps of the number of ship reports in each two degree square for July, and are taken from Reynolds (Ref. 4). Most of the data are in the northern hemisphere, along ship routes from the United States to Japan and from the United States to Europe. Reynolds states that there are over three million observations for July. Since there were about 40,000,000 observations altogether in the marine weather report set, this would indicate that the climatological November was created from about 3,000,000 observations also. The STD, CTD, XBT, and Nansen cast data number about 4% of the ship weather reports, so there should be about 100,000 of these for November. Since the distribution of ship weather reports and Nansen cast, STD, CTD, an XBT reports are similar, on average the ship reports will outnumber the casts 25 to 1. Assuming all data have Gaussian error distributions, the error in the average ship temperature will be reduced by a factor of five relative to the cast error reduction. Climatologies created from cast reports do not compare well with climatologies created from ship reports as a consequence (Ref. 8).

3. Comparison of Climatologies

The Reynolds climatology was created to fill the need for a climatology based on the "largest amount of SST observations currently available, (which) minimizes the subjective and objective processing of the observations, and maximizes the spatial resolution" (see Ref. 4). Other climatologies do not have the one-degree resolution of this climatology, or have a heterogeneous mixture of data sources, or use a mixture of subjective and objective processing (see Ref. 8).

The Reynolds climatology is not perfect; there is an anomalously cold region at around 10°N in the eastern Pacific in July which apparently is the result of mislocated ships. There are fluctuations in the data-sparse southern hemisphere with scales of 500 to 1000 km, which Reynolds could not smooth without damage to the rest of the field.

4. Ship Data Coverage for McLain and Pazan

Figure 4-3 is a data distribution plot of edited ship reports for the globe for the month of November, 1979. There were about 97,300 radioed ship reports in this month; after editing, there were 50,000. Figure 4-4 is a histogram of the percent of reports/hour for a mean day. About two-thirds of the observations occur at the synoptic hours of 00 GMT, 06 GMT, 12 GMT, and 18 GMT. (Because the histograms have been rounded off, the percentages do not add up to 100%.)

C. OTHER SEA SURFACE TEMPERATURE DATA SETS

Several other regional sea surface temperature data sets desirable by reason of their quality, or because they form time series from a stationary platform or from a moving platform, were archived or will be archived by PODS.

1. FGGE Buoy Data Set

During November, 1979, between 127 and 133 drifting buoys in the Southern Hemisphere reported sea surface temperature several times a day (Ref. 9). In Figure 4-5, the distribution of buoys is shown for this month on a polar stereographic projection. The worm tracks indicate the path each buoy took during that month.

As part of the First GARP Global Experiment the Marine Environmental Data Service of Canada volunteered to receive the data from these buoys and to prepare near-realtime maps of SST and SST anomalies every five days. The buoys were an average of 1000 km. from each other, well distributed from 20°S to Antarctica. The data, as edited by the Marine Environmental Data Service of Canada, were obtained by PODS but could not be processed in time for Workshop-I. Results of comparisons using these data will be studied in the next workshop.

2. TRANSPAC Pacific XBT Data Set

The TRANSPAC program at the Scripps Institution of Oceanography is sampling the Pacific Ocean with hundreds of XBTs from ships of opportunity traveling between North America, Japan, New Caledonia, Hawaii, Tahiti and the Panama Canal (Figure 4-6). Radio reported cast data archived by FNOC are included and the whole is edited and analyzed at SIO. Bimonthly contour maps of surface temperature (and 12 subsurface fields) are provided using the method of optimal analysis (Ref. 10). The optimal analysis is used to edit the data further, producing a very clean and consistent data set of cast sea surface temperatures. The data volume is adequate to produce monthly anomaly maps of sea surface temperature on the major trade routes between Japan and the United States in the central North Pacific, around Hawaii, and in areas north of Tahiti and New Caledonia/Fiji.

PODS has received and will receive cast data from the edited TRANSPAC file for the workshop months. For the month of November, 1979, there were 444 casts from the North Pacific ships of opportunity program run by SIO; 112 casts from the Tropical Pacific ships of opportunity program; 131 casts from Doug McLain at the PEG in Monterey; and 1031 Pacific casts from the FNOC radio report archives. These data were not processed in time for Workshop-I but will be included in subsequent comparisons.

TRANSPAC Mapping 11-12/79. Figure 4-7 shows the TRANSPAC analysis of sea surface temperature anomalies for the bi-month of November and December, 1979. The analysis uses optimal objective mapping techniques (Ref. 11). The anomalies are with respect to a 1968-1974 climatology (see Ref.10) derived from the historical archive. Therefore, these anomaly patterns are completely independent of the McLain or Pazan analyses. The pattern of sea surface

temperature in the North Pacific in this analysis shows a positive-negative-positive anomaly pattern running from the northwest to the southeast, just as in the ship analyses. The strengths of the anomalies shown are also much the same. (See discussion in Section VI.)

3. NDBO Buoy Data Set

The National Data Buoy Office has 19 instrumented buoys in locations around the periphery of the United States and its immediate neighbors. PODS has data tapes of this buoy data for October–November, 1979.

4. EPOCS SST Sections

As part of the Equatorial Pacific Ocean Climate Study (EPOCS) experiment, ships have been equipped with externally mounted thermistors that are automatically polled along meridional sections at about 110° W. These experiments were run during February through October, 1979; November, 1981; and May, 1982. Although these are all periods before or after the principal observing periods, they allow for comparisons of essentially synoptic in situ measurements through areas of high thermal gradients with satellite measurements at the same or nearly the same time. Patricia Pullen of the Pacific Marine Environmental Laboratory (PMEL) in Seattle has volunteered to supply these data for the workshops.

D. HIGHLIGHTS OF THE CHARACTERISTICS OF BINNED AND CONTOURED DATA

1. Global Reynolds Climatology

The climatological North Pacific November (Figure 4-8a) shows the meridional poleward cooling expected in both southern and northern hemisphere temperate zones. Warm temperatures and high thermal gradients are evidenced in the region of the Kuroshio. There is the expected warm Western Pacific and cool Eastern Pacific, and evidence of upwelling off Peru and the Gulf of Tehuantepec. In the Atlantic (Figure 4-9a), poleward meridional cooling is evidenced in the Northern Hemisphere temperate zones. The Gulf Stream is clearly shown and has higher thermal gradients than the Kuroshio, as the evidence indicates it should. The topographically connected bend in the isotherms at 50° N is also there, as well as another topographically connected feature between 40° and 50° S (not shown). It can be said, therefore, that this climatology passes at least a superficial test of consistency with oceanographic experience.

2. Global McLain SST

McLain Pacific and Atlantic SSTs were contoured (Figures 4-8b and 4-9b) for the month of November, 1979. The picture is limited to the Northern Hemisphere because of the lack of data south of 20° N. However, in the regions which can be mapped, the fields show a marked similarity to those of the Reynolds Climatology. In fact, if the Pacific maps are overlaid, the

McLain isotherms are displaced south of the climatological isotherms along a meridional axis at about 160° W. Conversely, temperatures seem warmer south of Japan and southwest of North America during 1979. These displacements are equivalent to one degree anomalies, approximately (see Figure 6-3b). If the Atlantic maps are overlaid, the McLain SST isotherms and climatological isotherms align very well, except in the southeast, where gradients are lower.

3. Global Pazan SST

The Pazan analysis for the Pacific (Figure 4-8c) is noisier than the McLain analysis, apparently because the editing has not removed isolated bad data points, which introduce "bullseyes" in the contour field. The McLain SSTs were subtracted from the Pazan SSTs and the result contoured (Figure 4-10). In the Pacific, with the exception of areas at about 28° N and 175° W, and 47° N and 192° E, the sea surface temperatures differ by less than a degree. The weak patterns that do show up do not evidence either consistent zonal or meridional gradients, nor do they evidence a shift in a major current. If there are changes in upwelling patterns, they are very weak.

E. SUMMARY OF THE COMPARISONS OF SHIP VERSUS SHIP AND SHIP VERSUS CLIMATOLOGY

The evidence indicates that November 1979 was a very "climatological" month, certainly in the Atlantic. This must make us particularly wary of deviations from climatology anywhere on the globe during this period.

The McLain and Pazan SST analyses are identical to within a degree. The Pazan ship data need to be edited against climatology in order to remove "bad" ship data.

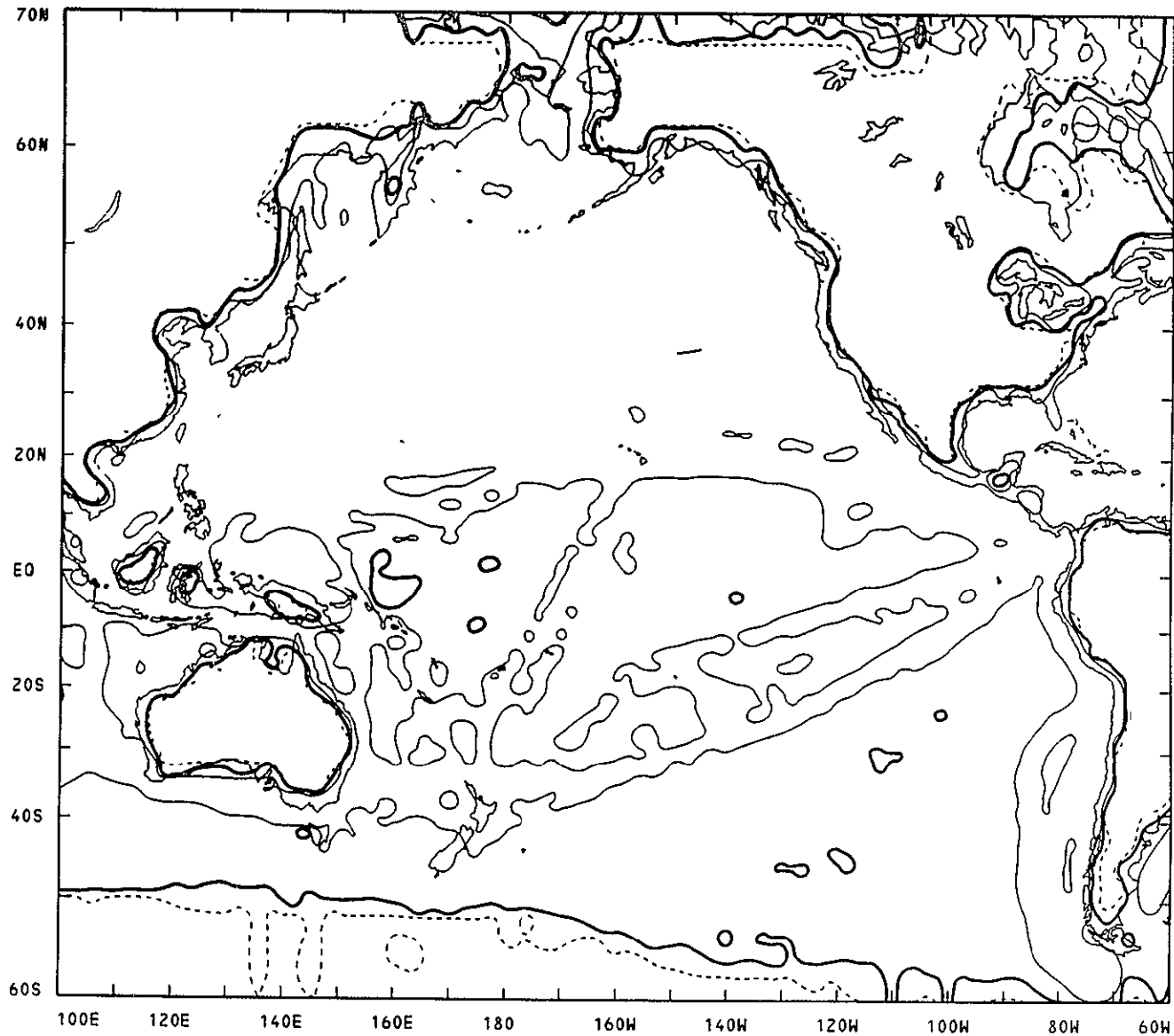
ORIGINAL PAGE IS
OF POOR QUALITY

Figure 4-1. Number of ship reports per 2° lat-lon square in Pacific Ocean for July. The dashed line indicates a contour level of one report per grid square, the heavy solid line indicates ten reports, and the light solid line indicates 100 reports. (Source: Ref. 4)

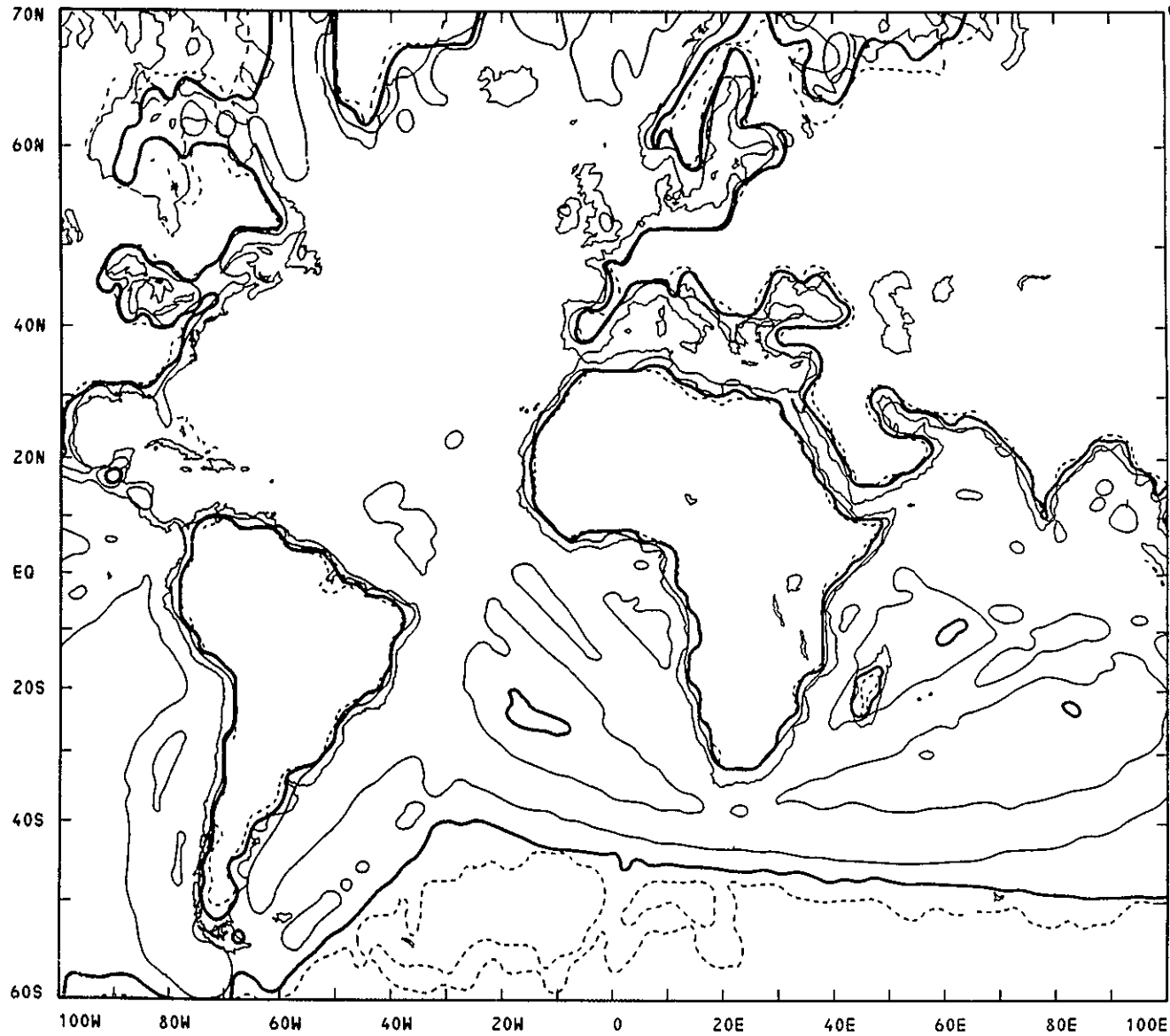
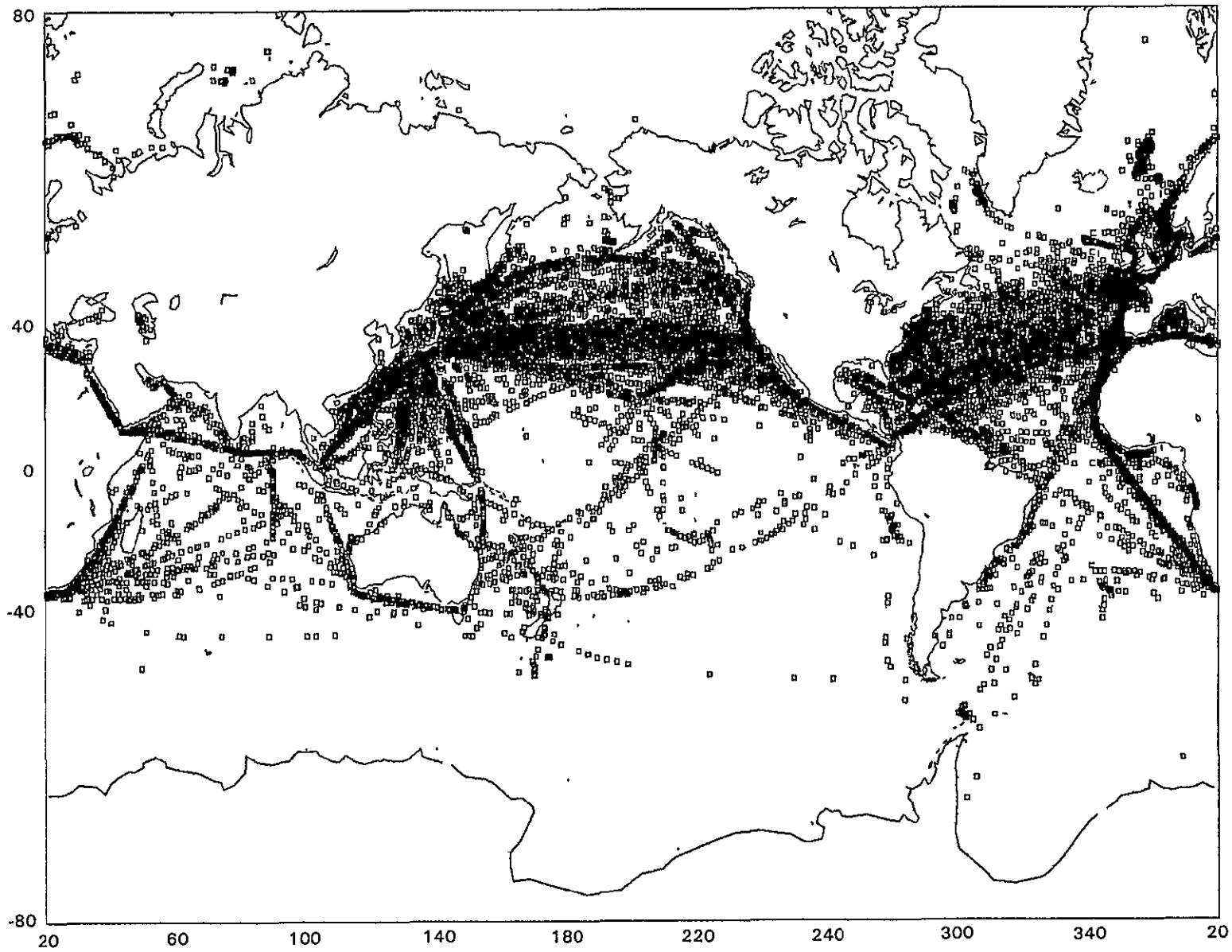
ORIGINAL PAGE IS
OF POOR QUALITY

Figure 4-2. Number of ship reports per 2° lat-lon square in Atlantic and Indian Oceans. The dashed line indicates a contour level of one report per grid square, the heavy solid line indicates ten reports, and the light solid line indicates 100 reports. (Source: Ref. 4)

6-7



ORIGINAL PAGE IS
OF POOR QUALITY

Figure 4-3. Distribution of edited FNOC ship reports for first part of November 1979

ORIGINAL PAGE IS
OF POOR QUALITY

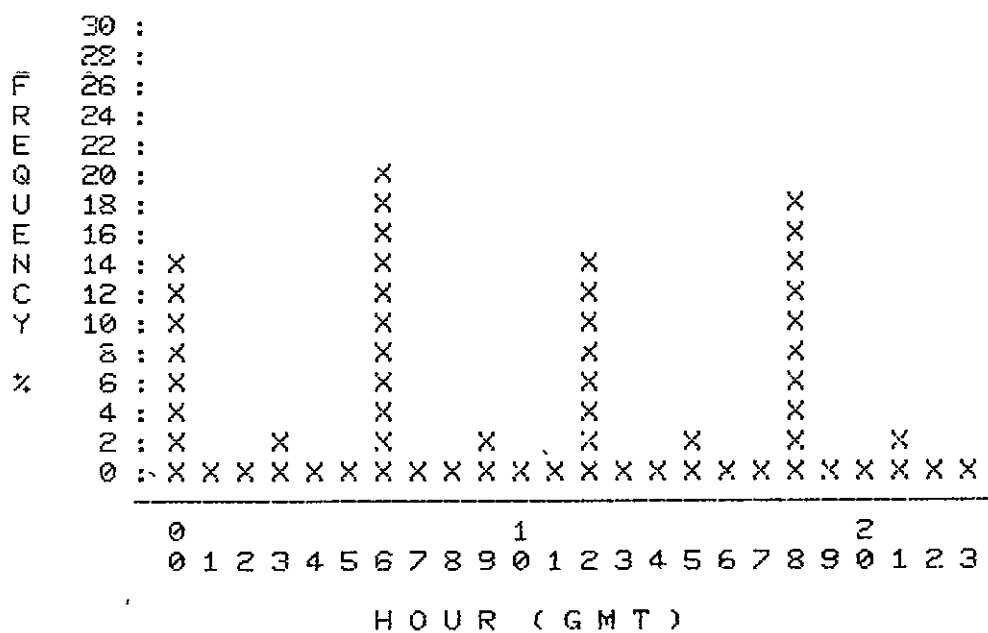


Figure 4-4. Histogram of the percent of reports/hour for a mean day

ORIGINAL PAGE IS
OF POOR QUALITY

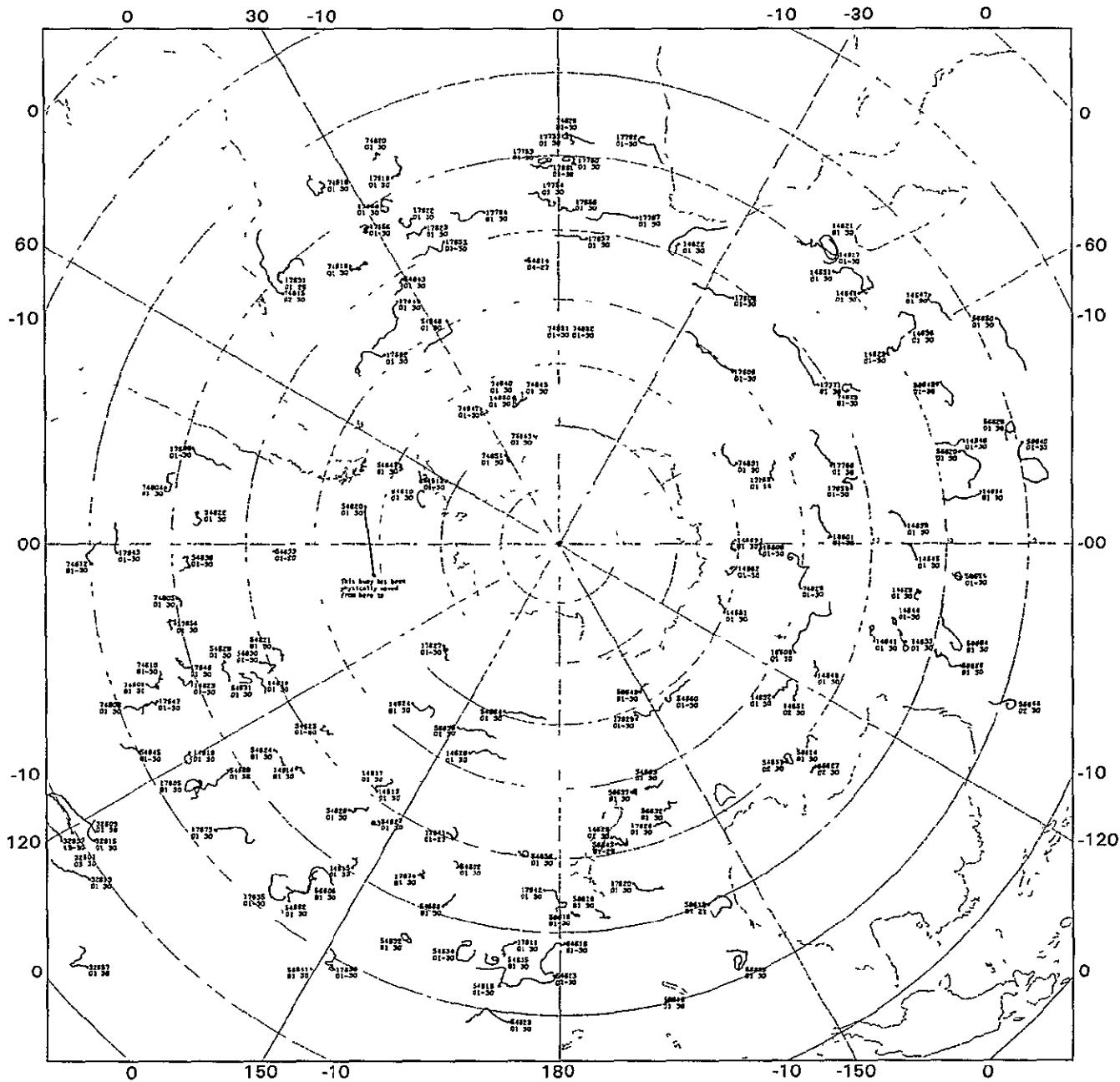


Figure 4-5. Distribution of Southern Ocean FGGE drifting buoys during 1979 (Source: Ref. 9)

ORIGINAL PAGE IS
OF POOR QUALITY

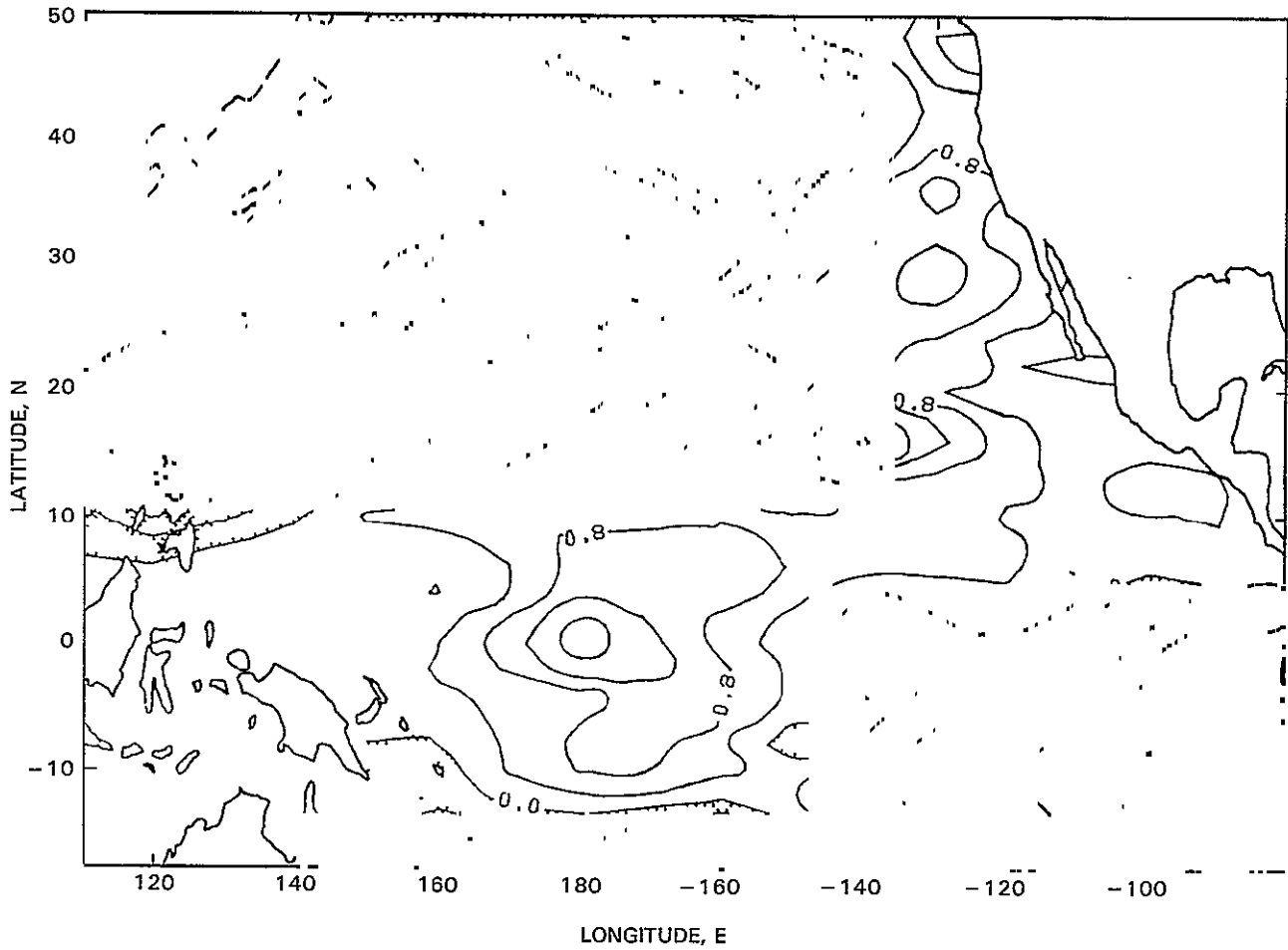


Figure 4-7. TRANSPAC bimonthly SST anomaly map for November - December, 1979

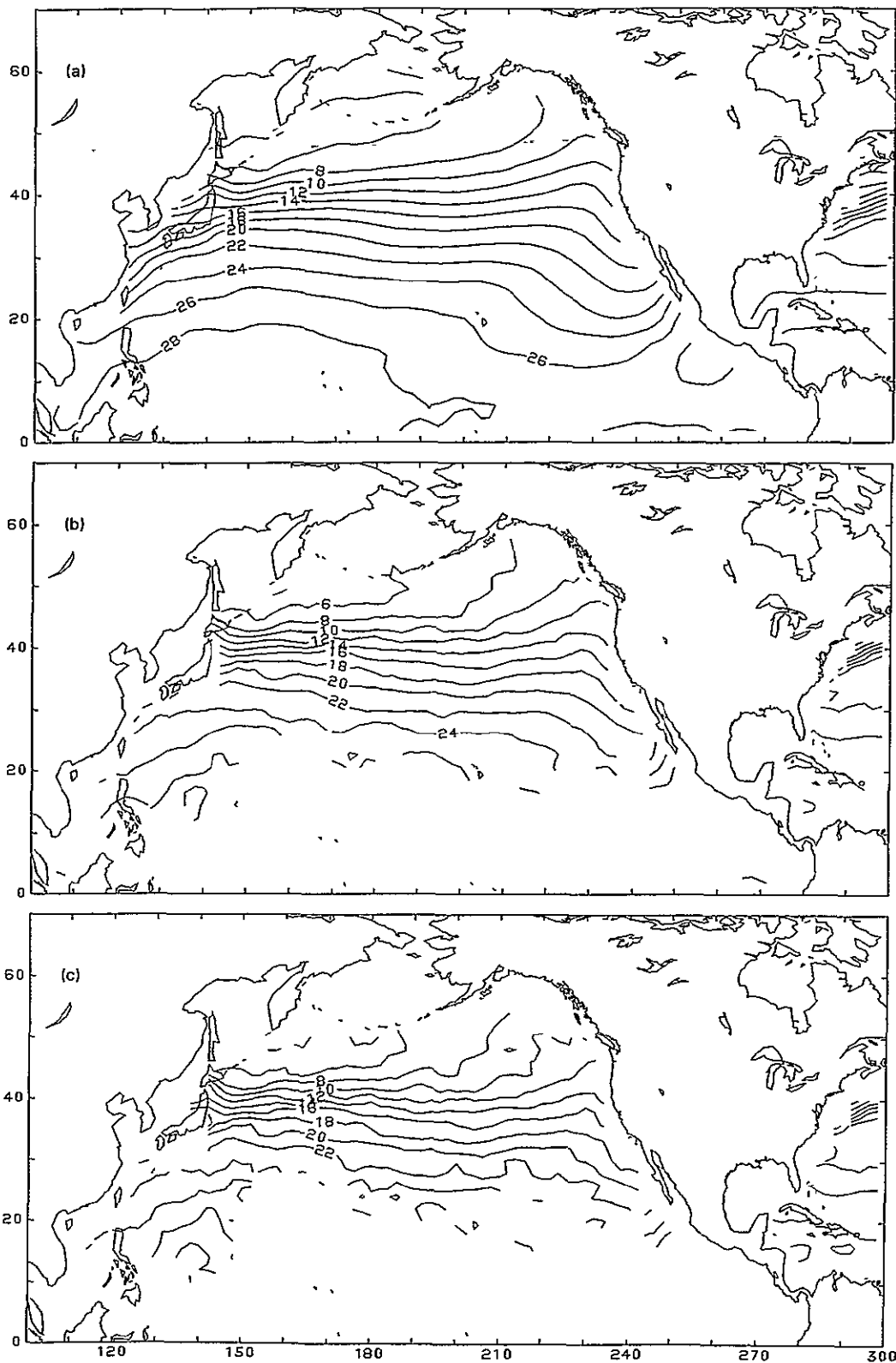


Figure 4-8. Contour map of SST in North Pacific Ocean: (a) Reynolds Climatology for November (b) McLain monthly mean for November 1979 (c) Pazan (JPL) monthly mean for November 1979

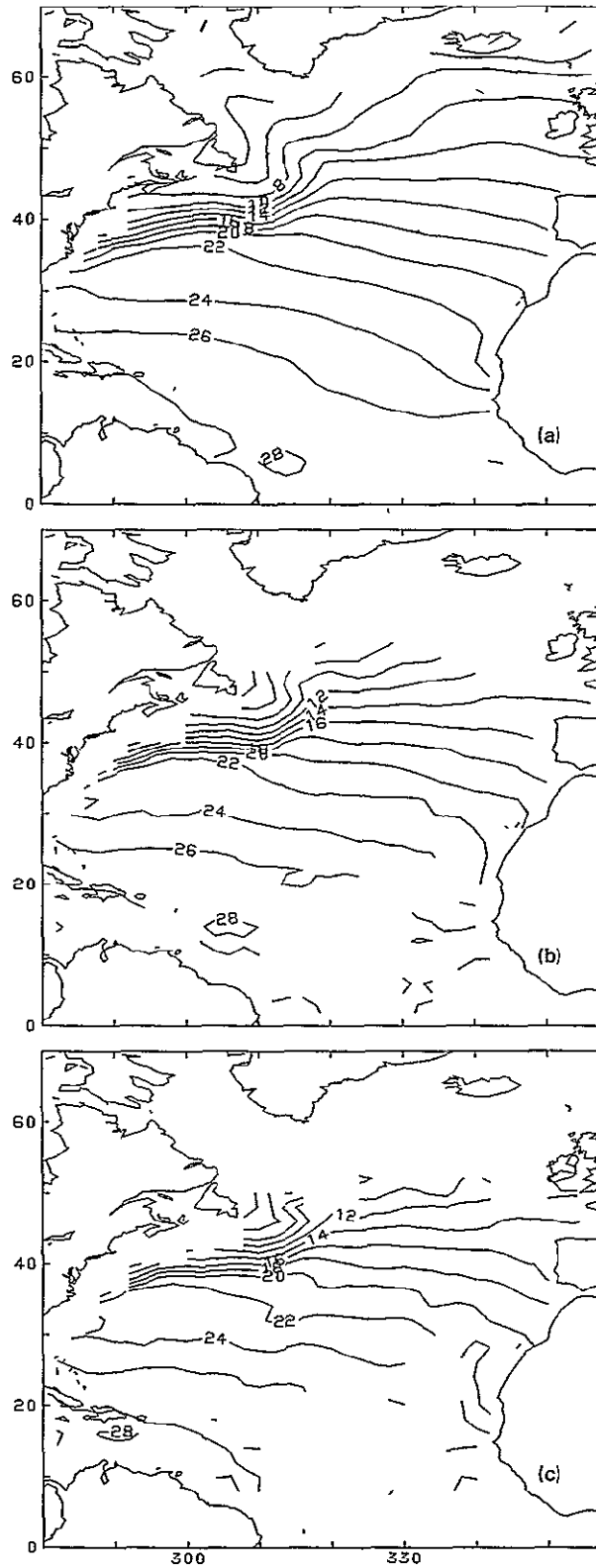
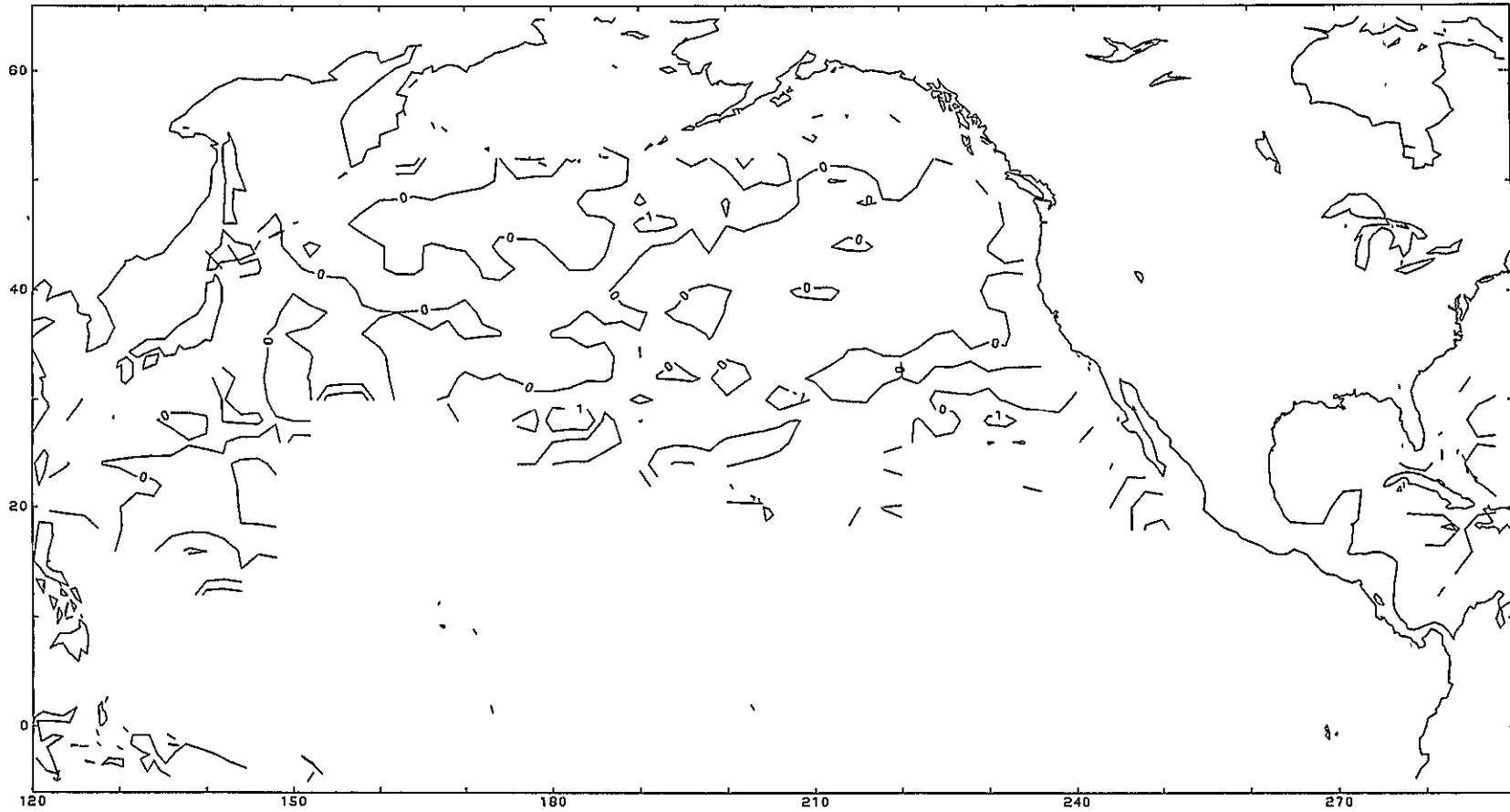


Figure 4-9. Contour map of SST in North Atlantic Ocean: (a) Reynolds Climatology for November (b) McLain monthly mean for November 1979 (c) Pazan (JPL) monthly mean for November 1979



ORIGINAL PAGE IS
OF POOR QUALITY

Figure 4-10. Pazan (JPL) minus McLain monthly mean SST in the North Pacific Ocean, November 1979

SECTION V

SATELLITE DATA

E. Njoku

Three satellite SST data sets were analyzed in Workshop-I, all derived from the Scanning Multichannel Microwave Radiometer (SMMR) on the Nimbus-7 satellite. The SMMR is a ten-channel instrument flown also on the Seasat satellite (now defunct) and was designed to measure SST in addition to other oceanographic and meteorological parameters (Ref. 12). The three SMMR data sets were referred to in the workshop as SMMR-I, -II, and -III. SMMR-I and -II were produced by T. Wilheit and A. Milman, SMMR-II being an updated and refined version of SMMR-I. A description of the algorithms used is provided in Appendix A. SMMR-III was provided by C. Prabhakara and was obtained by a different retrieval approach from the others. The procedure is described in Appendix B. For consistency with the file code conventions listed in Table 3-1 and to avoid confusion in future workshops, SMMRs I, II, and III have been renamed SMMR-A, SMMR-D, and SMMR-C, respectively, in this report.

Figure 5-1 shows coverage of the three data sets after averaging into 2° latitude-longitude bins. As discussed in Section III, SST data outside the range 0 to 35°C were not binned. Thus, no data appear over land, and in ocean areas there are occasional gaps due to islands and other data anomalies. Although the coverage of SMMR-C extends right up to the continental boundaries, antenna sidelobe contamination by land will cause errors in SST in these coastal regions. Anticipating this, SMMR-A and -D were sent to JPL containing no data within 600 km of major land areas. Pacific Ocean data only were provided in SMMR-D. These disparities in data coverage must be taken into account when comparing global histograms and scatterplots. In future workshops, standardized coverage and editing procedures will be adopted for all data sets (see recommendations in Section VII).

Figures 5-2 and 5-3 show SST contour maps of the Pacific Ocean from SMMR-D and SMMR-C data, respectively. The data have been smoothed prior to contouring, using a 6° longitude running mean filter. This reduces the data noise and permits the contouring package to produce legible contour lines and labels (similar smoothing was done for all contour plots appearing in this report). The SMMR-D map of Figure 5-2 contains night/twilight data only, since the authors of this data set experienced calibration problems with daytime data and suggested separate evaluation. In regions where there are data, the SMMR-D contours represent the SST field quite well by visual comparison with ship fields and climatology (see Section VI for a more detailed discussion). The SMMR-C map of Figure 5-3 contains both night/twilight and daytime data. The original contour map contained only night/twilight data for consistency with the SMMR-D map. However, due to the different retrieval approach, fewer useful data points were obtained in SMMR-C, thus leaving several gaps in the binned data coverage and resulting in illegible contours. Even with the addition of daytime data some gaps still occur, as can be seen in Figure 5-1(c). While correct SST trends are seen in Figure 5-3, the SMMR-C data appear to be noisier than SMMR-D.

To attain consistency between data sets, a 600-km coastal mask was applied at JPL to all three binned data sets prior to generating the histograms and scatterplots shown in this section. For additional consistency, data were restricted to the range 55°S to 55°N latitude and 120°E to 280°E longitude (i.e., Pacific Ocean). Night/twilight and daytime data were not mixed.

In Figure 5-4 histograms of the night/twilight data are shown for SMMR-A, -D and -C. As expected, SMMR-A and -D appear quite similar since the latter is a derivative of the former. SMMR-C has a higher percentage of data in the middle SST range, which probably reflects its noisier nature in mid-latitudes. Figure 5-5 shows similar histograms using daytime data for SMMR-D and -C (no daytime data were provided in SMMR-A). It is noticeable from Figure 5-5b that the SMMR-C daytime distribution is different from nighttime. This is due partly to fewer retrievals in the daytime between 13 and 19°C, and partly to having more points above 28°C. There are fewer retrievals overall in the daytime due to the approach used in generating this data set (see Appendix B). The SMMR daytime data are biased high relative to nighttime due to calibration problems, as has been discussed by Milman/Wilheit in Appendix A. In SMMR-D, however, these daytime calibration anomalies have been corrected, resulting in data of similar quality to nighttime (Figure 5-5a).

Prabhakara has provided his observations of these effects in Table 5-1. This shows statistics for histograms of the SMMR-C raw data (i.e., unbinned) presented by 20° latitude bands. By looking at the mean values it is apparent that the daytime values are lower than night/twilight in the northern hemisphere but considerably higher in the southern hemisphere. It is not readily apparent which data sets (night/twilight or day) are more correct in which hemisphere, although investigators place more confidence in the night/twilight data. For more evaluation of the night/twilight data see Section VI.

Finally, in Figure 5-6, scatterplots of the night/twilight data are shown. Figure 5-6a shows the similarity between SMMR-A and -D, SMMR-D being the better of the two. Figure 5-6b plots SMMR-C against SMMR-D and illustrates features discussed previously.

Table 5-1. Global Statistics of SMMR-C raw SST retrievals, grouped by latitude and separated between night/twilight and day (provided by G. Prabhakara)

LATITUDE, deg	NIGHT/TWILIGHT			DAY		
	Number of Retrievals	Mean	Standard Deviation	Number of Retrievals	Mean	Standard Deviation
-60 to -40	1,272	6.9	4.2	363	10.2	4.5
-40 to -20	2,341	16.8	4.1	365	20.7	3.9
-20 to 0	1,003	24.9	3.5	297	26.7	2.7
0 to 20	784	27.5	2.1	546	27.4	2.4
20 to 40	479	21.9	3.7	811	21.5	3.2
40 to 60	451	14.1	5.0	618	12.4	5.4
-55 to 55	4,950	18.6	7.9	2,684	20.4	7.0

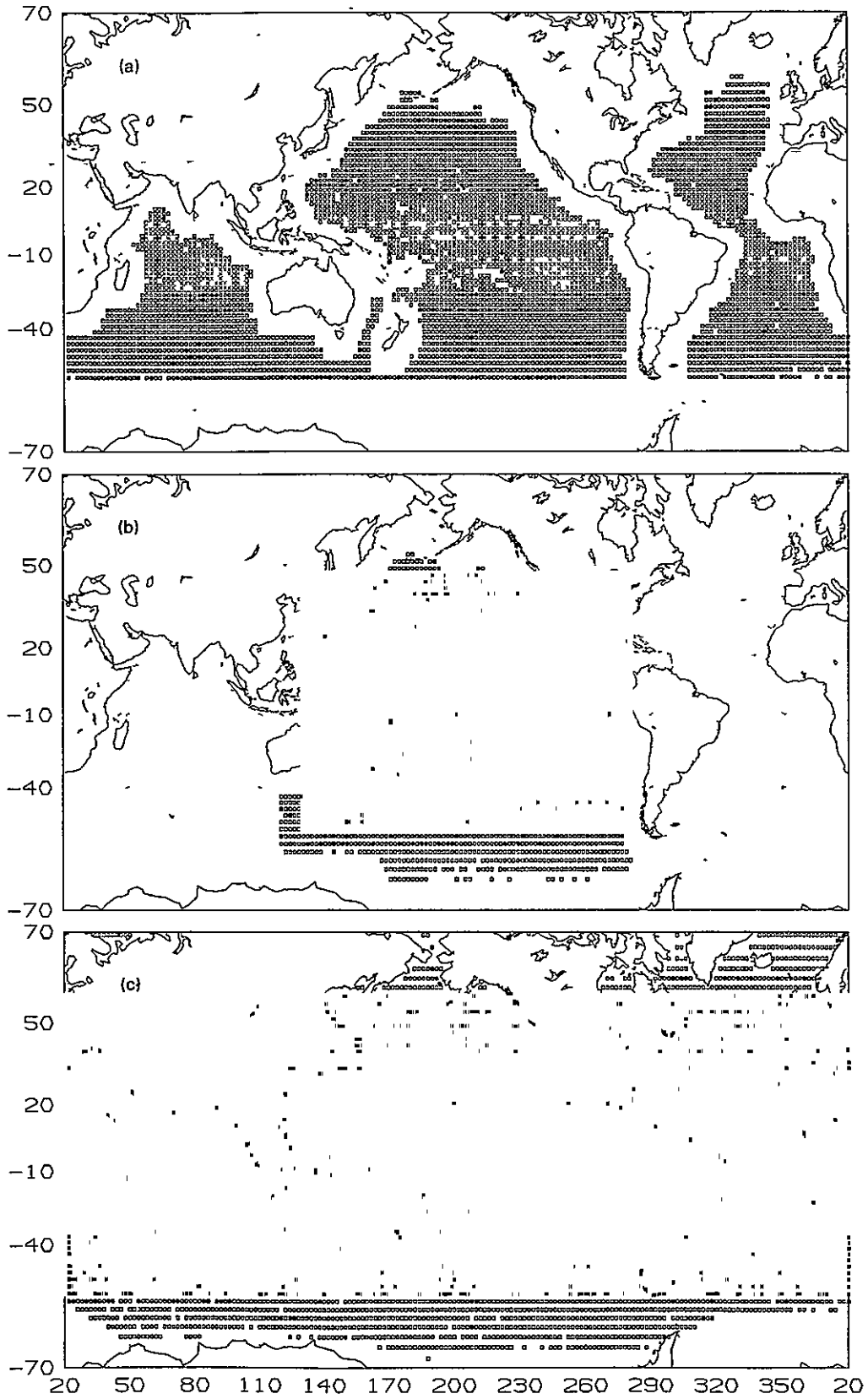


Figure 5-1. Distribution of 2° lat-lon binned data sets: (a) SMMR-A (b) SMMR-D
(c) SMMR-C

ORIGINAL PAGE IS
OF POOR QUALITY

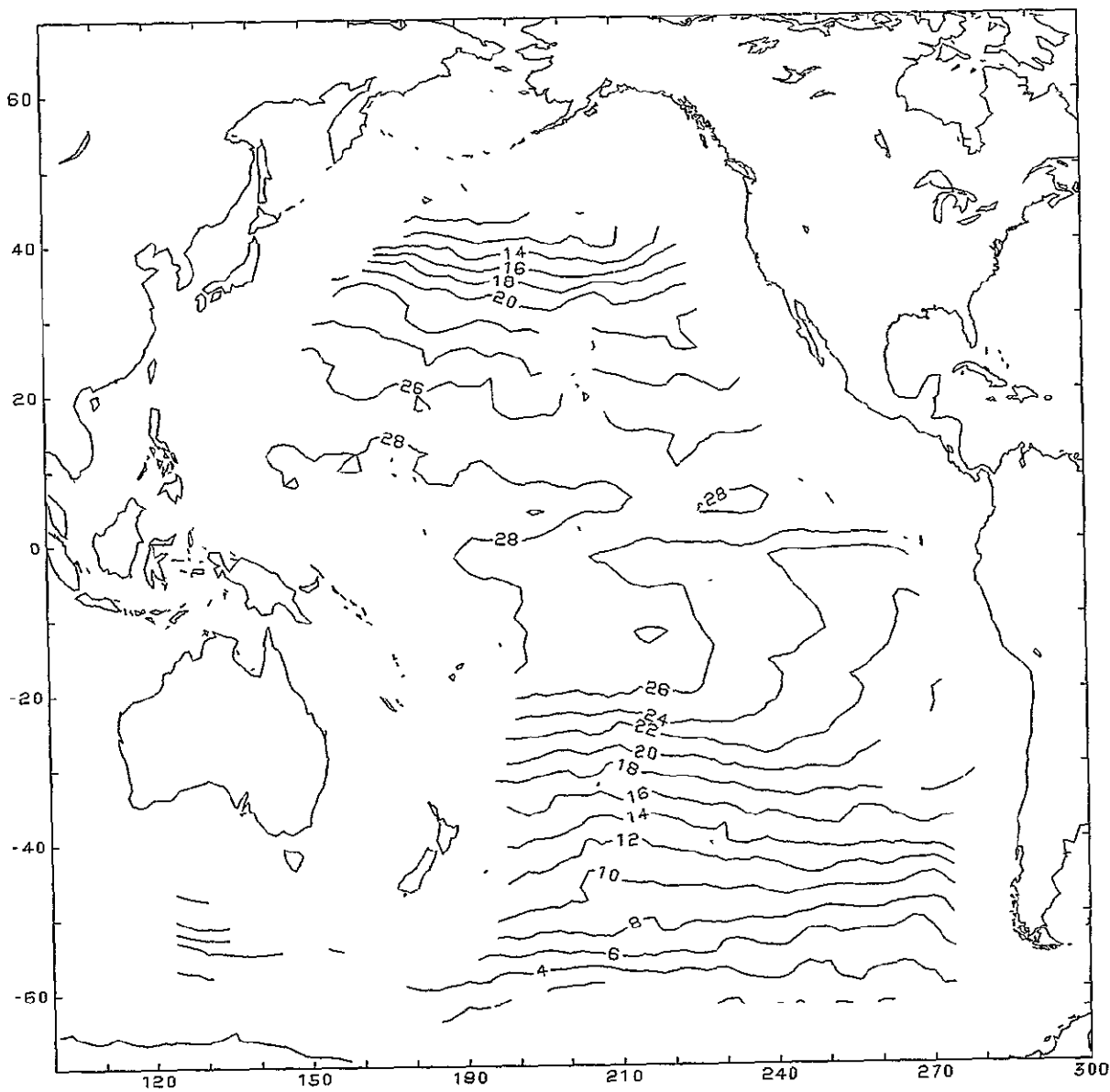


Figure 5-2. Contour map of SMMR-D SST in Pacific Ocean

ORIGINAL PAGE IS
OF POOR QUALITY

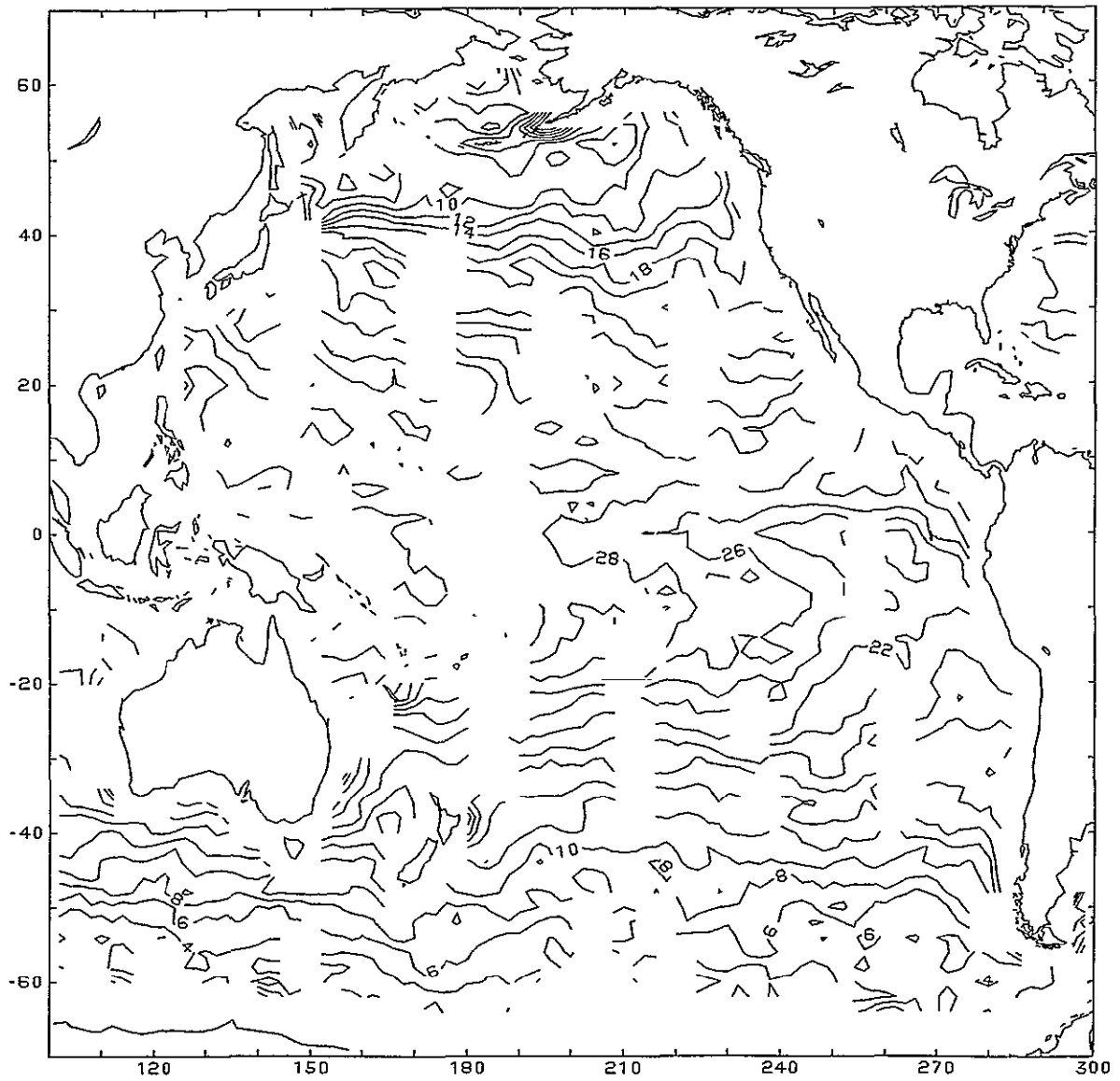


Figure 5-3. Contour map of SMMR-C SST in Pacific Ocean

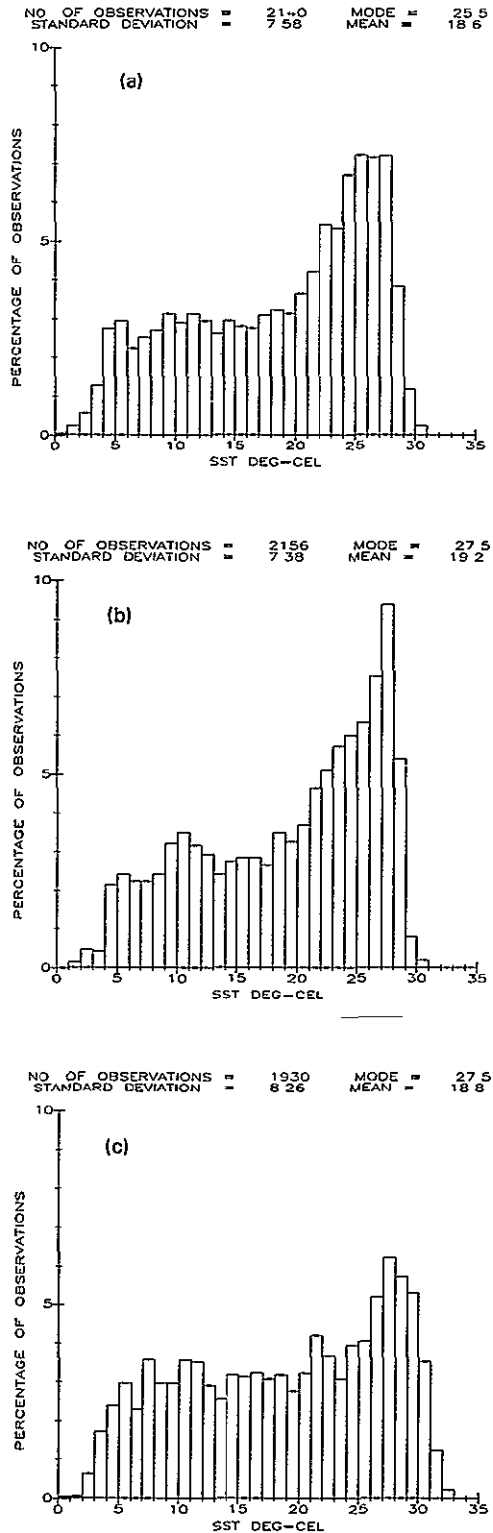
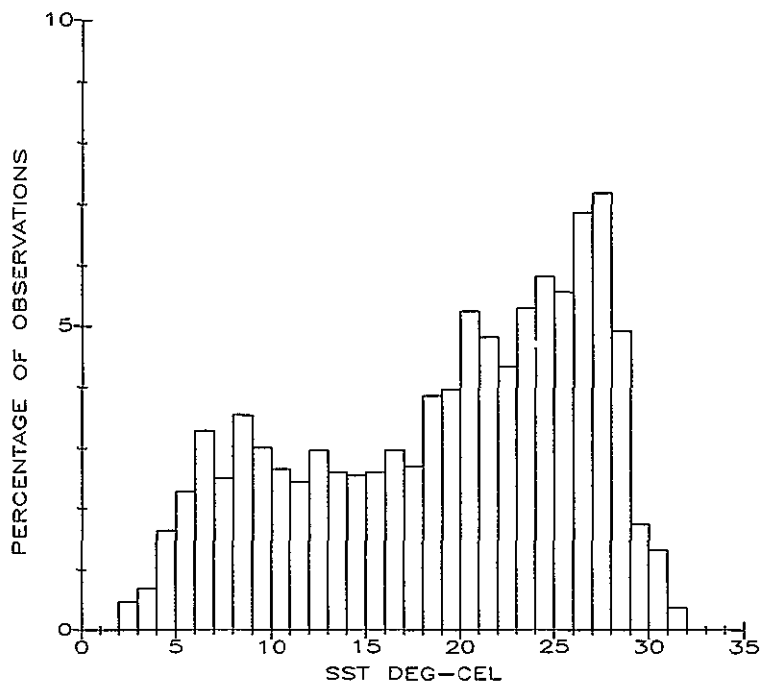


Figure 5-4. Histograms of binned SST in Pacific Ocean between 55°S and 55°N latitude, and 120°E and 280°E longitude. Data within 600 km of land were edited and night/twilight data only were used: (a) SMMR-A (b) SMMR-D (c) SMMR-C

ORIGINAL PAGE IS
OF POOR QUALITY

NO OF OBSERVATIONS = 1893 MODE = 27.5
STANDARD DEVIATION = 7.47 MEAN = 19.1



NO OF OBSERVATIONS = 1141 MODE = 27.5
STANDARD DEVIATION = 7.06 MEAN = 21.1

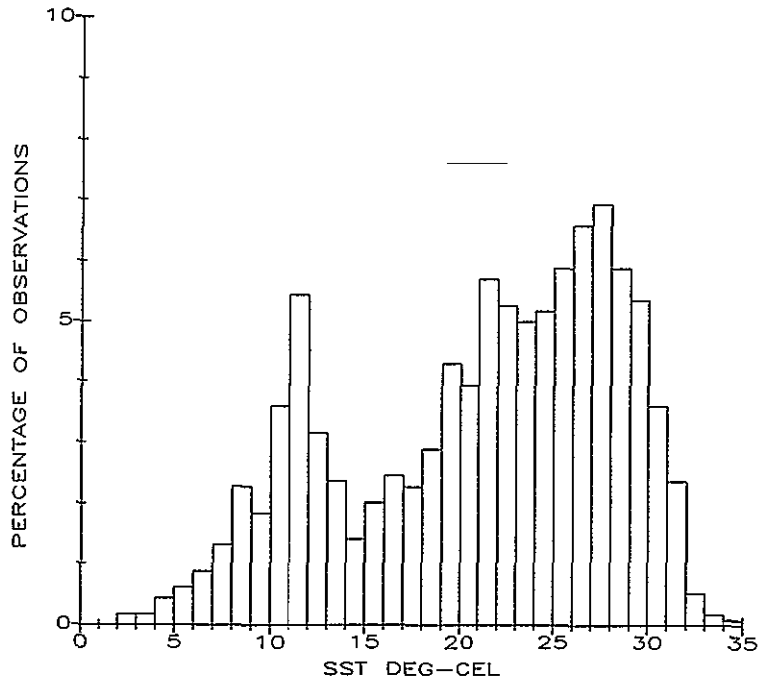


Figure 5-5. Histograms of binned SST in Pacific Ocean between 55°S and 55°N latitude, and 120°E and 280°E longitude. Data within 600 km of land were edited and daytime data only were used: (a) SMMR-D (b) SMMR-C.

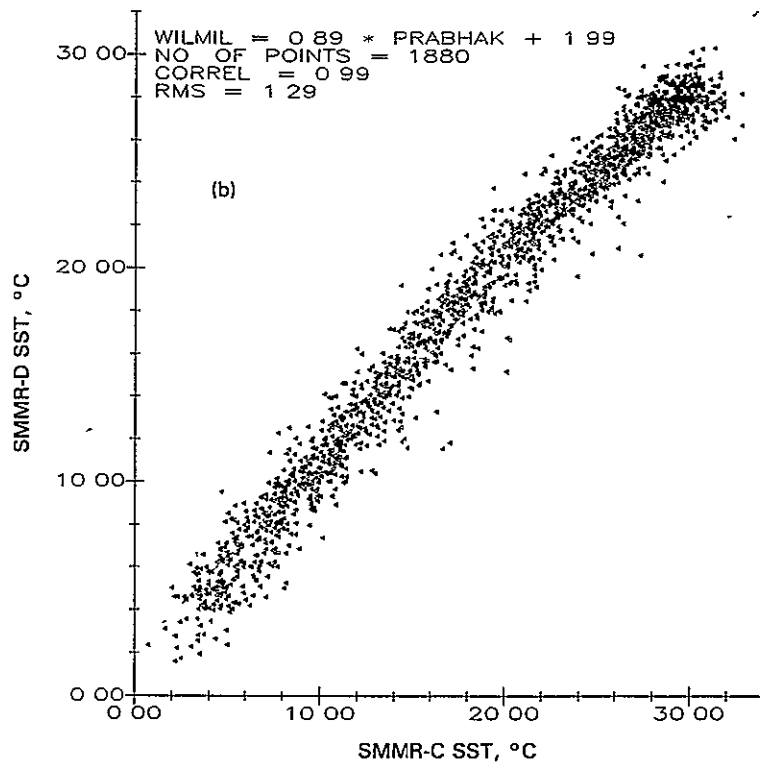
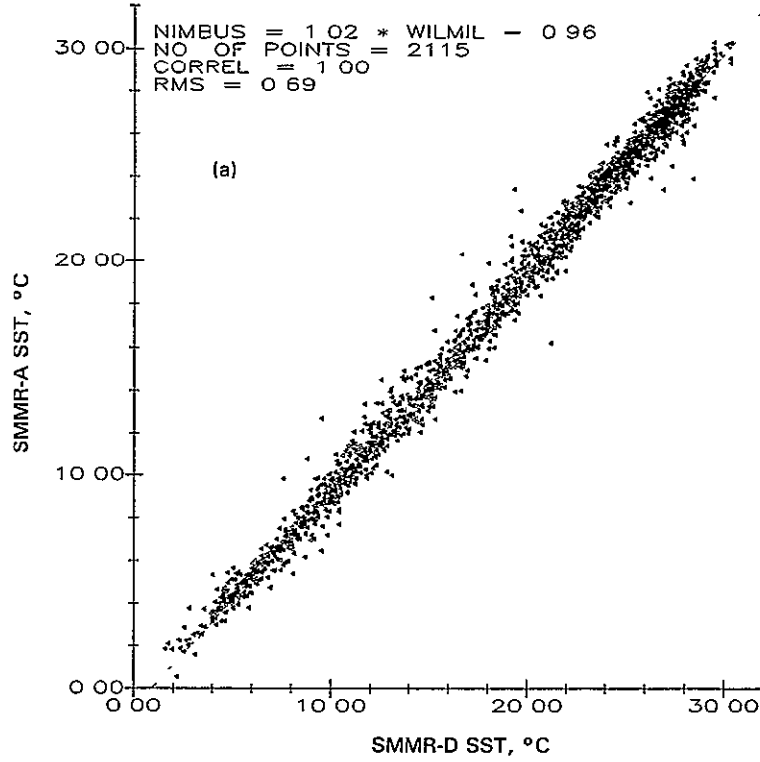


Figure 5-6. Scatterplots of data displayed in histograms of Figure 5-4: (a) SMMR-A versus SMMR-D (b) SMMR-D versus SMMR-C

SECTION VI

COMPARISON OF SATELLITE AND IN SITU DATA

R. Bernstein

A variety of data sets were available and analyzed for Workshop-I. The data sets discussed here are:

- (1) SMMR-A: The Nimbus Project data release.
- (2) SMMR-D: The revised SMMR version produced by Wilhelm and Milman.
- (3) SMMR-C: The SMMR version produced by Prabhakara
- (4) Fleet Numerical Oceanography Center (FNOC): The individual ship reports.
- (5) Reynolds Climatology.

Data from SMMR and FNOC ships were compared in three different ways:

- (1) The difference between individual ship and SMMR observations which were close in space and time.
- (2) The difference between the 2° lat-lon one-month averages for SMMR and ship, respectively.
- (3) The difference between the 2° averages and climatology, for both SMMR and ship.

A number of comments can be made, based on the data analysis performed so far. First, both SMMR-A and SMMR-D maps of SST visually appear to resemble climatology, and also resemble the SST maps produced by the ship data where it is sufficiently abundant in the 20°N to 60°N latitude range. In fact, from examination of gross statistics it may be argued that both SMMR data sets, when averaged over 2° lat-lon, and one month (referred to as "binned"), agree better with climatology than do the binned ship results. This may be seen in Figure 6-1 where all data sets are plotted against climatology between 55°S and 55°N. Note that the SMMR-A rms difference with respect to climatology is 1.36°C, the SMMR-D rms is 1.22°C, the SMMR-C runs is 1.92°C, and the ship rms is 1.81°C. It is apparent that most of the increase in the ship rms over that of SMMR-A and SMMR-D is the result of extreme outliers. The ship data is known to be notoriously noisy. Where sufficient ship data exist, for example in the 20°N to 40°N band, the monthly averages become more reliable, then Figure 6-2 shows that the rms difference between SMMR and ship averages is about 1.3°C.

The important point is that on larger space and time scales sea surface temperature rarely deviates from the climatological norm by more than 1 or 2°C. In view of the above rms differences, then, the only way to really compare the monthly SMMR and ship data is as departures from climatology. Such SST maps (based on ship data) have been used for many years by investigators of large-scale air-sea interaction. Figure 6-3 shows the monthly anomaly patterns for SMMR-A, -D, and ship data in the mid-latitude North Pacific where ship data is sufficiently abundant. Negative anomalies are shaded. Note that SMMR-A and -D resemble each other much more than they resemble the ship data. Of the two, SMMR-A perhaps is a little closer to resembling the ship map. These results suggest that if the actual anomaly patterns had been more intense, say 2 to 3°C, then there would have been a more pleasing correspondence. Yet 1°C is a typical intensity, and SMMR accuracies sufficient to map such features will be a requirement for the data to be useful in large-scale air-sea interaction studies.

Figure 6-4 shows a similar SST anomaly chart constructed by NOAA, using the Tiros-N AVHRR and HIRS/2 sensors. In this case, the interpolation procedure used to grid the data is one developed by NOAA and differs from the approach employed to create the panels of Figure 6-3. Also, the climatology used by NOAA was the NCAR climatology. Reynolds (Ref.8) has compared his climatology with the NCAR climatology and finds differences of 0.5°C in the mid-latitude North Pacific. It is also important to keep in mind that these NOAA data are from a period prior to the introduction of the AVHRR multi-channel processing procedures. Yet even with these discrepancies, there is substantial pattern correlation between the Tiros-N and FNOC maps. The large region of negative anomaly in the 40 to 50°N band, the warm anomalies extending east from Japan, west from California, and in the Gulf of Alaska, all are in reasonable agreement. When the individual Tiros-N SST estimates are binned and referenced against the Reynolds climatology, a more quantitative comparison can be made.

In the region of abundant ship data, for example 20°N to 60°N in the North Pacific, the difference map between binned ship and binned SMMR-A or SMMR-D data (Figure 6-5) on an absolute basis rarely exceeds 2°C. Over the map area, one of the major areas of disagreement occurs as one proceeds north of 40°N, where SMMR minus ship differences become increasingly more positive. The tendency for a temperature dependent bias has already been seen in Figure 6-2, for 20°N to 40°N, and becomes even more evident between 40°N and 60°N (Figure 6-6). Near 40°N in this month sea surface temperatures run around 7 to 10°C, thus according to Figure 6-6 the SMMR estimates should be about 2°C too warm. By inspection of Figure 6-3 we can see that a temperature-dependent correction of this type would substantially improve the agreement between the ship and SMMR anomaly patterns.

Previously unpublished work with the SMMR-A data set in the North Pacific, but for a different month, gave clear evidence of the same temperature-dependent bias. In that case, the ship data were first edited to remove erroneous reports deviating by more than 5°C from climatology and were mapped with a somewhat more involved procedure than simple binning. The same procedures were also applied to the SMMR data. Figure 6-7 gives the two SST

maps for the ship and SMMR, while Figure 6-8 crossplots the two map estimates, grid point by grid point. While the rms difference is 1.25°C , the scatter about a best fit line is only 0.67°C .

The source of the temperature-dependent bias is unknown but was noted earlier by Chester at the Jet Propulsion Laboratory while he was developing the Seasat SMMR data set, and that data set in fact had a correction then built into it. The Nimbus SMMR bias may be of the same unknown origin. Comparison of northern and southern hemisphere data will be essential to addressing the problem, but the southern data is already strongly affected by an instrument problem tied into the sun-satellite geometry (see discussion in Appendix A).

ORIGINAL PAGE IS
OF POOR QUALITY

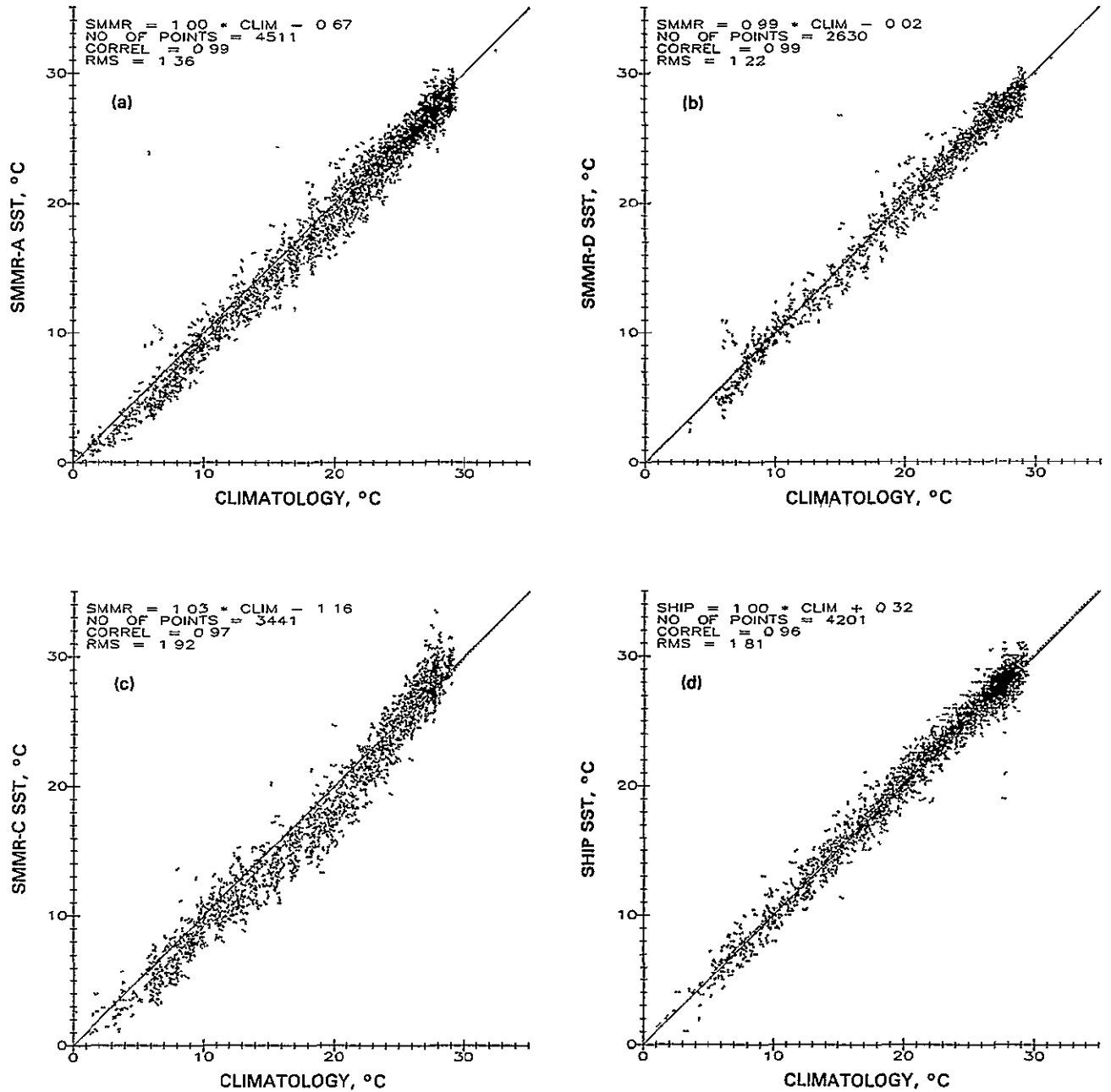
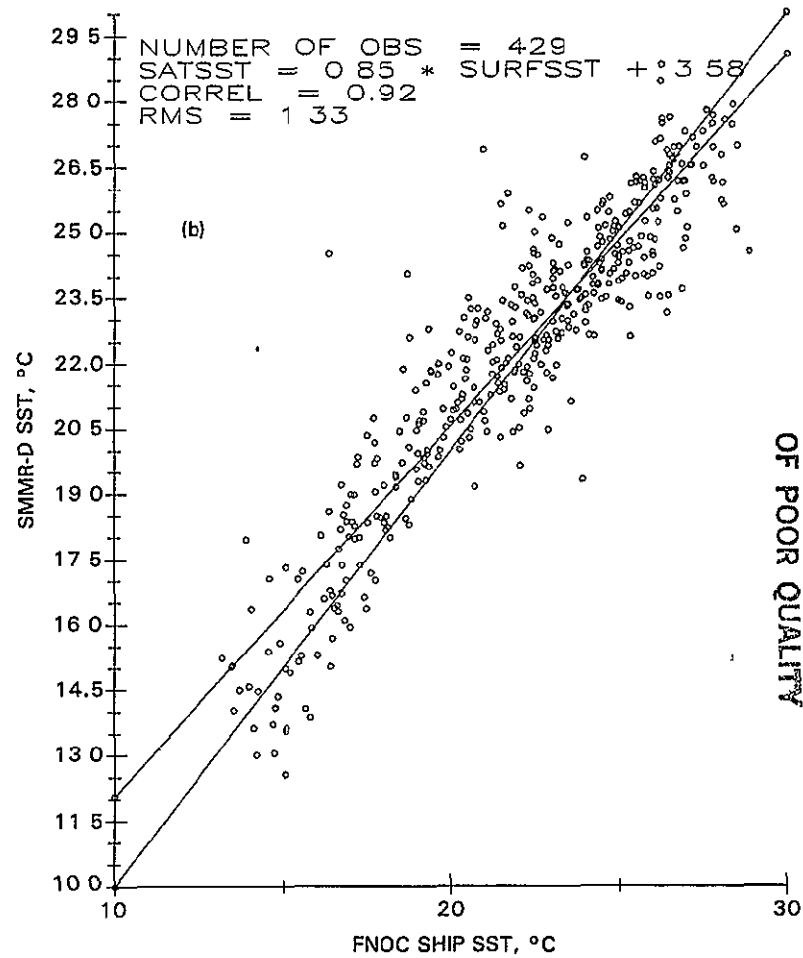
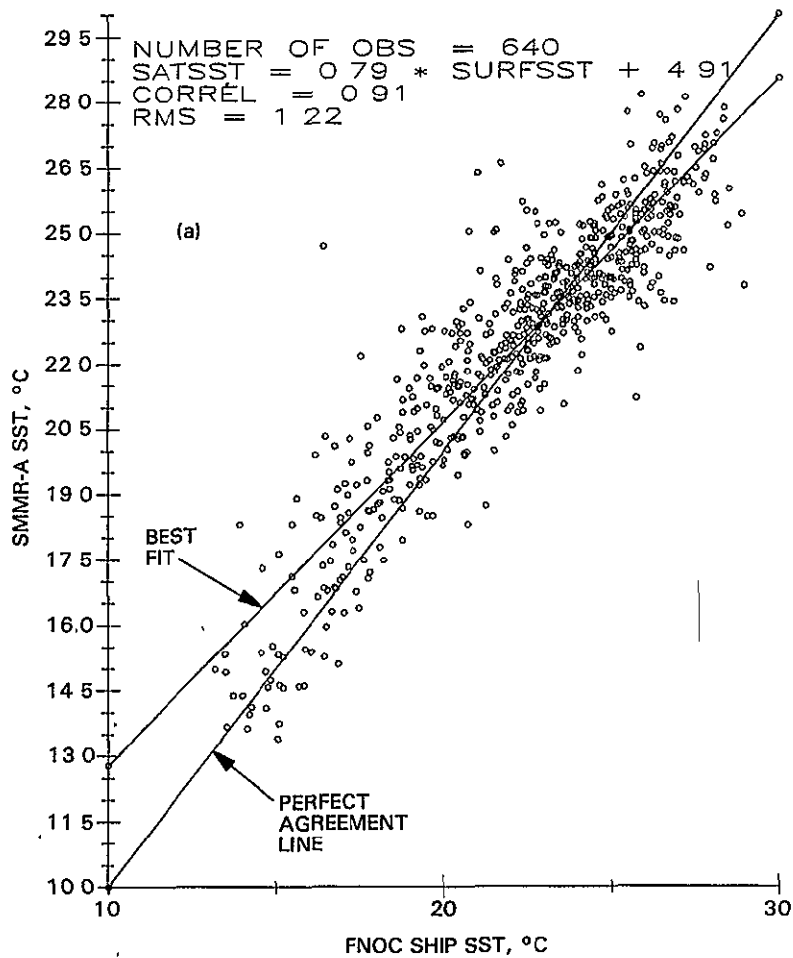


Figure 6-1. (a) Scatterplot of SMMR-A versus Reynolds Climatology for all binned average data in range 55°S to 55°N. (b) Same as (a) except for SMMR-D. (c) Same as (a) except for SMMR-C. (d) Same as (a) except for FNOC ship observations.



ORIGINAL PAGE IS
OF POOR QUALITY

Figure 6-2. Scatterplot of SMMR versus FNOC ship data for binned averages in the range 20°N to 40°N latitude (a) SMMR-A (b) SMMR-D

ORIGINAL PAGE IS
OF POOR QUALITY

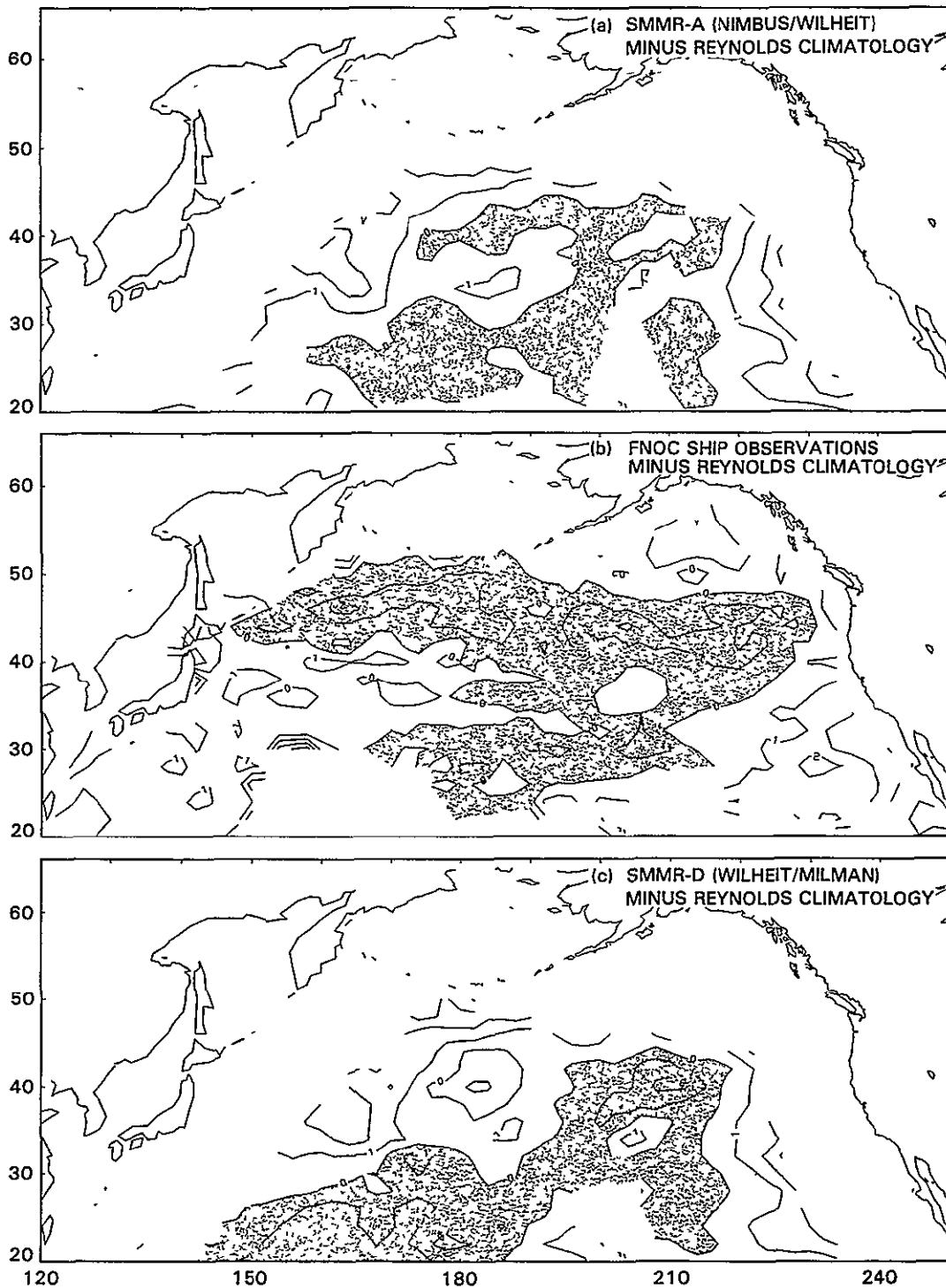
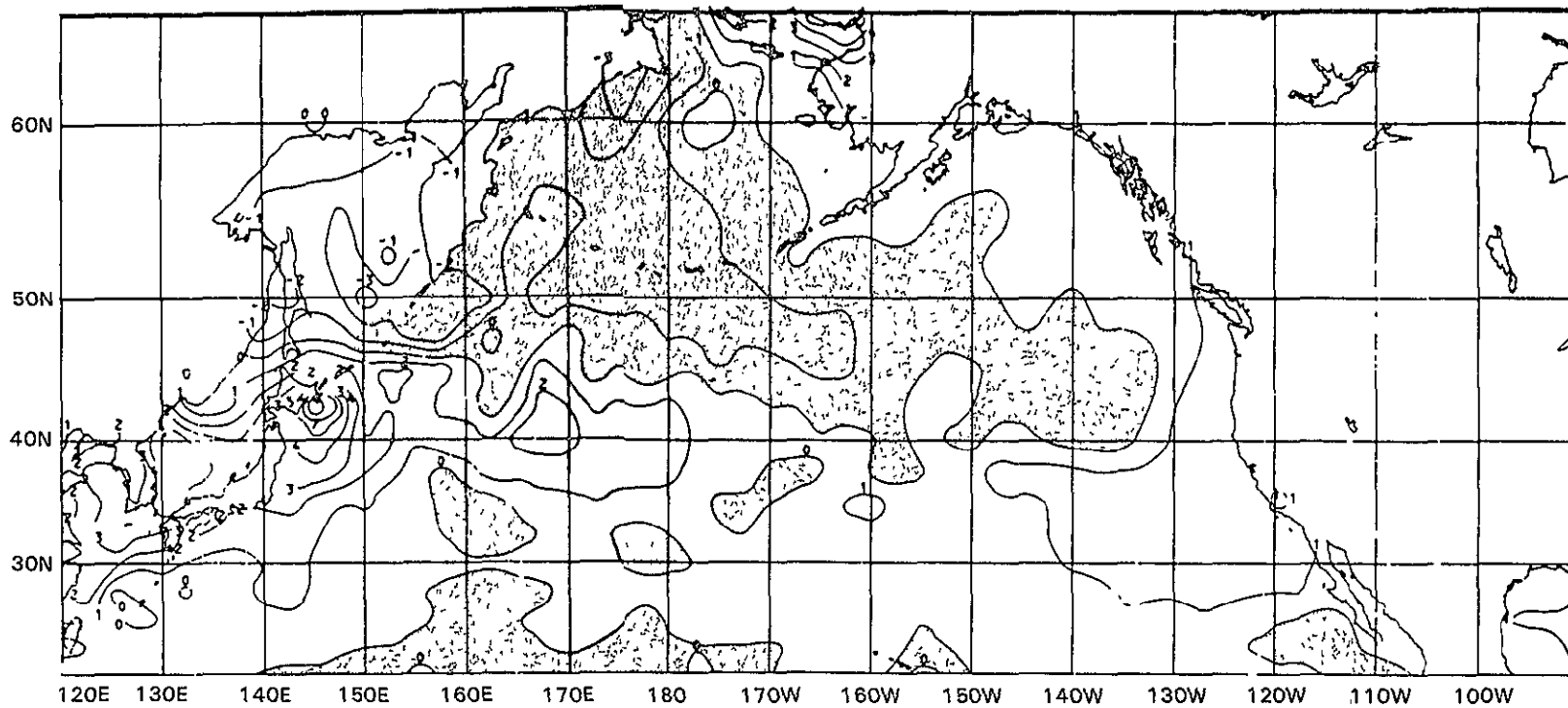


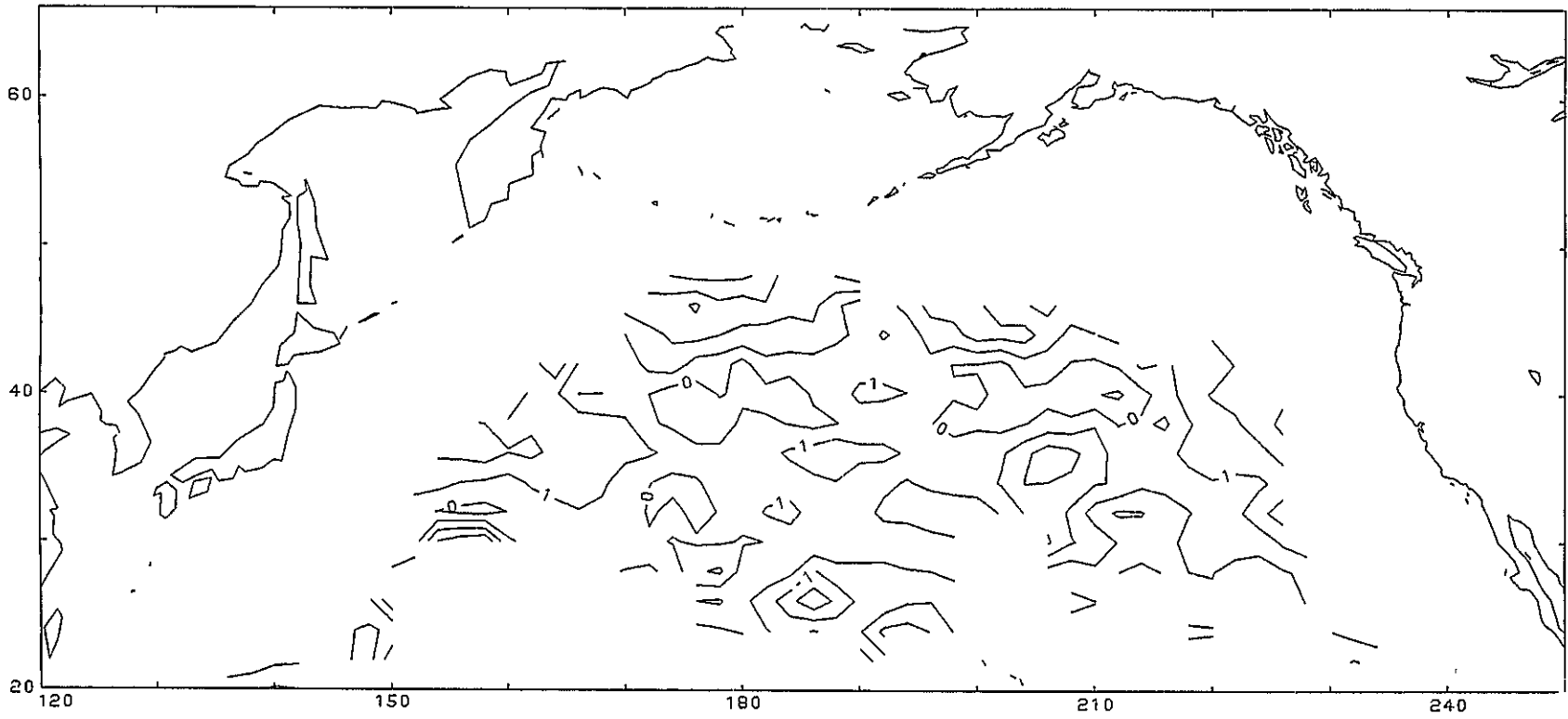
Figure 6-3. Differences between (a) SMMR-A, (b) FNOC, and (c) SMMR-D and Reynolds Climatology in mid-latitude North Pacific (negative differences are shaded)



ORIGINAL PAGE IS
OF POOR QUALITY

Figure 6-4. Difference between TIROS-N AVHRR and NCAR Climatology, November 1979

6-8



ORIGINAL PAGE IS
OF POOR QUALITY

Figure 6-5. Difference between SMMR-A and FNOC ship data in mid-latitude North Pacific

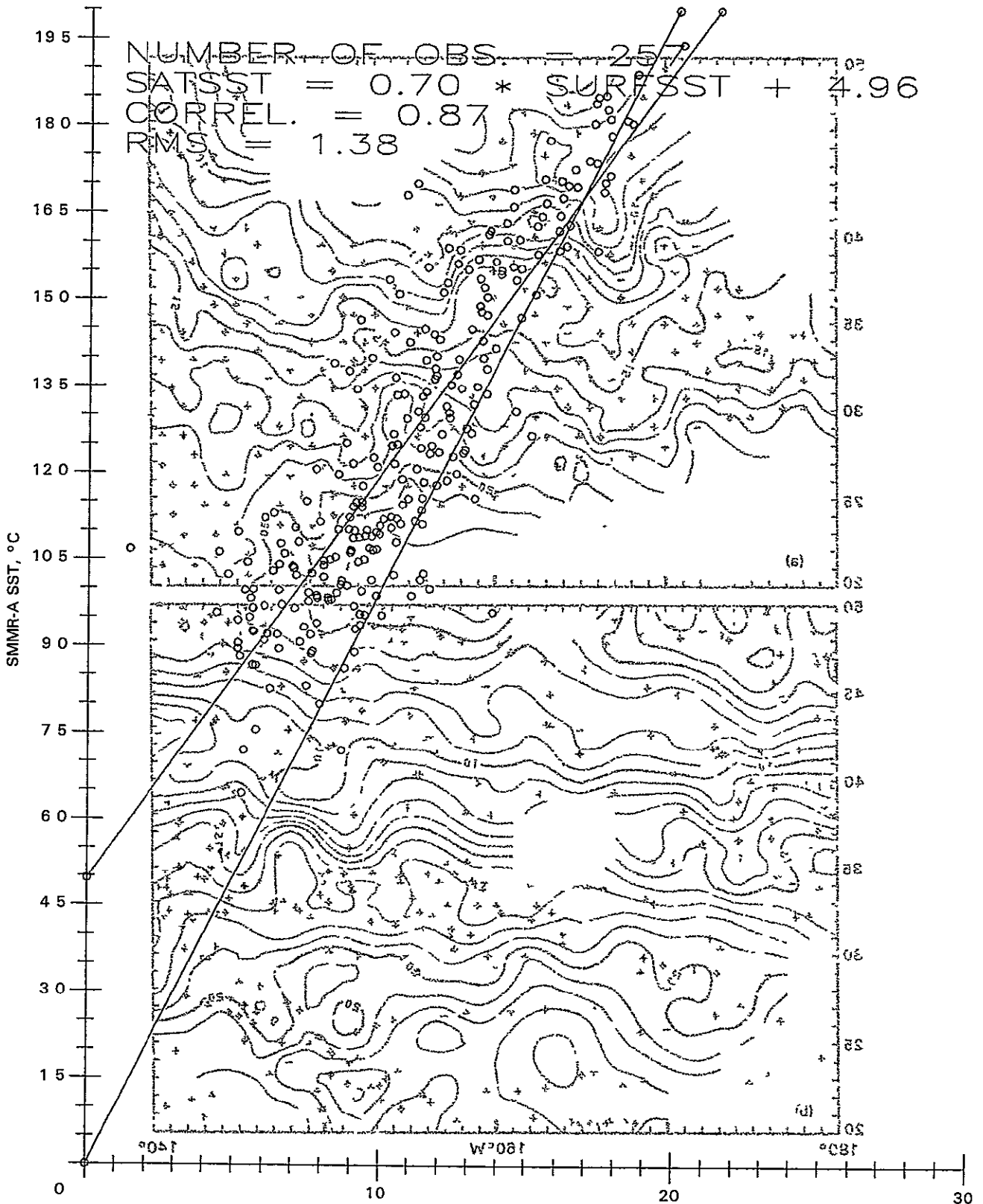


Figure 6-6. Scatterplot of SMMR-A versus FNOG ship data for binned averages in the range 40° to 60°N latitude (note temperature-dependent bias)

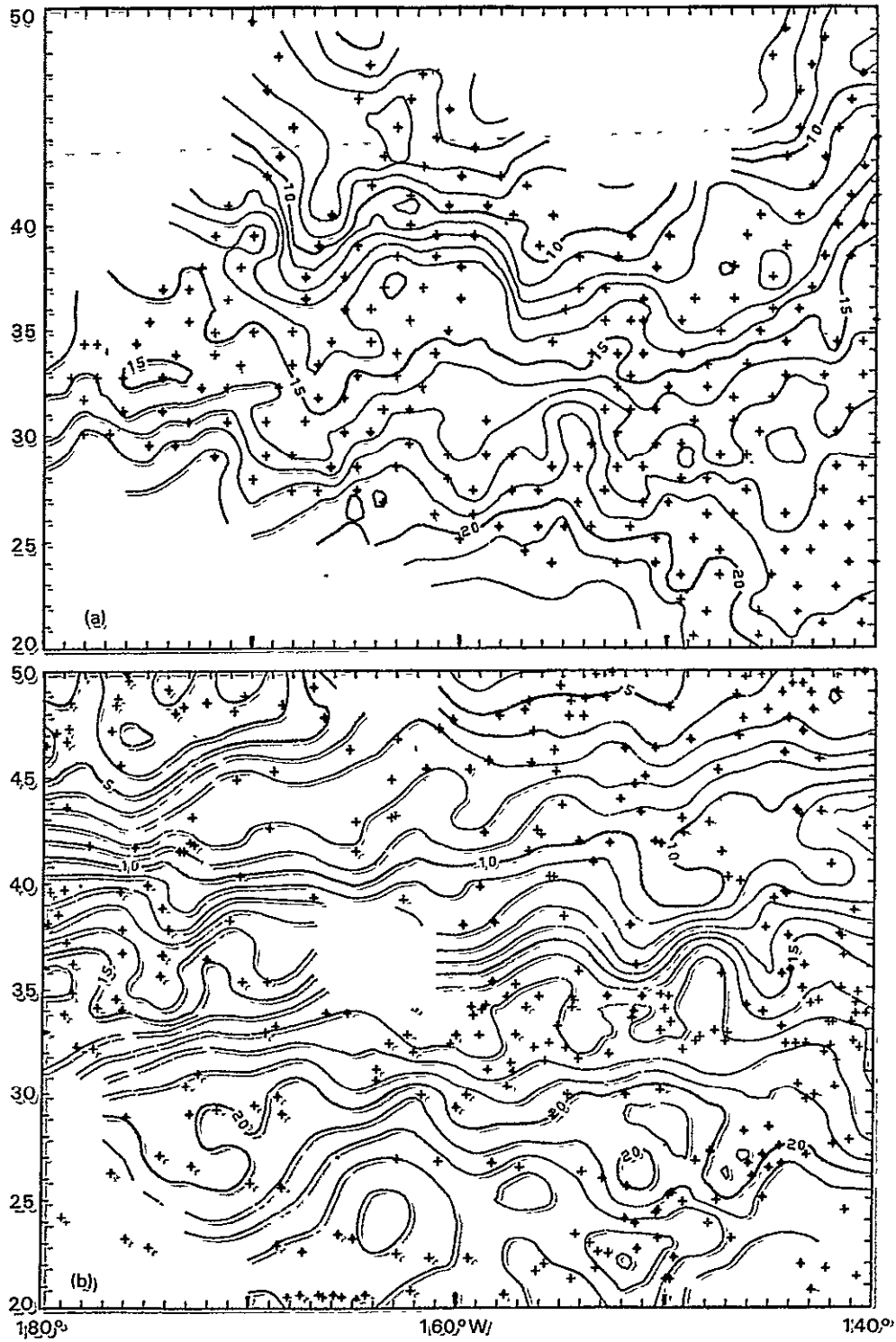
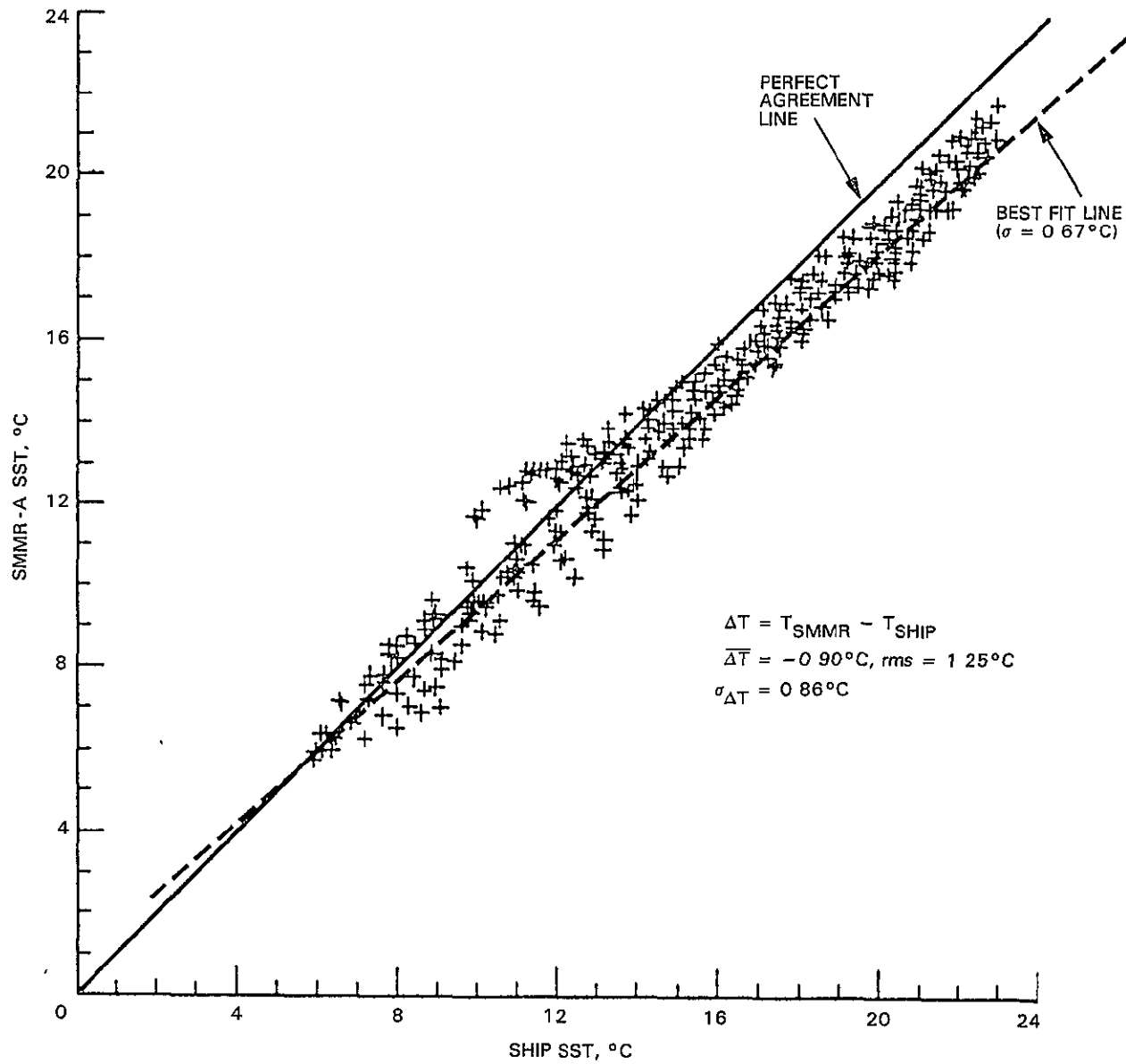


Figure 6-7. Distribution of (a) SMMR-A and (b) ship observations and SURFACE II mapping of data in Central North Pacific from February 15 to 19, 1979



ORIGINAL PAGE IS
OF POOR QUALITY

Figure 6-8. Scatterplot of SMMR-A ship data for the period February 15 to March 9, 1979, in central North Pacific. Statistics indicated in Figure (Source: Bernstein, unpublished).

SECTION VII

CONCLUSIONS AND RECOMMENDATIONS

During the first day and a half of Workshop-I, participants heard a variety of presentations on sensors and algorithms and had an opportunity to look through the package of satellite and in situ data displays provided for the workshop. Most of the second day was given over to discussion of recommendations for future comparisons. Because time available at the workshop was so limited, only rather general conclusions concerning data quality were drawn at the meeting. It was agreed that better comparisons could be made with more time to peruse the results, when improved analysis techniques were implemented, and when data from other sensors and in situ sources were available for study. This section of the report is a synthesis of contributions from several participants and a summary of recommendations arising out of the workshop discussions.

From the analyses performed thus far, it is clear that the ship data must be treated with great care in any satellite comparisons because of their high noise level. At the very least, the ship data should be screened to eliminate observations deviating unreasonably from climatology. In fact, a two-pass screening may be better, with the second pass screening out data deviating unreasonably from the first pass mapping attempt. Even with screening, the noise level is comparable with that of the satellite data and, particularly in spot comparisons, should not be used to evaluate the accuracy of the satellite data. Consideration also should be given to more sophisticated mapping procedures than simple binning-averaging. Procedures that attempt local least-squares fitting to individual observations would give better results because they would then be less sensitive to the spatial distribution of the data.

It is evident that the major satellite problems are systematic rather than random. This was observed to a marked degree in the presentation of SMMR data for this workshop. A wider geographic range of in situ data is needed for comparison purposes to identify better the systematic errors. The ship data used thus far are so noisy that they may only be used in the data-rich mid-latitude northern hemisphere. Research quality data from XBTs and drifting buoys must be included. For addressing the large systematic errors in the southern hemisphere with the SMMR, the FGGE drifting buoy network is of key importance. Because these buoy data were not available after November 1979, it is probably best to continue the examination of SMMR data for this month.

Several suggestions were made to enhance the quantitiveness and simplicity of future workshops. These have been grouped into the six following sub-headings.

1. Bounds on Data Products

It was recognized that 44 plots per sensor (the quantity of graphics generated for Workshop-I) is too much to assimilate. This would especially become a problem in future workshops where up to 10 sensor/

algorithm combinations may be represented. (The term "sensor" can refer to satellite, ship, or buoy measurements, and also climatological SST values). The revised list of primary data products, given at the end of this section, reduces the number from 44 to 11 plots per sensor. The capability for providing additional plots on demand will be maintained, however. It was agreed that emphasis in global comparisons would be placed on the spatially and temporally averaged fields. The time and space averages used in Workshop-I would be continued, i.e. binned monthly averages over 2° latitude-longitude regions. Since much of the in situ data are noisy, spot comparisons of raw (i.e., un-binned) satellite versus in situ data will be considered of secondary importance and restricted to the higher quality data available from buoys and XBTs. Spot comparisons will become more important when evaluating the VAS sensor, which has limited global coverage.

2. Reference and Difference Fields

On a global basis, SST departures from climatology are more meaningful quantities for evaluation than the SSTs themselves. The recently published Reynolds Climatology was decided upon as the "reference" against which all other sensors would be compared. Obviously, differences between sensor-derived SST and climatology are not necessarily indicative of errors in the sensor because these differences may be due to deviations of the true SST from climatology. However, deviations of each sensor from climatology can be compared with each other to indicate differences between the sensors. There are two primary motivations for this procedure. First, although observed temperatures in the ocean range from approximately -2 to 32°C , deviations of SST from climatology rarely exceed 3°C anywhere in the oceans. We expect the remote sensors to measure SST with an error of less than a degree. Clearly the dynamic range of SST is much greater than the measurement error and scatterplot comparisons of SST measured by different sensors always appear "good." By subtracting the climatological SST from a sensor SST measurement, the global dynamic range of "anomalous" SST is reduced by a factor of 3 to 5, and problem areas in SST retrieval become much more apparent in scatterplots and contour maps.

A second and perhaps more important motivation for the use of anomalies is that SST can vary in some regions of the ocean by 2 to 3°C across 2° of latitude. Because of these strong gradients, non-uniform sensor samplings of a particular 2° lat-lon square can result in a bias of the monthly average for that 2° region. The following example illustrates this point. Consider the case where the true SST in a particular 2° lat-lon square is equal to the climatological value for that square. Suppose the satellite sampled the 2° square only at the northeastern corner over the one-month averaging period. Suppose further that the climatological SST in this corner is 1.5°C colder than the climatological SST averaged over the entire 2° lat-lon region. Then, even if the sensor measured temperature perfectly, the difference between the sensor 2° lat-lon "average" SST and climatology would be 1.5°C , which might be carelessly interpreted as an error in the sensor measurement. If the sensor samples all 2° squares uniformly, this problem does not arise. However, in the more general case, this apparent error could erroneously influence the performance evaluation of the sensor.

A simple way around this problem is to compute the deviation from climatology for any particular SST observation prior to forming the 2° lat-lon averages. Davis (Ref. 13) has shown that year-to-year variations in anomalous SST (deviations from climatology) have much larger spatial scales than the climatological SST itself. Thus, if the deviation from climatology for any particular SST observation is computed prior to forming the 2° lat-lon averages they will then be more representative of actual anomalous conditions over the 2° region. In this way the requirement of uniform spatial sampling of the 2° lat-lon squares can be relaxed when analyzing anomalies.

Thus, for future SST workshops, the raw sensor SSTs provided by the various investigators will be converted to anomalous SSTs in the following manner. For each raw observation, the climatological SST will be interpolated in time and space to the lat-lon coordinates of the observation using simple bi-linear interpolation between the nearest four 1° lat-lon gridded climatology values. This interpolated climatological SST will then be subtracted from the observed value to form the anomaly. The resulting raw anomalies will then be averaged over all 2° lat-lon bins to form global maps of anomalous SST.

3. Data Editing Standardization

Much thought was given to standardized editing procedures to enable objective comparisons of the data sets. As a starting point, investigators will be asked to submit to JPL their raw SST retrievals for a given month, having been subjected only to "sensor-unique" filters. These filters are allowed to reject data for specific cases in which the retrieval techniques are known to fail, (e.g., clouds for IR, rain for SMMR, etc.). The only requirement is that these filters must be objective, and they must be clearly spelled out at workshops. A preliminary list of rejection criteria for each sensor is provided in Table 7-1.

Upon submittal to JPL, data from each sensor will be subjected to exactly the same methods of anomaly calculation, further data editing, and binning. Investigators themselves should not filter "bad" data (other than allowed in Table 7-1) in the products delivered to JPL. Further editing at JPL will exclude from the binned averages all raw sensor SST observations differing from climatology by more than 5.5°C. The requirement that investigators provide all data allows a uniform determination at JPL of the percentage of "bad" data retrievals for each sensor, a quantity that may be of interest for operational applications. It was recognized that a climatology filter may tend to bias retrievals slightly towards the climatology, and if set too low could erroneously "clip" retrievals in regions of high SST anomaly. On consideration of experience with ship data, 5°C was judged a sufficiently wide filter, and 5.5°C was chosen for compatibility with the graphics products contour levels.¹

Investigators are responsible for filtering land-contaminated observations from their data using any method they desire. However, JPL will provide a 600-km "shadow" land mask, equivalent to that used by Wilhelm/Milman, at the request of investigators.

¹When observing "El Nino" months of 1982, etc., this filter may need to be widened

Table 7-1. Rejection Criteria for Satellite Data

Satellite Data	Rejection Criteria
AVHRR	Cloud and aerosols Data within 50 km of land
SMMR	Rain Daytime data (sensor heating, sun glint) Data within 600 km of land End cells of swath (polarization correction anomaly) Internal algorithm consistency check (data transmission errors, gain shifts)
HIRS/MSU	Cloud overcast Data within 60 km of land Internal algorithm check (non-convergent solution)
VAS	Cloud and aerosols Nighttime data (difficulty with cloud filter) Data within 50 km of land

Investigators are allowed to use climatology in adjustment of their retrieval algorithm coefficients if they so desire. It is understood, however, that global-scale statistics only should be used. Detailed regional tuning to climatology will obviously produce a zero anomaly map and useless sensor data set. It is preferred that investigators not use any in situ data in algorithm tuning, if at all possible. It is recognized that all sensors need some in situ data for final algorithm adjustment and calibration, but the data and technique used should be clearly spelled out at the workshops.

4. Graphics Display Products

An opinion shared among the workshop participants was that some aspects of the Pilot Ocean Data System (PODS) graphics displays could be improved in several ways:

- (1) The scatterplot and histogram routines should be rewritten to handle user-specified maxima and minima on both the ordinate and the abscissa, rather than using only self-scaling. This will result in all plots having common scaling, which greatly simplifies mental assimilation of the results and intercomparisons.
- (2) More mnemonic labelling of all plots would greatly simplify and speed interpretation of the data.
- (3) Regression information on the scatterplots is of little value. The scatterplot data should be plotted only with the

perfect fit line and with printed statistical information consisting of bias, standard deviation, and correlation.

- (4) Capabilities of gray-shade maps should be developed as an alternative to contour maps. This type of display enables a more rapid assimilation of the data characteristics because the human eye is able to integrate or filter gray shades much more effectively than contours.

5. June Workshop Products

It was decided that the next workshop (Workshop-II, to be held in June, 1983) would use December 1981 as the primary month for study. (This was in accordance with the sequence November 1979, December 1981, and July 1982, agreed to at the first workshop planning meeting). The addition of March 1982 was discussed and adopted for study (along with July 1982) at a workshop subsequent to June 1983 (Workshop-III). The motivation for including March 1982 was that it is the only month for which VAS data are available without probable contamination by the eruption of El Chichón. It was mentioned also that AVHRR channel 3 had begun to degrade slightly by July 1982. By including March as well as July 1982 all infrared sensors will be evaluated in both favorable and unfavorable environmental conditions.

For Workshop-II, SST data for December 1981 were required for delivery to JPL by April 30, 1983. This date was set in order that the Primary Analysis Techniques (see below) could be implemented in time for products to be mailed to investigators for perusal and feedback prior to Workshop-II.

The SST data received at JPL will be subjected to the following analysis techniques on a first-come-first-served basis:

- (1) Primary Analysis Techniques
 - (a) Raw SST observations will be converted to raw anomaly observations using the method described previously. The anomaly values will be written to a disk file together with the interpolated climatological SST value at the observation location.
 - (b) Raw anomaly observations will be binned into 2° lat-lon monthly averages centered at odd latitudes and longitudes.
 - (c) "Absolute" SST will be computed by adding the 2° binned anomaly SST values to the climatological average SST for the center of each particular 2° lat-lon region.
 - (d) A global contour map of 2° binned "absolute" SST will be generated (1 plot).
 - (e) A global gray shade map of 2° binned anomaly SST will be generated (1 plot).

- (f) A global histogram of raw anomaly SST observations will be generated. These histograms will be labelled with statistical information consisting of mean value, standard deviation about the mean value and total number of observations in histogram (1 plot).
- (g) Global and 20° latitude band scatter plots of 2° binned anomaly SST versus Reynolds climatological SST will be generated. These scatter plots will be labelled with statistical information consisting of bias, standard deviation about the bias, correlation and the total number of 2° lat/lon values in the scatter plot (7 plots).
- (h) A global gray shade map of 2° binned anomaly SST data density will be generated with gray shades corresponding to varying numbers of raw observations per 2° lat-lon region (1 plot).

When all sensor data is received, two additional analysis capabilities will be implemented:

- (i) A table of cross correlations between 2° binned anomaly SST from all sensors will be generated. Statistical information included in the table for each sensor pair consists of correlation, mean difference (bias), standard deviation about the bias and the number of 2° lat-lon values included in the statistics (1 table).
- (j) Tables of three-way partitioning of sensor measurement error will be generated for all possible sensor triplets (see Appendix G for description of method) (1 table per sensor).

In addition to the Primary Analysis Techniques described above, the following secondary capabilities will be made available to investigators on request for any specified geographical region:

(2) Secondary Analysis Techniques

- (a) Regional contour maps of 2° binned "absolute" SST.
- (b) Regional gray shade maps of 2° binned anomaly SST.
- (c) Regional histograms of raw anomaly SST.
- (d) Regional scatter plots of 2° binned anomaly SST versus Reynolds climatological SST.
- (e) Regional gray shade maps of 2° binned anomaly SST data density.
- (f) Regional histograms of the number of raw observations per 2° lat-lon region.

- (g) Regional maps of raw data locations (plotted with a dot at latitude and longitude coordinates of observations).
- (h) Regional gray shade maps of the difference between 2° binned anomaly SST for any pair of sensors.
- (i) Regional scatter plots of 2° binned anomaly SST by one sensor versus 2° binned anomaly SST by another sensor. These plots will be labelled with statistical information consisting of mean difference (bias), standard deviation about the bias, correlation and the number of 2° values in the scatter plot.
- (j) Regional scatter plots of 2° binned anomaly SST differences between any pair of sensors versus the number of raw observations per 2° lat-lon region for either of the sensors.
- (k) Regional scatter plots of raw anomaly SST versus interpolated climatology. (This is the same capability as 4 above except it is implemented on raw rather than 2° binned data.)
- (l) Regional scatter plots of raw anomaly SST by one sensor versus raw anomaly SST by another sensor within any specified time and space separation.

Finally, two additional analysis techniques are being explored for implementation in future workshops. These include objective analysis of the data sets in the method summarized by Gandin (Ref. 11) and statistical comparison of the various 2° binned anomaly SST data sets using the method summarized by Preisendorfer and Barnett (Ref. 14). The Preisendorfer and Barnett method involves essentially the same computations as those described above (the mean difference and standard deviation). The virtue of their method is that it provides an estimate of the statistical significance of the bias and standard deviation. That is, it investigates the question of whether or not differences between two sensor data sets are statistically significant. Implementation of these last two methods may not be ready in time for Workshop-II.

6. General Approach

Participants generally felt that Workshop-I had been productive in terms of understanding the characteristics of the different data sets and agreeing upon specific ways to evaluate them. This was seen, however, as only the beginning of a difficult process, since quantitative accuracy determinations must take into account many factors and require intensive examination of the data. At least one workshop subsequent to June 1983 will be required, with much work in between, to complete analysis of the four months of data in question. In addition, the workshops should not lose sight of the wider issue of recommendations to be made once the present sensors have been evaluated.

It is perhaps not premature even now to begin thinking of future sensors or techniques that combine the merits of existing methods and include new improvements in technology. Several interesting ideas are being developed along these lines, such as more numerous and modified IR channels, dual looks from two polar-orbiting satellites, dual looks from a polar-orbiting and geostationary satellite, dual looks from the same instrument on a polar-orbiting satellite, combined microwave and infrared sensors, and perhaps other ideas also. In part to attract discussion on some of these new ideas, and to supplement the global SST comparisons with high-resolution regional IR studies, future workshops will include a day of symposium-type presentations. These will be announced as interest dictates.

omit to
P. A-1

REFERENCES

1. McClain, P., Pichel, W., and Strong, A., "Ocean Surface Temperatures from Space - A Multispectral Approach," submitted to Science, 1983.
2. Susskind, J., Rosenfeld, J., Reuter, D., and Chahine, M., "The GLAS Physical Inversion Method for Analysis of HIRS/MSU Sounding Data," NASA Technical Memorandum No. 84936, Goddard Space Flight Center, Greenbelt, Maryland 20771, 1982.
3. Njoku, E., and Swanson, L., "Global Measurements of Sea Surface Temperature, Wind Speed, and Atmospheric Water Content from Satellite Microwave Radiometry," submitted to Monthly Weather Review, 1983.
4. Reynolds, R., A Monthly Averaged Climatology of Sea Surface Temperature, NOAA Technical Report NWS 31, Silver Spring, Maryland, 1982.
5. U.S. Navy Marine Atlas of the World, IX, NAVAIR 50-1C-65, Washington, D.C., 1981.
6. Tabata, S., "An Evaluation of the Quality of Sea Surface Temperatures and Salinities Measured at Station P and line P in the Northwest Pacific Ocean, J. Phys. Oceanog., Vol. 8, pp. 970-986, 1982.
7. Tabata, S., Comparison of Observations of Sea Surface Temperatures at Ocean Station P and NOAA Buoy Stations and Those Made by Merchant Ships Traveling in Their Vicinities in the Northeast Pacific Ocean, J. Appl. Meteorol., Vol. 17, pp. 374-385, 1982.
8. Reynolds, R., "A Comparison of Sea Surface Temperature Climatologies," J. Clim. Appl. Meteorol. (accepted), 1983.
9. Keeley, J., and Taylor, J., Data Products from the First GARP Global Experiment, Marine Science and Information Directorate Manuscript Report No. 57, Department of Fisheries and Oceans, Ottawa, Canada, 1981.
10. White, W. and Bernstein, R. "Design of an Oceanographic Network in the Mid-Latitude North Pacific, J. Phys. Oceanog., Vol. 9, pp. 592-606, 1979.
11. Gandin, L.S., "Objective Analysis of Meteorological Fields," Israeli Program for Scientific Translations, IPST 1373, Jerusalem, 1965. (U.S. Dept. of Commerce Publication #TT65-50007, Springfield, VA).
12. Wilheit, T., and Chang, A., "An Algorithm for Retrieval of Ocean Surface and Atmospheric Parameters from the Observations of the Scanning Multi-channel Microwave Radiometer," Radio Science, Vol. 15, pp. 525-544, 1980.
13. Davis, R.E., "Predictability of Sea Surface Temperature and Sea Level Pressure Anomalies over the North Pacific Ocean," J. Phys. Oceanog., Vol. 6, pp. 249-266, 1976.
14. Preisendorfer, R.W., and Barnett, T.P., "Numerical Model/Reality Intercomparison Tests Using Small-Sample Statistics," J. Atm. Sci. (in press), 1983.

APPENDIX A

SEA SURFACE TEMPERATURES FROM THE NIMBUS-7
SCANNING MULTICHANNEL MICROWAVE
RADIOMETER

SEA SURFACE TEMPERATURES FROM THE NIMBUS-7 SCANNING
MULTICHANNEL MICROWAVE RADIOMETER

A. Milman and T. Wilheit

A. INTRODUCTION

This report describes how the algorithm was developed to determine sea surface temperature (SST) from the Nimbus-7 Scanning Multichannel Microwave Radiometer (SMMR) data. The SST algorithm has evolved over the last several years; this report describes the final version that will be applied to the 1979 SMMR data (more tuning may be needed for later data). Four different stages in the development are reported here (they are called Versions I to IV); each version has evolved out of its predecessor either because newly processed data became available or because significant problems were uncovered in earlier versions.

What herein are called Version III and Version IV were submitted to the SST Workshop-I (Jet Propulsion Laboratory, January 17-18, 1983), and were called SMMR-I and SMMR-II in that workshop. (Note that these are now referred to as SMMR-A and SMMR-D, respectively, in the main body of this report.) Version IV (SMMR-II) produces better SSTs than Version III (SMMR-I) and was meant to supersede it.

The data presented in this report have all been screened so that they refer to positions at least 600 km from large land masses. Because of the side lobes of the SMMR antenna, SSTs are systematically very wrong closer to land than that, even after an antenna pattern correction is applied (as it was with these data). In addition, data from the end positions of the scan (cells 1 and 5) were not used. Data were also rejected if the C-band polarization ratio $(V - H)/(V + H)$ was not in the range of 0.245 to 0.28.

B. DEVELOPMENT OF THE SEA SURFACE TEMPERATURE ALGORITHMS

1. Version I

The SST algorithm for the Nimbus-7 SMMR has undergone a process of development over the last several years. The original version (Version I) was derived from an ensemble of models of brightness temperature over the ocean (Ref. 1). The SST algorithm is affected by the calibration constants used to derive the SMMR antenna temperatures; the Version I algorithm was used in conjunction with pre-launch calibration constants that were determined from thermal-vacuum test data by regression analysis.

The result of comparing SSTs from Version I with ship data was that there was a large (about 20°C) bias in the SMMR SSTs, and there was a large variance with respect to the ship measurements.

2. Version II

Improvements were made to the SST algorithm to produce Version II. The ensemble of models used to derive the algorithm was modified to allow some correlation between SST and the amount of atmospheric liquid water (with a correlation coefficient $r^2 \approx 0.5$). This stabilized the algorithm by removing some combinations of SST and water vapor column density that cannot occur in nature. The SST algorithm was used with an improved calibration algorithm for the antenna temperatures that takes into account losses in the SMMR instrument.

In addition, an empirically-derived filter was used to screen out raining or otherwise contaminated data. The SST algorithm performance up to this point is described in Ref. 2.

No quantitative use was made of ground truth in deriving Version II, except for one degree of freedom to correct for an overall bias in the SST.

The Version II algorithm, then, was as follows:

Let

$$\begin{aligned} T'' = & 1.7 V_{6.6} - 0.37 H_{6.6} \\ & + 56 (285 - H_{10.7}) / (285 - V_{10.7}) \\ & - 245 (285 - H_{18}) / (285 - V_{18}) \\ & - 326 \ln(280 - V_{18}) \\ & + 370 \ln(280 - H_{18}) - 11 \ln(280 - H_{21}) \\ & - 3 \theta_i - 73.15, \end{aligned} \tag{1}$$

where V and H refer to the vertically and horizontally polarized components of the brightness temperature, and the subscripts refer to the frequency in GHz; θ_i is the incidence angle. The coefficients used to calculate T'' were determined by regression from the ensemble of models.

Next, a correction is applied for the change in emissivity with temperature:

$$T' = T'' - 1.34 - 0.2(7.5 - T''(1 - 0.025T'')). \tag{2}$$

Equations (1) and (2) are the Version II algorithm. When the results were compared with climatology, it was found that there were several kinds of systematic errors. The later versions of the SST algorithm (Versions III and IV) add corrections to T' to get rid of the systematic errors.

Figure A-1 shows the result of using the Version II algorithm for the year 1979, for the center cell only. The SMMR SSTs were calculated for each location and time that SMMR observed the ocean, and the climatological value of SST for that location and time was subtracted; call this difference between the SMMR measurement and climatology $\delta T'$ (since Version II was used). For each day, the values of $\delta T'$ were averaged over all longitudes; the vertical and horizontal axes in Figure A-1 are latitude and day of the year. Plotting the data in this way allows us to look at one year's worth of data on one page.

Since the diurnal change in SST is very small (about 0.5°C or less), systematic differences between the daytime and nighttime data (Nimbus-7 is in a near-polar, sun-synchronous orbit) must be due to changes in the SMMR instrument caused by different heating of the components. Figure A-1 shows the difference between the day and night SSTs; note particularly the arc of high SSTs in the southern hemisphere that reaches up to 20°S about day 180. Figure A-2 shows the nighttime SSTs; therefore, the arc of high SSTs in Figure A-1 is due to SMMR overestimating the SSTs in the daytime. Figure A-3 shows the temperature of the antenna feed horn for the daytime; it seems clear that the arc of high SSTs in Figure A-1 is due to failure to correct properly for the heating of the antenna feed horn.

Additional problems with the Version II SSTs are that, in the northern hemisphere, the SSTs are too high (by 2°C) in the fall and winter and are too low (by 3°C) in the spring and summer.

Because of the large footprint of the SMMR antenna (about 150 km at 6.6 GHz), we would expect that variations of the true SST from climatology will be small; the next sections of this report describe the effort to tune the SST algorithm to get rid of the 2 to 3°C differences between the SMMR SSTs and climatology.

3. Version III

Versions III and IV of the SST algorithm represent slightly different corrections to the Version II algorithm that produces T' (Equations 1 and 2). The corrections are in the form

$$T = T' + \sum a_i p_i \quad (3)$$

where the a_i are constants and the p_i are parameters that may be measured antenna temperatures, instrument temperatures, other instrument parameters, or incidence angle. In every case, the coefficients a_i were found by regression to minimize the difference between SST and climatology. (Note that no surface data from 1979 were used to derive the corrections; only climatology was used).

The choice of which parameters could be used was a difficult one, as was the choice of how many different sets of coefficients should be used for different time periods, or for day and night, and so forth. For example, the use of a quadratic function of latitude in the correction was tried. The result was, that since SST depends strongly on latitude, about 60% of the variance of the SST could be explained without using the SMMR data at all. Including latitude as an independent parameter resulted in a correction to the Version II algorithm that gave little weight to the SMMR antenna temperatures. This clearly was not a satisfactory algorithm for SST. We therefore limited ourselves to using parameters for which it is physically reasonable to expect a meaningful correction.

The Version III algorithm, then, works as follows: a correction to the Version II algorithm was created that uses the following parameters:

$$\begin{aligned}
k_{iii} = & -0.09815 (V + H)_{10.7} + 0.01246 (V - H)_{10.7} \\
& -0.20162 (V - H)_{18} + 13.36 + \\
& \begin{pmatrix} 9.16 \\ -1.20 \end{pmatrix} t_1 + \begin{pmatrix} -11.0 \\ 1.51 \end{pmatrix} t_2 + \begin{pmatrix} 2.45 \\ 0.23 \end{pmatrix} t_3 - \begin{pmatrix} 0.80 \\ 0.83 \end{pmatrix} \theta_i \quad (4)
\end{aligned}$$

where k_{iii} is the correction to be added to T' ; the upper (lower) set of coefficients is applied to nighttime (daytime) data; t_1 to t_3 are the temperatures of the X-band ferrite switch, the K-band ferrite switch, and the C and X calibration horn. A plot of the results of the Version III algorithm ($\delta T_{iii} = T' + k_{iii} - T_{cli}$) is shown in Figure A-4. Figure A-4 shows the day-night difference in SST; Figure A-5 shows the nighttime SST. Note that the error in the nighttime SSTs in the northern hemisphere has been reduced considerably and that the effects of the heating of the antenna horn have been reduced.

4. Version IV

Version IV of the SST algorithm uses a different correction to the Version II algorithm than the one described above. Version III was meant to apply to all of the SMMR data from December, 1978 through December 1979. To create Version IV, it was decided to break the data into several time periods and to use nine instrument variables (eight temperatures and the C-band crystal current) instead of three. The coefficients of the antenna temperatures were derived first and apply to all of the data, day and night, and all times; they are virtually the same as those found for Version III.

$$k_{iv} = -0.0968 (V + H)_{10.7} - 0.1974 (V - H)_{18} + f(\{t_i\}), \quad (5)$$

where f is a linear function of the instrument variables $\{t_i\}$. The coefficients of these instrument variables are different for day and night and

different for different time periods; the time periods are shown in Table A-1, along with the reasons for changing the coefficients. The reasons for adopting the last two time intervals were that an algorithm was needed for this workshop (hence one period ends in November 1979) and that the data after December 1979 are not yet available for analysis.

Figures A-6 and A-7 show the SSTs from Version IV; Figure A-6 shows the day-night difference, and Figure A-7 shows the nighttime SST-climatology difference. Comparison between Versions III and IV shows that the Version-IV algorithm works better than the Version-III algorithm, especially for the northern hemisphere spring and summer months.

Figure A-8, A-9, and A-10 are comparisons between SMMR and climate, ship and climate, and between SMMR and ship data, respectively; for these comparisons, SMMR data are compared with surface reports that are within about 75 km and 24 h of a given SMMR observation. About 18,700 coincidences were found for 1979. The surface measurements were rejected if they were more than 5°C different from climatology. The SST algorithm (Version IV) works over the range from 0 to 32°C, and comparison among the three figures suggests that the SMMR SSTs are at least as good as the surface measurements.

Table A-1. Time Periods for Version IV Coefficients

Time Period	Reason for Changing Coefficients
December 1978 - January 1979	-----
February 1979 - March 1979	Instrument Change
April 1979 - September 1979	Seasonal Change
October 1979 - November 1979	Seasonal Change
October 1979 - December 1979	Workshop Requirements

C. PROBLEMS WITH THE SCANNING MULTICHANNEL MICROWAVE RADIOMETER INSTRUMENT

There are three aspects of the SMMR as it was designed and flown on Nimbus-7 that cause problems with interpretation of the data. A considerable effort has gone into correcting for instrument errors in the data. These design aspects are discussed briefly below. A microwave instrument that corrected these problems in design would provide much better data than the current SMMR instrument.

1. For each of the four lowest frequencies, one radiometer is switched to measure the V and H polarizations alternately. This scheme increases the complexity of the hardware, provides extra pathways for leakage effects, and makes it harder to interpret the data. In particular, the leakages between antenna ports contribute to a rotation of the polarization vector that adds an offset, which may be variable, to the scan angle. (This is discussed further in the next paragraph.)

2. In order to conserve space, the SMMR instrument was designed so that the antenna scans conically, but the feed horn is fixed. The result is that the ports in the antenna that measure orthogonally polarized radiation at each frequency each measure a linear combination of the vertical and horizontal polarizations; this linear combination depends on the scan angle. Let ϕ be the scan angle, let X and Y be the two antenna temperatures measured, and let V and H be the incident brightness temperatures. Then

$$\begin{aligned} X &= V \cos^2 \phi + H \sin^2 \phi \\ Y &= V \sin^2 \phi + H \cos^2 \phi. \end{aligned} \tag{6}$$

This system of equations must be inverted to get V and H from the measurements of X and Y. In practice, it has not been possible to do this correctly for the SMMR data when ϕ is large because of leakage in the ferrite switches and uncertainties in the calibration of the antenna temperatures.

3. The calibration of the antenna temperatures is done by looking alternately through the main antenna and a separate antenna that provides a cold calibration. A separate (internal) hot load is used as a hot reference. The result is that the data, cold reference, and hot reference signals come over different paths, and it is impossible to compensate fully for the different losses in the different paths. That this is a significant problem for determining SSTs can be seen by comparing the antenna horn temperature (Figure A-3) with the day-night difference in SST (Version II; Figure A-1). An external source of hot and cold reference measurements would be preferable for any future microwave instrument.

Of all these problems, the sharing of radiometers should be easiest to fix in future systems. Recent advances in technology make it possible to construct a SMMR of the same external dimensions, but with four more radiometers.

Overall, these three effects combine to degrade the quality of the data, making the calibration of the antenna temperatures untrustworthy and degrading the data at large scan angles. Some of these effects have not been seen in the data presented above because only the 60% of the data nearest the scan center were used.

Even with the problems discussed above, it seems that the SMMR instrument can provide useful SSTs; the quality of the SST product will be tested in future workshops. Most of the residual errors can be traced to problems that are inherent in the design of this particular instrument and can be corrected in future microwave instruments.

REFERENCES

1. Wilheit, T., and Chang, A., "An Algorithm for Retrieval of Ocean Surface and Atmospheric Parameters from the Observations of the Scanning Multichannel Microwave Radiometer," Radio Science, Vol. 15, pp. 525-544.
2. Wilheit, T. T., J. Greaves, J. Gatlin, D. Han, B. M. Krupp, A. S. Milman, and E. Chang, "Retrieval of Ocean Surface Parameters from the Scanning Multichannel Microwave Radiometer (SMMR) on the Nimbus-7 satellite," submitted to IEEE Trans. Geosci. Rem. Sens., 1983.

A-11

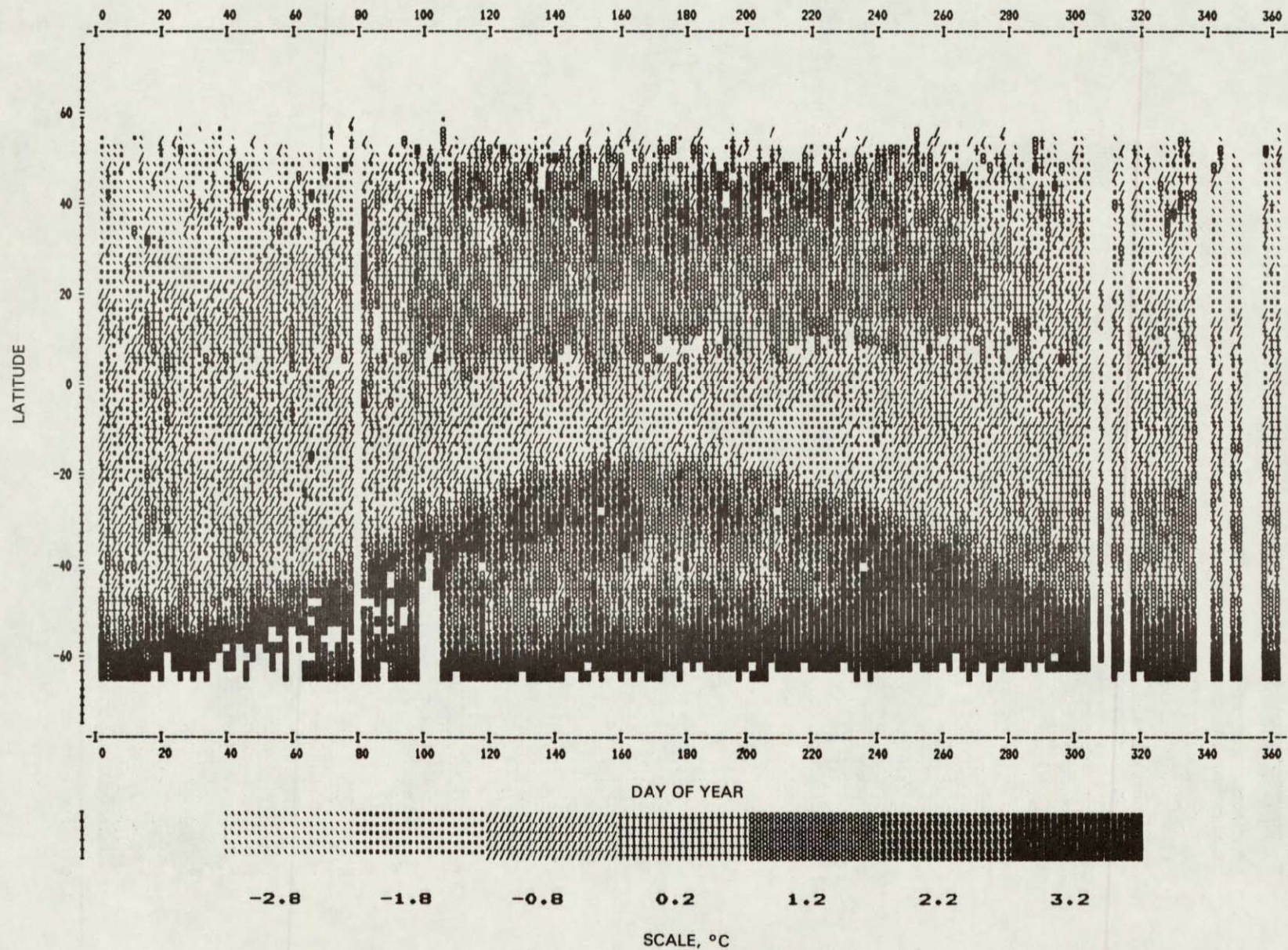


Figure A-1. Difference between Daytime and Nighttime SST Anomaly, i.e., $(\text{SMMR-Climatology})_{\text{Day}} \text{ minus } (\text{SMMR-Climatology})_{\text{Night}}$, Using Algorithm Version II

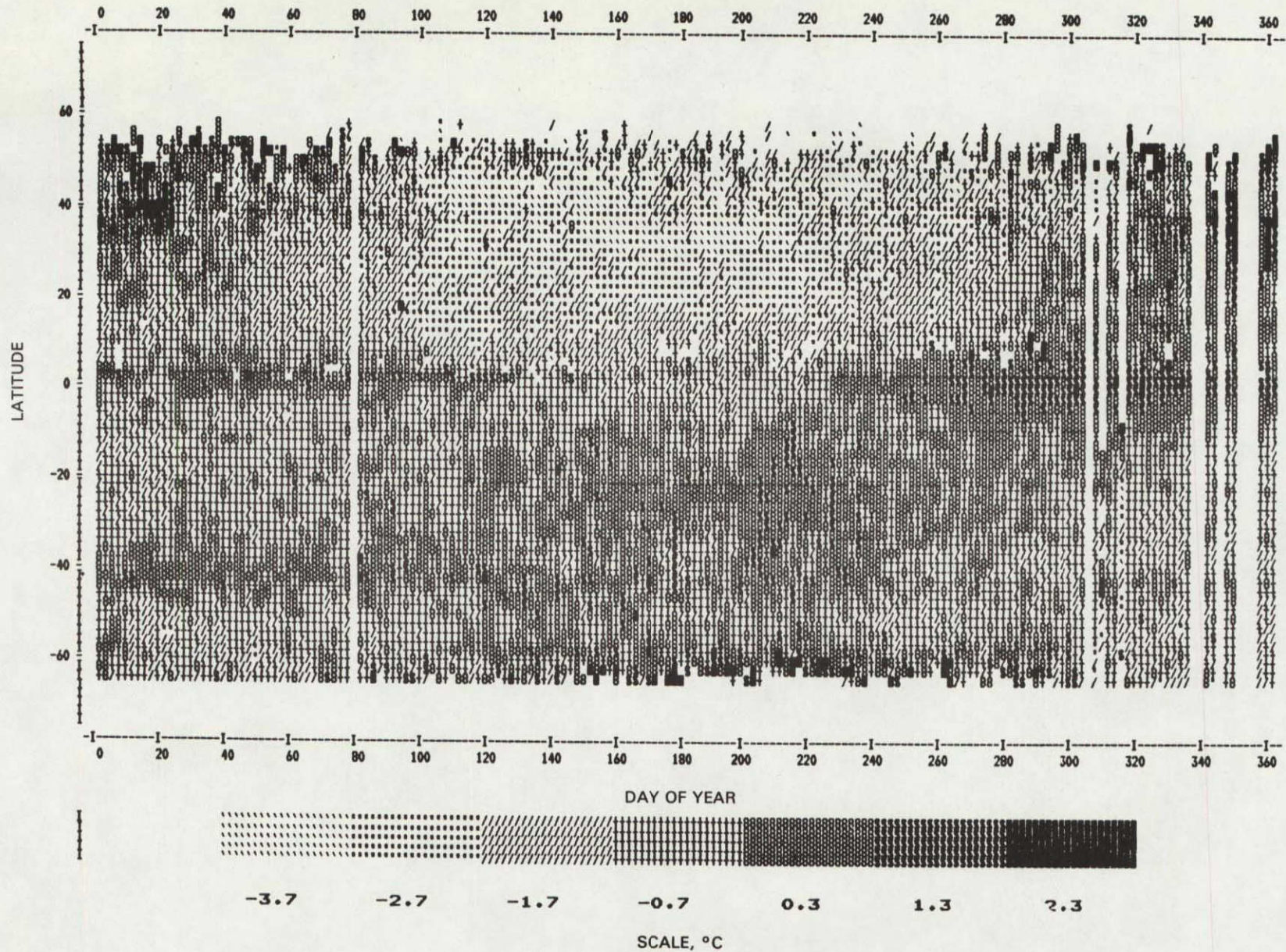
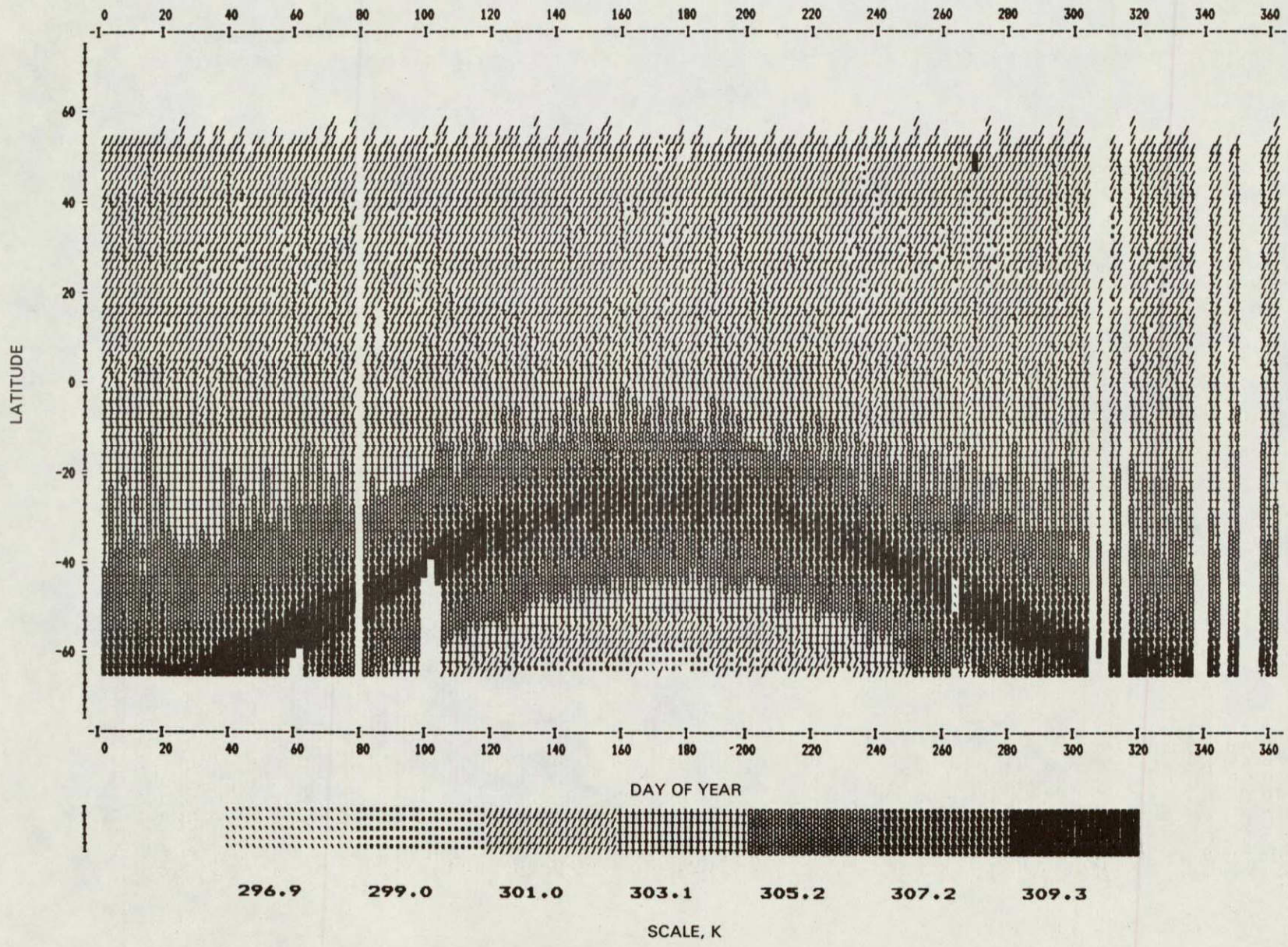


Figure A-2. SST Anomaly (SMMR minus Climatology) for Night/Twilight Data, Algorithm Version II

e-7
A-13



ORIGINAL PAGE IS
OF POOR QUALITY

Figure A-3. Daytime Temperature of SMMR Antenna Feed Horn

A-14

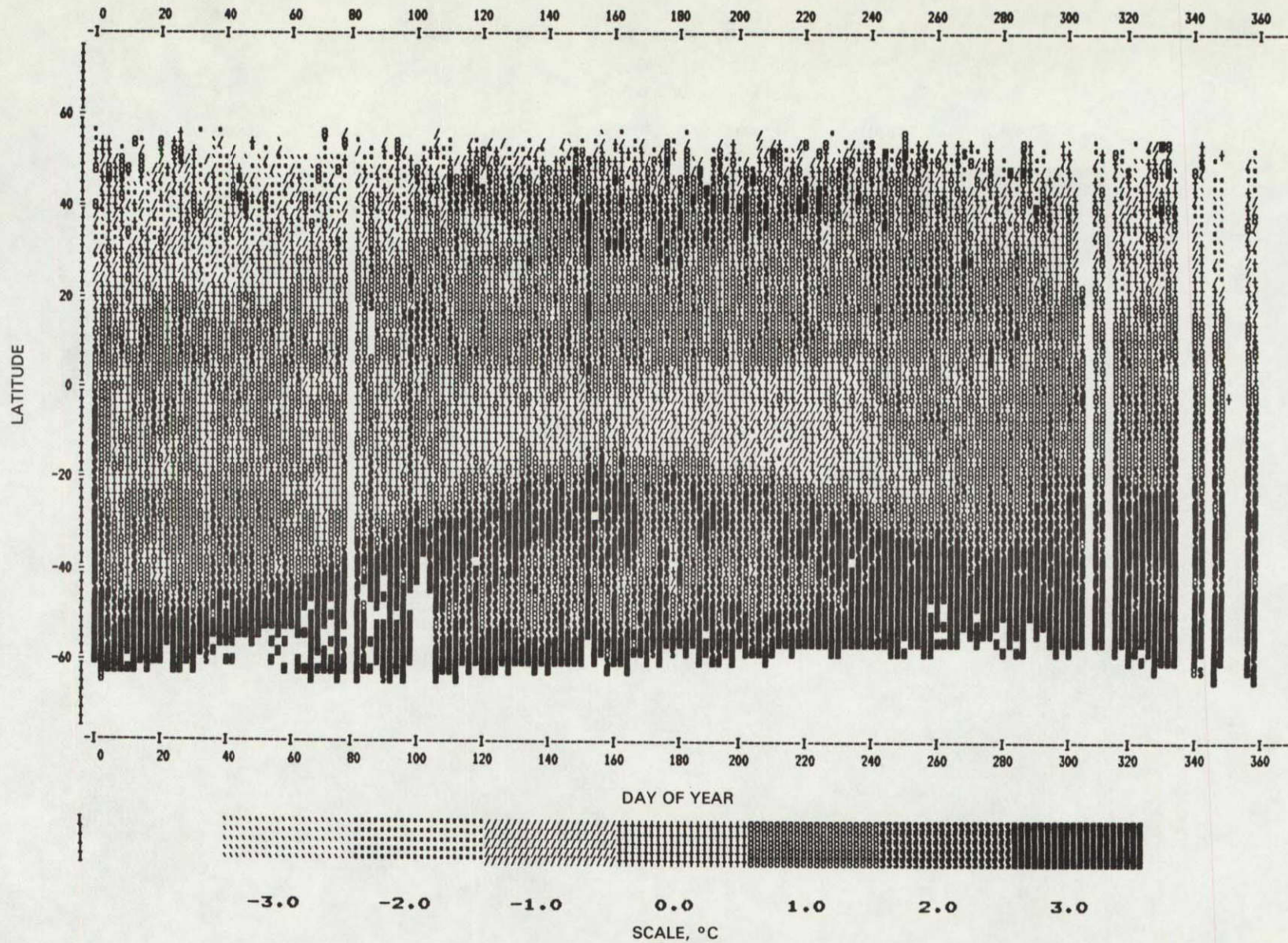


Figure A-4. Difference between Daytime and Nighttime SST Anomaly, i.e., $(\text{SMMR-Climatology})_{\text{Day}}$ minus $(\text{SMMR-Climatology})_{\text{Night}}$, Using Algorithm Version III

A-15

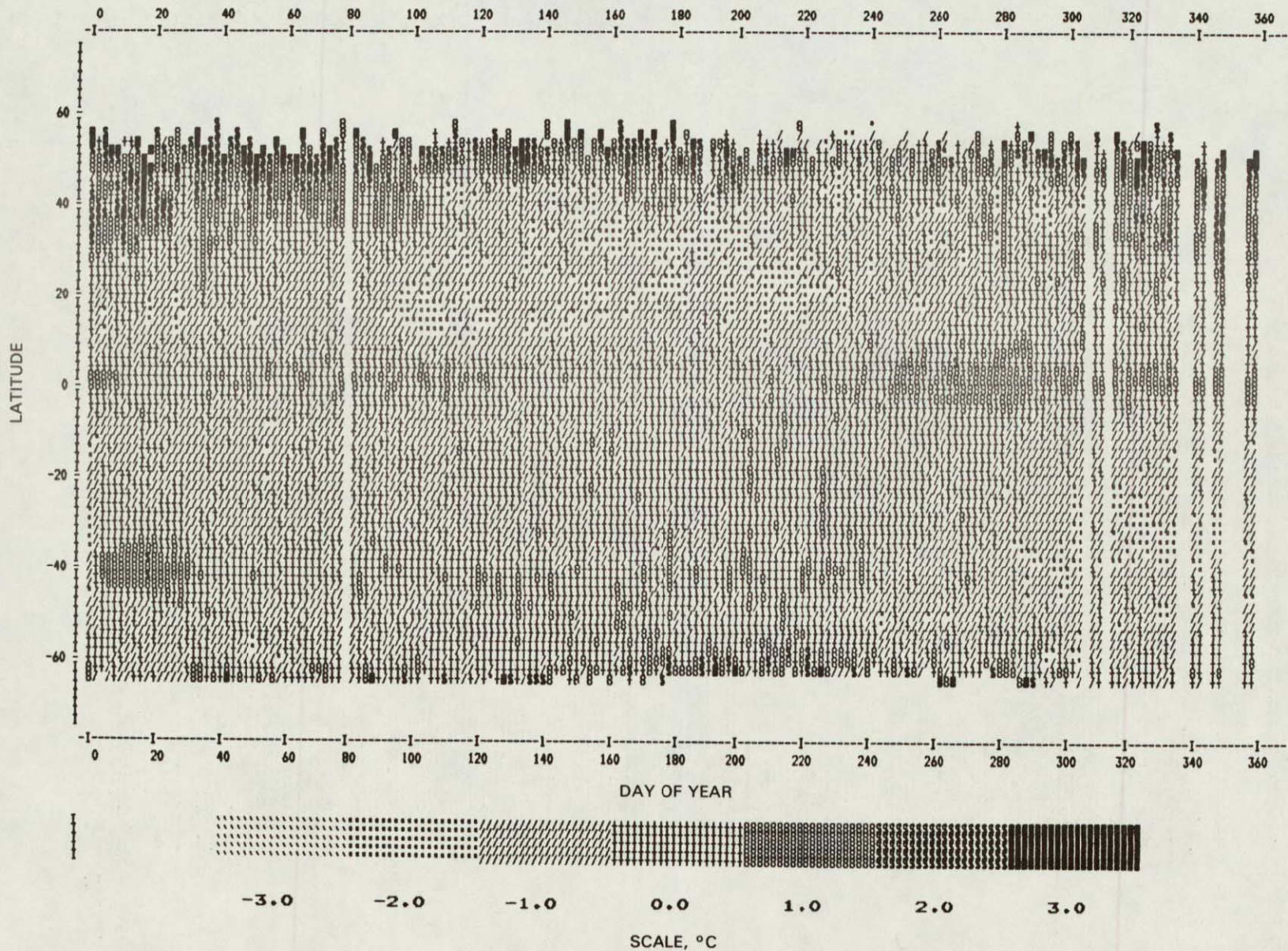
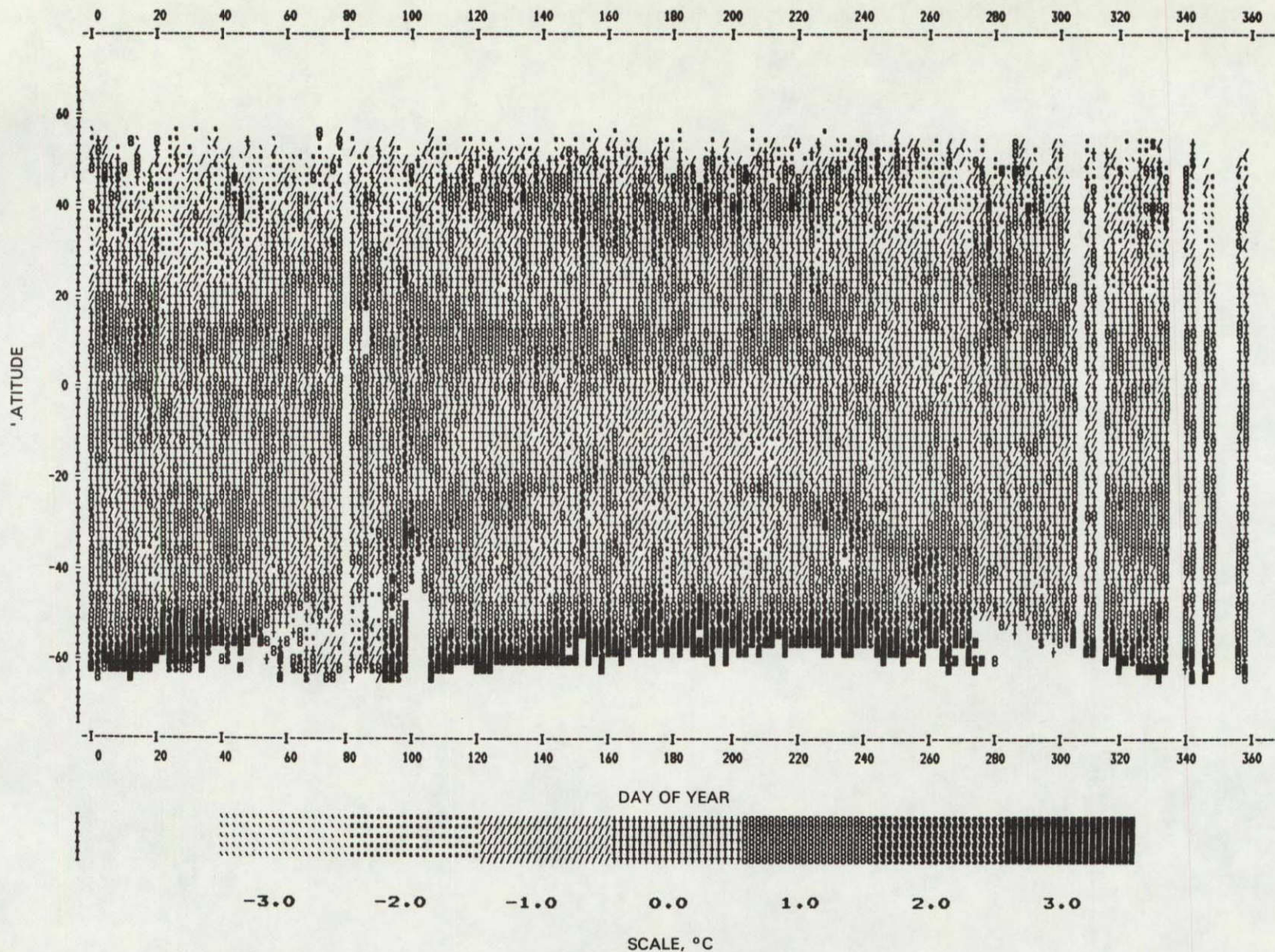


Figure A-5. SST Anomaly (SMMR minus Climatology) for Night/Twilight Data, Using Algorithm Version III

A-16



ORIGINAL PAGE IS
OF POOR QUALITY

Figure A-6. Difference between Daytime and Nighttime SST Anomaly, i.e., $(\text{SMMR-Climatology})_{\text{Day}} - (\text{SMMR-Climatology})_{\text{Night}}$, Using Algorithm Version IV

A-17

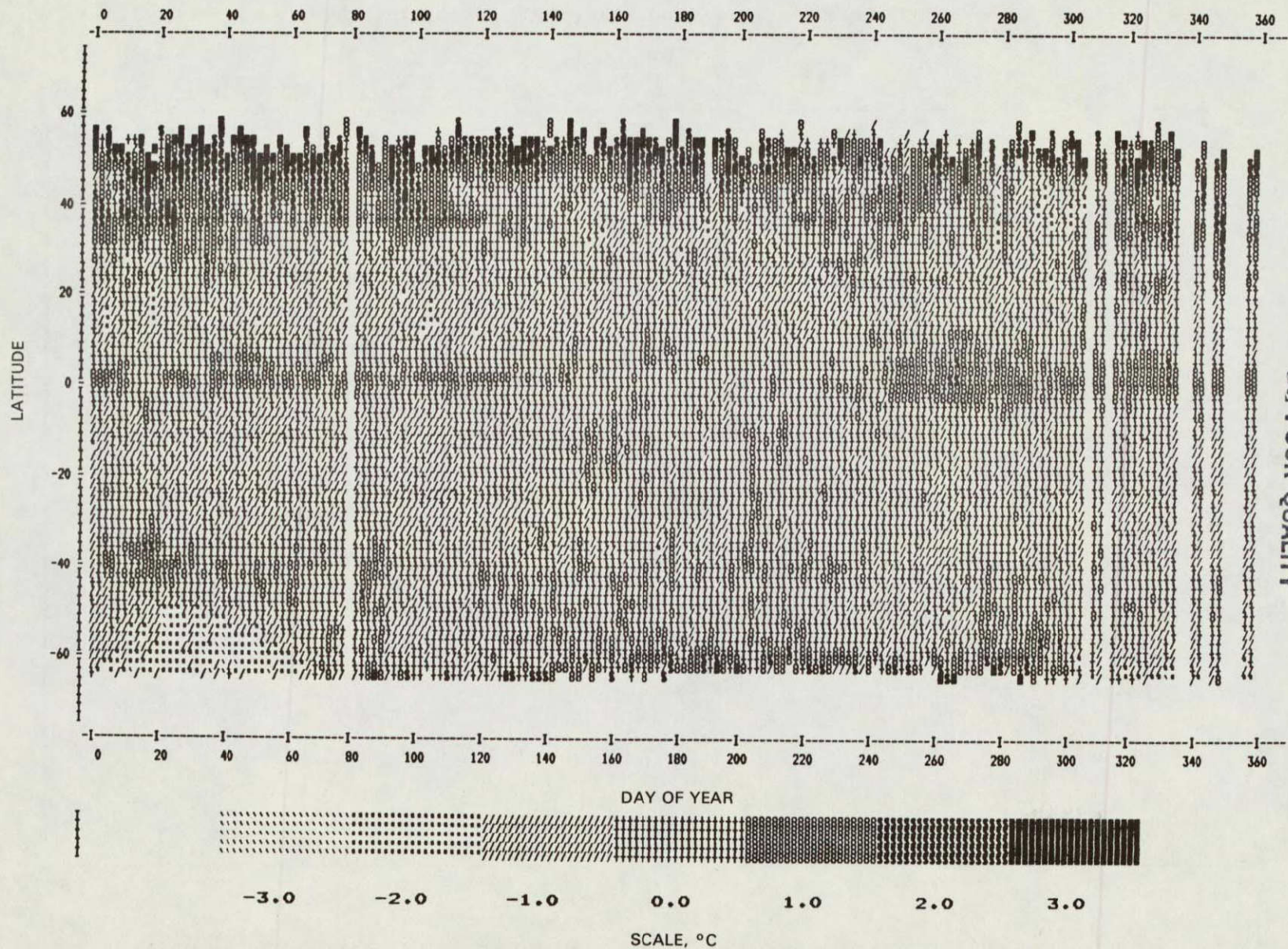
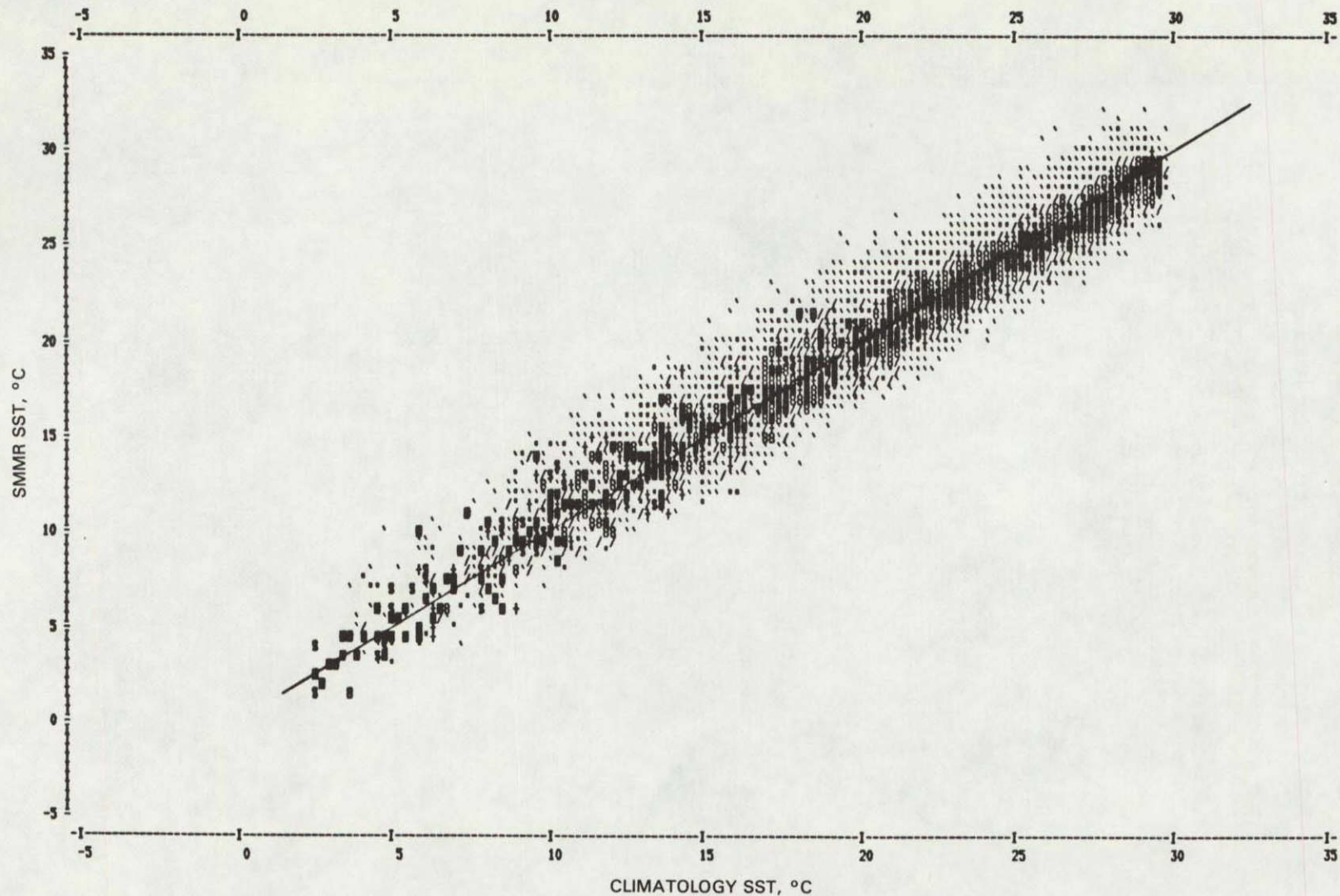


Figure A-7. SST Anomaly (SMMR minus Climatology) for Night/Twilight Data, Using Algorithm Version IV

SMMR & CLIMATE COMPARISON

n = 18702 av. = 0.09 rms = 1.41



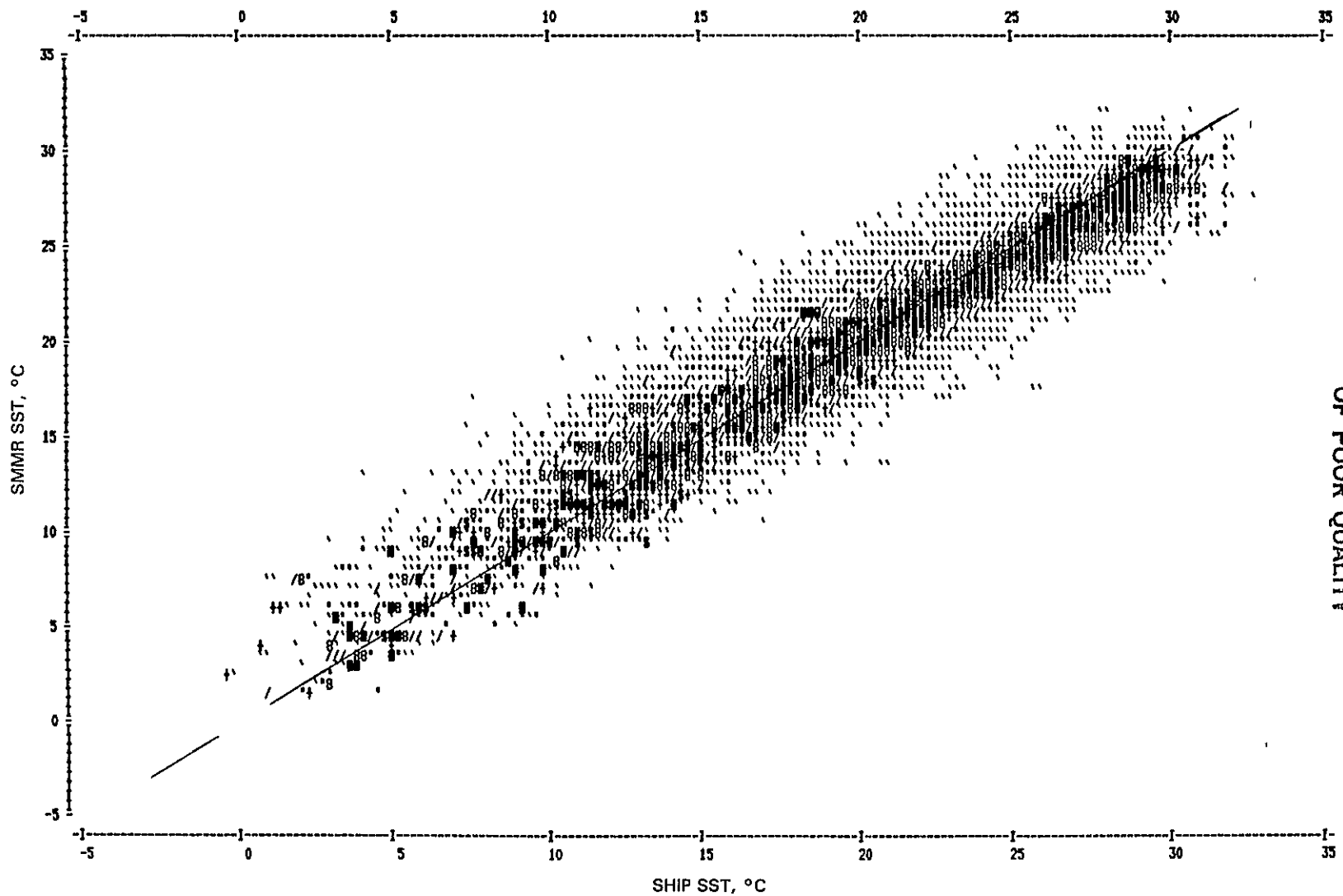
A-18

ORIGINAL PAGE IS
OF POOR QUALITY

Figure A-8. Scatterplot of SMMR (Version IV) SST versus Climatology

SMMR & SHIP COMPARISON

n = 18702 av. = 0.04 rms = 1.79



A-20

ORIGINAL PAGE IS
OF POOR QUALITY

Figure A-10. Scatterplot of SMMR (Version IV) SST versus Ship SST

APPENDIX B

A STATISTICAL METHOD TO SENSE SEA SURFACE TEMPERATURE FROM THE
NIMBUS-7 SCANNING MULTICHANNEL MICROWAVE RADIOMETER

A STATISTICAL METHOD TO SENSE SEA SURFACE TEMPERATURE FROM THE
NIMBUS-7 SCANNING MULTICHANNEL MICROWAVE RADIOMETER

C. Prabhakara and I. Wang

Among the five channels in the Scanning Multichannel Microwave Radiometer (SMMR), the brightness temperature measured at 6.6 GHz vertical polarization is least affected by the atmospheric water vapor and liquid water in clouds or rain (Table B-1). Furthermore, as the undisturbed sea surface emissivity at 6.6 GHz is nearly constant over the temperature range 275 to 300 K, this channel has the best sensitivity to sea surface temperature (SST). The 6.6 GHz channel on SMMR is specifically chosen for these reasons to measure SST.

Surface winds roughen the sea surface as well as form foam, thereby increasing surface emissivity. As a consequence the brightness temperature measured at the top of the atmosphere shows an increase. Thus in order to sense SST from 6.6 GHz measurements one has to apply appropriate corrections to account for the effects of surface winds, liquid water in the atmosphere, and water vapor. SMMR measurements at the 10.7, 18, 21 and 37 GHz channels in principle can provide information needed to make these corrections. In practice, however, the calibration errors that differ from channel to channel and between night and day cause considerable problems. Sun glint may introduce some contamination in the data. For these reasons we have developed a statistical technique that is suitable for the estimation of SST on a monthly basis.

When we examine the variance in the 6.6 GHz brightness temperature measured by SMMR in a geographic region during a month, we find this variance is principally due to the meteorological elements -- surface winds, liquid water, and water vapor in the atmosphere. The variance introduced by the SST is relatively smaller. Thus, in order to get a good estimate of SST, the meteorological noise has to be minimized.

Table B-1. Sensitivity of Scanning Multichannel Microwave Radiometer Brightness Temperatures (T_B)

ν (GHz)	Surface Channels				Atmospheric Channels					
	6.6	10.7	18	21	37					
Polarization	V	H	V	H	V	H	V	H	V	H
$\frac{\partial T_B}{\partial T_S}$ (K/K)*	0.5	0.3	0.5	0.3	0.3	0.2	0.2	0.1	0.1	-0.1
$\frac{\partial T_B}{\partial w}$ (K/g/cm ²)*	0.3	0.5	0.8	1.3	4.5	7.5	11.9	19.6	6	11
$\frac{\partial T_B}{\partial \ell}$ (K/10 ⁻² g/cm ²)*	0.3	0.5	0.7	1.1	1.6	2.7	1.5	2.5	4.2	7.8
$\frac{\partial T_B}{\partial \mu}$ (K/m/s)*	~0.5	~1.0	~0.5	~1.0	~0.5	~1.0	~0.5	~1.0	~0.5	~1.0

T_S - Sea surface temperature, °C

w - Total water vapor in the atmosphere, g/cm²

ℓ - Total liquid water content in the atmosphere, 10⁻² g/cm²

μ - Surface wind speed, m/s

*These sensitivities are calculated for a tropical model atmosphere having sea surface temperature of 298.6 K, 3.4 g/cm² of water vapor, 50 m g/cm² of liquid water droplets and no surface winds.

With the above considerations a statistical method has been developed to estimate SST from SMMR 6.6 GHz measurements on a monthly basis. Statistically when there are more than four Nimbus-7 SMMR observations in a grid box of 1° lat x 1° lon during a month, the minimum among those observations represents, with a high degree of probability, calm surface conditions with negligible liquid water in the atmosphere. Because the footprint of 6.6 GHz channel at the surface is about 155 km, this procedure amounts to over-sampling of the data by about a factor of two. The minimum 6.6 GHz vertical polarization brightness obtained in this fashion is corrected for water vapor absorption. For each gram of water vapor the 6.6 GHz brightness is decreased by 0.3°K. The amount of water vapor in the atmosphere is estimated from the 18 and 21 GHz SMMR measurements.

Because the water vapor in the atmosphere is present at all times and has a large scale character, the water vapor correction to 6.6 GHz measurements can be applied satisfactorily. The liquid water and surface winds, on the other hand, have larger variability both in time and space. For this reason no correction for these variables is applied. However, choosing a minimum brightness at 6.6 GHz helps in reducing the errors resulting from surface winds and liquid water in the atmosphere.

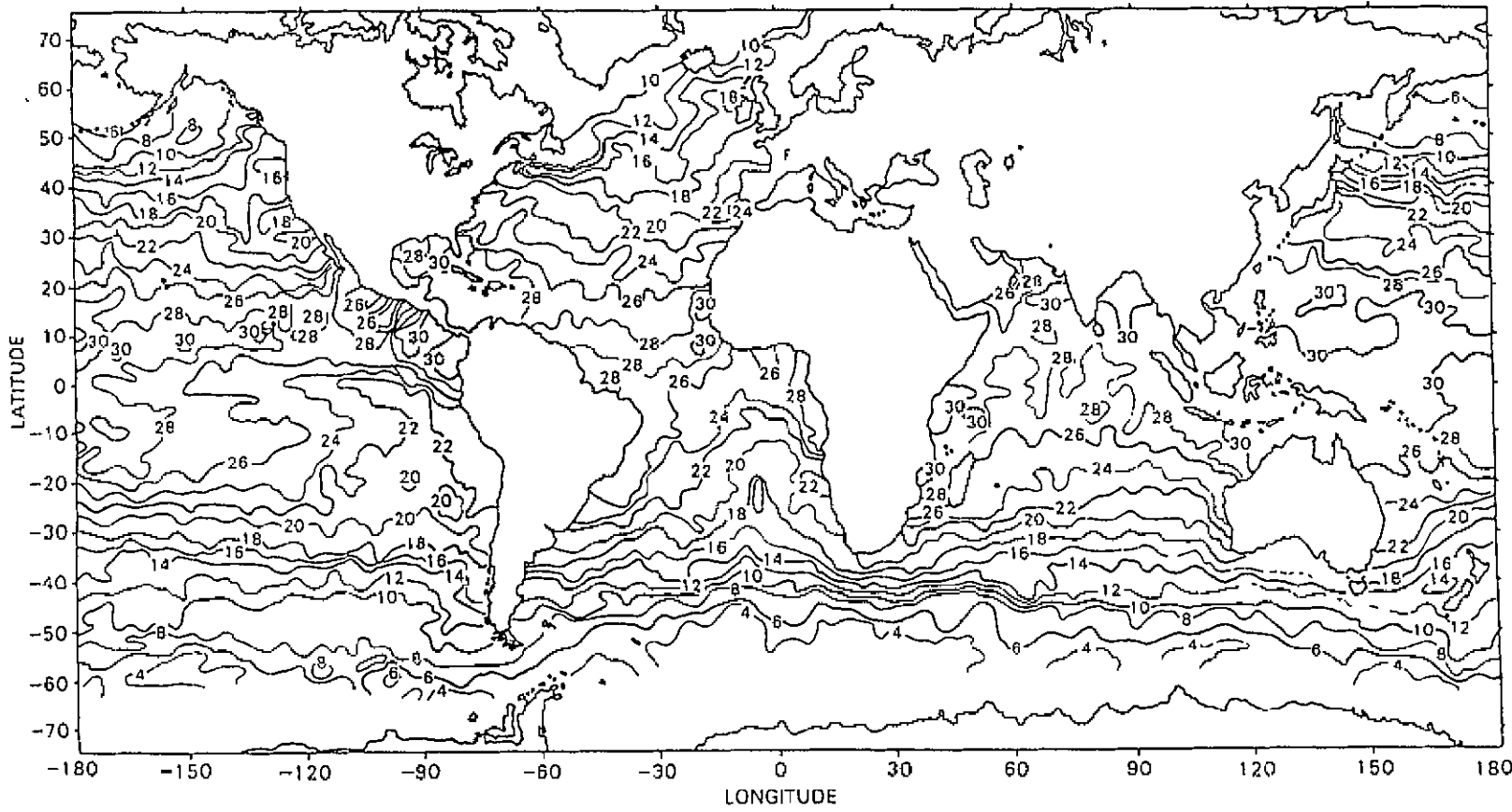
The ratio of 6.6 GHz brightness temperature in the vertical and horizontal polarizations, $T_{6.6}^V/T_{6.6}^H$, is a measure of the degree of polarization. This ratio decreases as the meteorological noise (surface winds, liquid water and water vapor in the atmosphere) increases. A maximum value of this ratio thus assures that the meteorological noise is near a minimum. When a minimum $T_{6.6}^V$ in a 1° x 1° grid box is chosen during a month it is found that the polarization ratio is near maximum.

An SST map for the period from October 25 to November 25, 1978, deduced with the method described above is shown in Figure B-1. Although the SST information shown in Figure B-1 near the coasts is not satisfactory, on the open oceans the SST patterns look good. In Figure B-2 SST data obtained from SMMR are compared with those of National Marine Fisheries Service (NMFS) from about 50°N to 30°S along 140°W and 165°W longitude. This comparison shows

that the SMMR measurements are within 1°C of NMFS data. Part of this discrepancy could be attributed to calibration errors in the SMMR data. One such calibration error is shown in Figure B-3. Notice from this figure that the minima in the Nimbus-7 SMMR 6.6 GHz vertical polarization brightness temperature differ systematically between day and night. When 6.6 GHz minimum data are selected regardless of night or day, as is done in generating the SST map shown in Figure B-1, a significant error is introduced in the results.

This study leads to the conclusion that the 6.6 GHz measurements, despite the large field of view, can be processed to get high quality SST information on a monthly basis over the open oceans. Supplementing this information with the infrared remote sensing of SST near the coastal areas will lead to comprehensive global mapping capability.

B-5



ORIGINAL PAGE IS
OF POOR QUALITY

Figure B-1. Monthly mean sea surface temperature ($^{\circ}\text{C}$) derived from Nimbus-7 SMMR for the period October 25 to November 15, 1978

ORIGINAL PAGE IS
OF POOR QUALITY

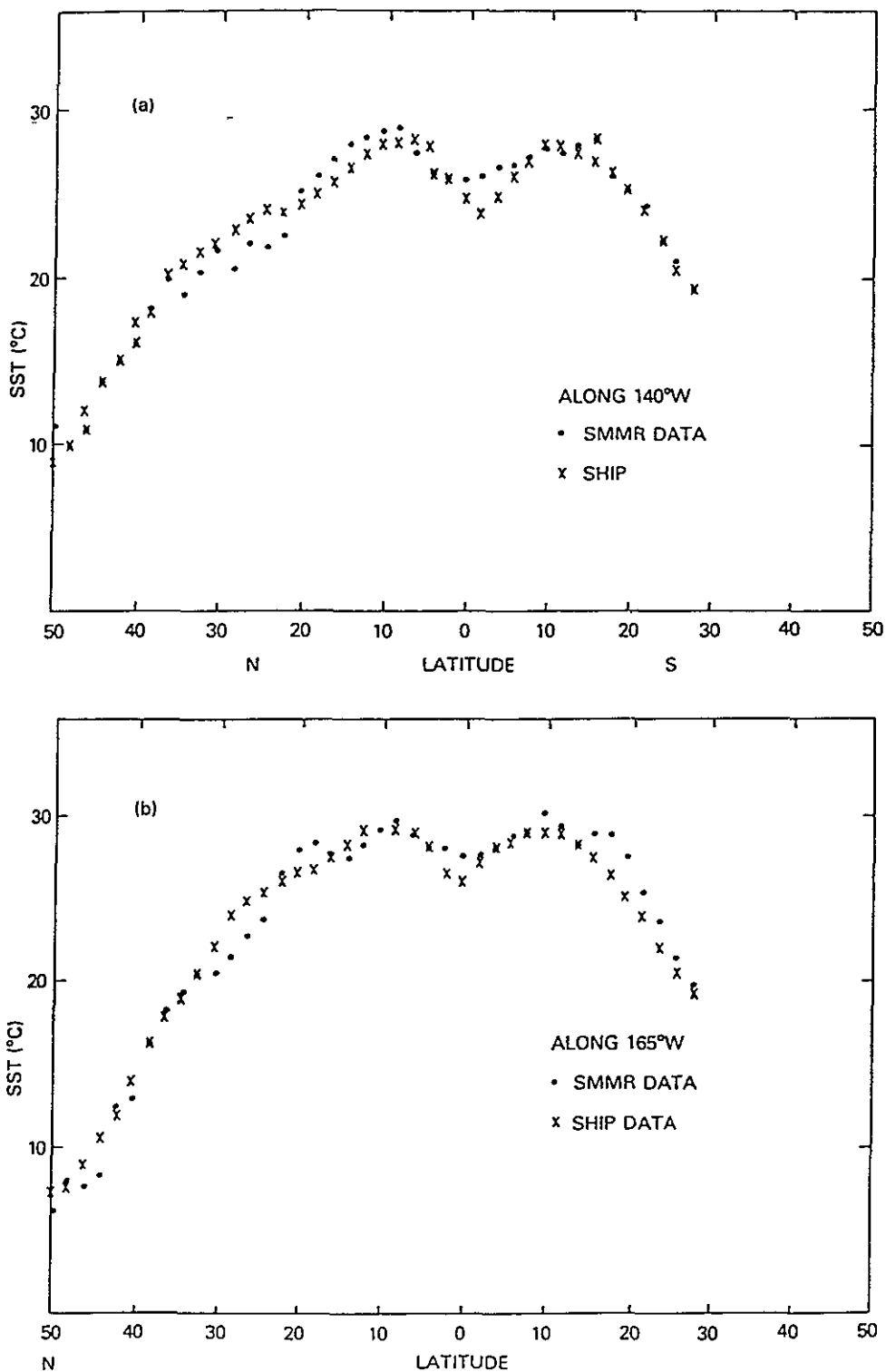


Figure B-2. Comparison of sea surface temperature derived from Nimbus-7 SMMR with that obtained from National Marine Fisheries Service for November 1978 (a) along 140°W longitude (b) along 165°W longitude

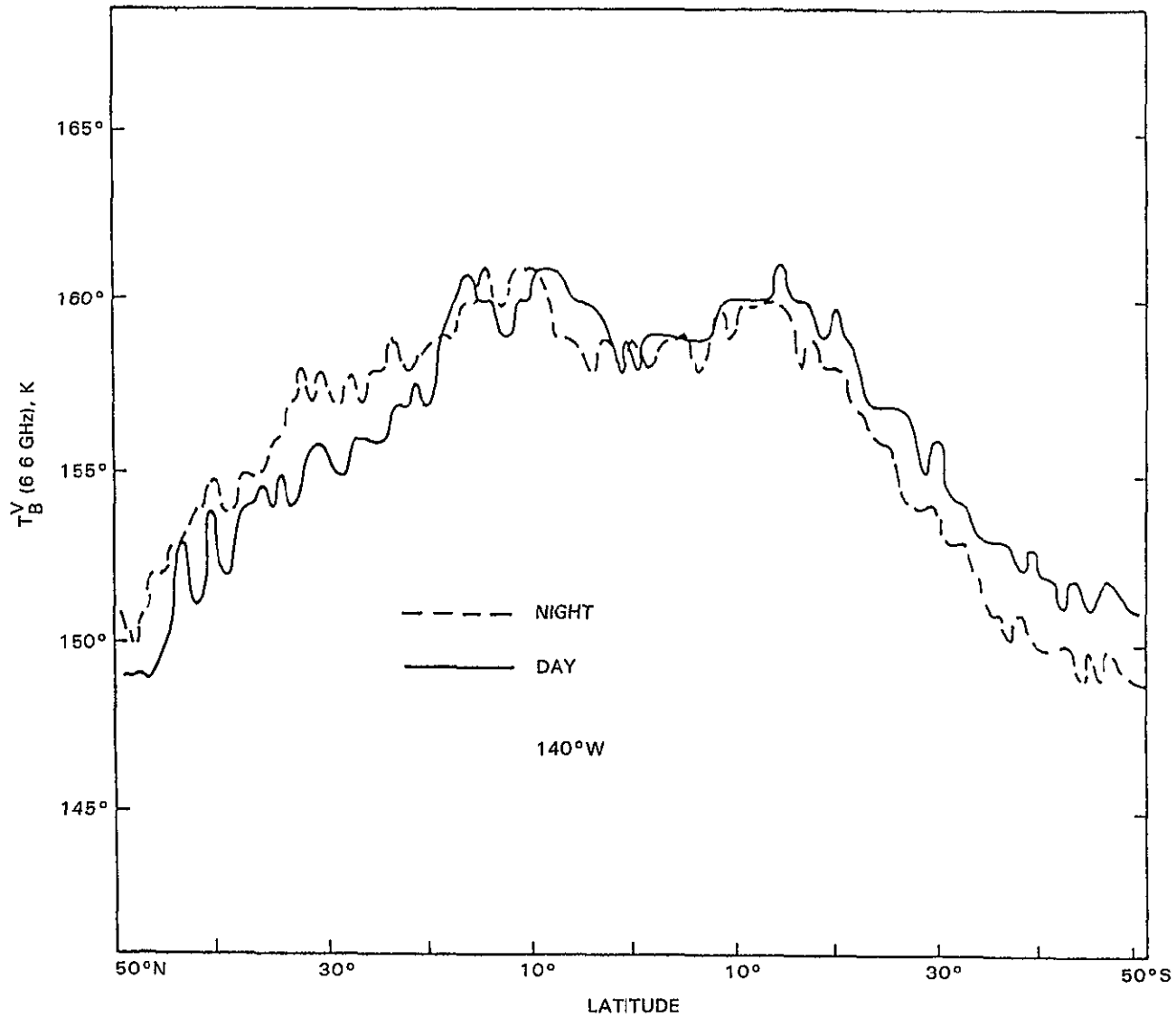


Figure B-3. Minima in the Nimbus-7 SMMR 6.6 GHz (Vertical Polarization) brightness temperature as a function of latitude, along 140°W longitude, obtained from night and day data

ORIGINAL PAGE IS
OF POOR QUALITY

N84 21965

D/10

APPENDIX C

NOAA SATELLITE-DERIVED OPERATIONAL SEA
SURFACE TEMPERATURE PRODUCTS

NOAA SATELLITE-DERIVED OPERATIONAL SEA SURFACE TEMPERATURE PRODUCTS

E. Paul McClain

The National Oceanic and Atmospheric Administration (NOAA) began processing global measurements of emitted radiation in the 10.5-12.5 μ m "atmospheric window" for purposes of deriving weekly composite and mean monthly sea surface temperature fields in the early 1970s. Atmospheric attenuation corrections, begun with empirical means, were accomplished chiefly with the aid of coarser-resolution measurements from atmospheric sounders aboard the same polar-orbiting spacecraft. Cloud filtering depended heavily upon the use of histogram techniques applied to 11 x 11 arrays of 8-km resolution Scanning Radiometer-Infrared (SRIR) data. Details of the SRIR processing for SST are found in a NOAA Technical Memorandum (Ref. 1).

After the launch of the first in the TIROS-N generation of NOAA operational environmental satellites in late 1978, the Global Operational Sea Surface Temperature Computation (GOSSTCOMP) was continued for several years in much the same way as before, but with several substantial improvements. The noise level of the new 4-km measurements from the Advanced Very High Resolution Radiometer (AVHRR) was far lower than with the earlier SR, spatial resolution of the SST retrievals improved from 100-km to 50-km, and an improved High-Resolution Infrared Sounder (HIRS) was employed both in the cloud filtering and atmospheric correction procedures. Only one of the two (later three) IR window channels, the one centered at 11 μ m, was used during this period (Ref. 2).

Figure C-1 is the global monthly mean SST for November 1979 derived by averaging all the 50-km resolution GOSSTCOMP retrievals falling into 2.5 x 2.5 degree lat-lon bins. Figure C-2 and C-3 are global charts of the number of satellite SST retrievals, and anomaly (satellite minus climatology (NCAR)) values, respectively. Table C-1 is a summary of the zonal mean (2.5° lat belts) and global statistics relative to satellite and climatological SST values.

Beginning in mid-November 1981, the totally new Multi-Channel Sea Surface Temperature (MCSST) became operational. Details of the conceptual and procedural basis of the MCSST method are found in McClain (Ref. 3) and McClain, et al (Ref. 4). Several types of cloud-detection tests are applied to 2 x 2 "unit arrays" of daytime 4-km visible (0.58 - 0.68 μm) or reflected-IR (0.725 - 1.1 μm) measurements within overlapping 11 x 11 target arrays centered every 25 km to isolate at least one unit array per target for further processing; the nighttime data are cloud-filtered using other tests. Brightness temperatures from the three IR window channels (3.55 - 3.93, 10.3 - 11.3, and 11.5 - 12.5 μm) are used in algorithms derived by simulation from a large and geographically diverse set of maritime atmospheric profiles of temperature and humidity (from radiosondes) and atmospheric transmittance models. SSTs predicted from this simulation process were regressed against matched buoy and XBT observations to obtain small but significant temperature-dependent bias corrections. After testing the bias-corrected equations with an independent set of buoy-satellite matchups to see if the bias had been eliminated (Table C-2), the equations became part of the operational procedures.

The MCSSTs have proven superior to the earlier GOSSTCOMP in accuracy (bias and RMS difference relative to buoys or ships), density of observations, and overall geographic coverage. GOSSTCOMP biases were 0.5 to 1.0°C globally (higher and often quite variable regionally), and GOSSTCOMP RMSDs were generally $\geq 1.5^\circ\text{C}$ relative to buoys and $\geq 2.0^\circ\text{C}$ relative to ships. MCSSTs have biases $< 0.1^\circ\text{C}$ globally and are generally $\leq 0.25^\circ\text{C}$ regionally.¹ MCSST RMSDs have been running $\leq 0.75^\circ\text{C}$ relative to buoys and $\leq 1.5^\circ\text{C}$ relative to ships. Coverage in the polar regions and in the deep tropics has been good.

¹An exception to this was a persistent negative bias of about 0.4°C in the nighttime retrievals during the first nine months of operation. This was eliminated by using a large set of drifting buoy/satellite matchups to re-derive the temperature-dependent bias corrections for the nighttime simulation equations (see Table C-3).

Figures C-4, C-5 and C-6 are monthly mean MCSSTs, numbers of observations, and anomalies, respectively, for March 1982. This month was chosen because it was the last before the eruption of El Chichón and the first using the Robinson-Bauer climatology, a climatology superior to the NCAR one used previously. Table C-4 presents the global and 2.5° zonal mean statistics for March 1982.

The eruption of El Chichón at the end of March and during the first few days of April 1982, combined with rapid degradation of the 3.7 μm measurements from the AVHRR on NOAA-7, resulted in a considerable loss of MCSST data density and several degrees of negative bias, particularly in the tropics and subtropics of the Northern Hemisphere, during the period from April through November 1982. Present indications are that the negative bias has now lessened somewhat in the tropical belt but has become relatively uniform elsewhere throughout the Northern Hemisphere at about -0.9°C. The magnitude and geographic distribution in the Southern Hemisphere is not well known. The noise level in the 3.7 μm channel had become so large by late 1982 that its use in the MCSST processing has been severely curtailed and may need to be abandoned altogether.

REFERENCES

1. Brower, R. L., Gohrband, H. S., Pichel, W. G., Signore, T. L., and Walton, C. C., Satellite-Derived Sea Surface Temperatures from NOAA Spacecraft, NOAA Technical Memorandum NESS 78, NOAA/NESS, Washington, D.C., 1976.
2. Walton, C. C., "Deriving Sea Surface Temperatures from TIROS-N Data," Remote Sensing of Atmospheres and Oceans, Academic Press, 1980, pp. 547-578.
3. McClain, E. P., "Multiple Atmospheric-Window Techniques for Satellite-Derived Sea Surface Temperatures," Oceanography from Space, Edited by J. F. R. Gower, Plenum Press, New York, 1980, pp. 73-85.
4. McClain, E. P., Pichel, W. G., Walton, C. C., Ahmad, Z., and Sutton, J., "Multi-channel Improvements to Satellite-Derived Global Sea Surface Temperatures," Preprint, XXIV COSPAR, Ottawa, Canada, 22-29 May 1982, 11 pp.

Table C-1. Summary of the Zonal Mean (2.5° lat belts) and Global Statistics Relative to Satellite and Climatological SST Values (November 1979 GOSSTCOMP)^a

	LAT	GRID PTS	No. OBS	OBS/PT	DELT-T	MEAN TMP	CLI TEMP
	-57.5	38	405	10.7	2.1	4.5	2.4
	-55.0	59	1559	26.6	2.3	5.7	3.4
	-52.5	70	2681	33.3	2.0	6.8	4.8
	-50.0	85	3810	44.8	1.8	7.8	6.0
	-47.5	127	6055	47.7	1.7	8.3	6.6
	-45.0	137	9029	65.9	1.5	9.7	8.2
	-42.5	139	12847	92.4	1.3	11.4	10.0
	-40.0	136	17688	130.1	1.4	13.5	12.1
	-37.5	137	24012	175.3	1.2	15.1	13.9
South	-35.0	133	31955	240.3	1.1	16.6	15.5
	-32.5	122	32890	269.6	1.0	17.9	16.9
	-30.0	115	33501	291.3	0.9	19.4	18.5
	-27.5	114	34030	298.5	0.8	20.6	19.8
	-25.0	112	34651	309.4	0.6	21.6	21.0
	-22.5	109	35771	328.2	0.6	22.5	21.8
	-20.0	107	28016	261.8	0.8	23.5	22.7
	-17.5	109	20418	187.3	0.9	24.6	23.6
	-15.0	109	12328	113.1	1.0	25.6	24.6
	-12.5	106	11850	111.8	0.8	26.4	25.5
	-10.0	110	11642	105.8	0.8	26.7	25.9
	-7.5	102	10654	104.5	0.8	27.0	26.1
	-5.0	96	9210	95.9	0.8	27.1	26.3
	-2.5	83	6717	80.9	0.8	27.0	26.2
	0.0	78	4337	55.6	0.8	27.1	26.2
	2.5	78	3436	44.0	0.8	27.3	26.5
	5.0	63	2247	35.7	0.6	28.0	27.3
	7.5	52	1665	32.0	0.5	28.2	27.7
	10.0	64	2550	39.8	0.3	28.1	27.8
	12.5	88	4949	56.2	0.5	28.3	27.8
	15.0	98	9353	95.4	0.4	28.0	27.6
	17.5	102	12276	120.4	0.4	27.6	27.2
	20.0	94	14718	156.6	0.5	27.1	26.6
	22.5	95	18119	190.7	0.4	26.3	25.9
	25.0	90	23311	259.0	0.4	25.7	25.2
North	27.5	86	25345	294.7	0.6	24.9	24.3
	30.0	83	25671	308.7	0.8	23.9	23.1

^aSatellite minus climatology monthly mean sea surface temperature difference, °C.

Table C-1. Summary of the Zonal Mean (2.5° lat belts) and Global Statistics Relative to Satellite and Climatological SST Values (November 1979 GOSSTCOMP)^a (contd)

	LAT	GRID PTS	No. OBS	OBS/PT	DELT-T	MEAN TMP	CLI TEMP
	32.5	77	23097	300.0	0.9	22.8	21.9
	35.0	83	22484	270.9	1.3	21.7	20.3
	37.5	82	16192	197.5	1.5	20.4	18.8
	40.0	80	13923	174.1	1.6	18.3	16.7
	42.5	72	10312	150.2	1.3	15.8	14.5
	45.0	71	9832	138.5	0.7	13.1	12.3
	47.5	63	9446	149.9	0.0	10.5	10.4
	50.0	60	7251	120.8	-0.3	8.8	9.1
	52.5	55	5683	103.3	-0.1	7.9	8.1
	55.0	56	4962	88.6	-0.2	6.7	7.0
	57.5	60	4971	82.8	-0.2	5.9	6.2
	60.0	57	4698	82.4	0.1	5.6	5.5
Global	999.0	4342.0	673000.0	155.0	0.9	19.6	18.7

^aSatellite minus climatology monthly mean sea surface temperature difference, °C.

Table C-2. Operational Equations for MCSST, and
Satellite-Buoy Comparisons^a

Daytime:

$$T_{11/12} = -283.93 + 1.035 T_{11} + 3.046(T_{11}-T_{12})$$

Nighttime:

$$T_{3.7/11} = -287.76 + 1.0574 T_{11} + 1.5044(T_{3.7}-T_{11})$$

$$T_{11/12} = -296.23 + 1.0760 T_{11} + 3.168(T_{11}-T_{12})$$

$$T_{3.7/11/12} = -289.55 + 1.0602 T_{11} + 1.0385(T_{3.7}-T_{12})$$

	Buoy/satellite matchup data used with original simulation equations		Independent data used with bias-corrected simulation equations		Equation
	DAY	NIGHT	DAY	NIGHT	
N	-	39	-	74	
Bias	-	-0.96°	-	+0.02°	Dual-Window
RMSD	-	1.25°	-	0.62°	(3.7/11 μm)
N	52	39	76	74	
Bias	-0.17°	-0.35°	+0.02°	-0.03°	Split-Window
RMSD	0.77	0.96	0.78°	0.63°	(11/12 μm)
N	-	39	-	74	
Bias	-	-0.78°	-	+0.02°	(Triple-Window)
RMSD	-	1.10°	-	0.58°	(3.7, 11, 12 μm)

^aThe 1-m temperatures from these environmental buoys ranged from 5-30C, and the locations were in the Western Atlantic, Eastern Pacific, Gulf of Mexico, and Great Lakes. The output MCSSTs are in deg. C from input brightness temperatures in deg. K. Although atmospheric corrections have been worked out for viewing angles substantially different from nadir, these have not been incorporated in the equations because they are not significant except in moist air masses at greater than 45° satellite zenith angles currently being used.

Table C-3. Revised MCSST Equations and Drifting Buoy Comparisons

The following NOAA-7 multichannel sea surface temperature (MCSST) equations became operational effective 9/14/82 (revised bias correction; satellite zenith angle = 0).

DAYTIME (°K, °C out)

Split-window $T_{4/5D} = 1.0209T_{11} + 2.5438(T_{11}-T_{12}) - 279.23$

NIGHTTIME (°K, °C out)

Split-window $T_{4/5N} = 1.0529T_{11} + 2.6235 (T_{11}-T_{12}) - 288.28$

Triple-window $T_{3/4/5} = 1.0305T_{11} + 0.9823 (T_{3.7}-T_{12}) - 280.43$

Dual-window $T_{34} = 1.0207T_{11} + 1.5195 (T_{3.7}-T_{11}) - 276.75$

Equation	Split-window		Triple-window	Dual-window
	Day	Night	Night	Night
N	51	94	94	94
Bias	-0.002	+0.060	+0.038	+0.019
RMSD	0.749	0.613	0.646	0.729

Table C-4. Global and 2.5° Zonal Mean Statistics for MCSST and Robinson-Bauer Climatology, March 1982^a

	LAT	GRID PTS	NO. OBS	OBS/PT	DELT-T	MEAN TMP	CLI TMP	RMS DIF
	-57.5	143	16070	112.4	-0.2	2.7	2.9	0.8
	-55.0	144	19961	138.6	-0.1	3.9	4.1	0.7
	-52.5	142	23093	162.6	-0.1	5.2	5.3	0.9
	-50.0	141	26908	190.8	-0.1	6.7	6.8	0.9
	-47.5	140	28095	200.7	0.0	8.7	8.7	1.0
	-45.0	140	29747	212.5	0.1	10.9	10.7	1.2
	-42.5	138	32934	238.7	0.2	13.2	13.0	1.3
	-40.0	136	37280	274.1	0.4	15.8	15.4	1.3
	-37.5	137	40469	295.4	0.6	18.1	17.5	1.3
South	-35.0	133	43547	327.4	0.5	19.9	19.3	1.0
	-32.5	122	39110	320.6	0.4	21.4	20.9	1.1
	-30.0	115	37672	327.6	0.2	22.7	22.4	1.0
	-27.5	113	36351	321.7	0.1	23.7	23.6	0.9
	-25.0	112	34031	303.8	0.1	24.6	24.5	1.0
	-22.5	108	29841	276.3	0.0	25.2	25.2	1.1
	-20.0	108	29656	273.7	0.0	25.8	25.9	1.1
	-17.5	110	32524	295.7	-0.1	26.4	26.5	0.9
	-15.0	109	29720	272.7	-0.1	26.8	27.0	0.8
	-12.5	111	28906	260.4	0.0	27.5	27.5	0.6
	-10.0	117	26920	230.1	0.0	28.0	27.9	0.6
	-7.5	108	21758	201.5	0.2	28.2	28.0	0.6
	-5.0	104	19254	185.1	0.3	28.4	28.1	0.8
	-2.5	100	19231	192.3	0.3	28.4	28.0	0.7
	0.0	102	25090	246.0	0.3	28.0	27.6	0.7
	2.5	104	23904	229.8	0.3	28.0	27.6	0.8
	5.0	109	15201	139.5	0.3	28.2	27.8	0.7
	7.5	103	13743	133.4	0.2	27.8	27.6	0.6
	10.0	102	15155	148.6	0.0	27.2	27.2	0.5
	12.5	108	16744	155.0	-0.1	26.6	26.7	0.5
	15.0	106	19510	184.1	-0.1	26.0	26.2	0.5
	17.5	102	22176	217.4	-0.1	25.4	25.5	0.5
	20.0	97	23175	238.9	0.0	24.6	24.7	0.5
	22.5	95	25702	270.5	0.0	23.8	23.8	0.6
	25.0	90	23971	266.3	0.0	22.7	22.6	0.8
	27.5	85	18603	218.9	-0.1	21.1	21.2	0.9
	30.0	83	14775	178.0	-0.3	19.2	19.5	1.2

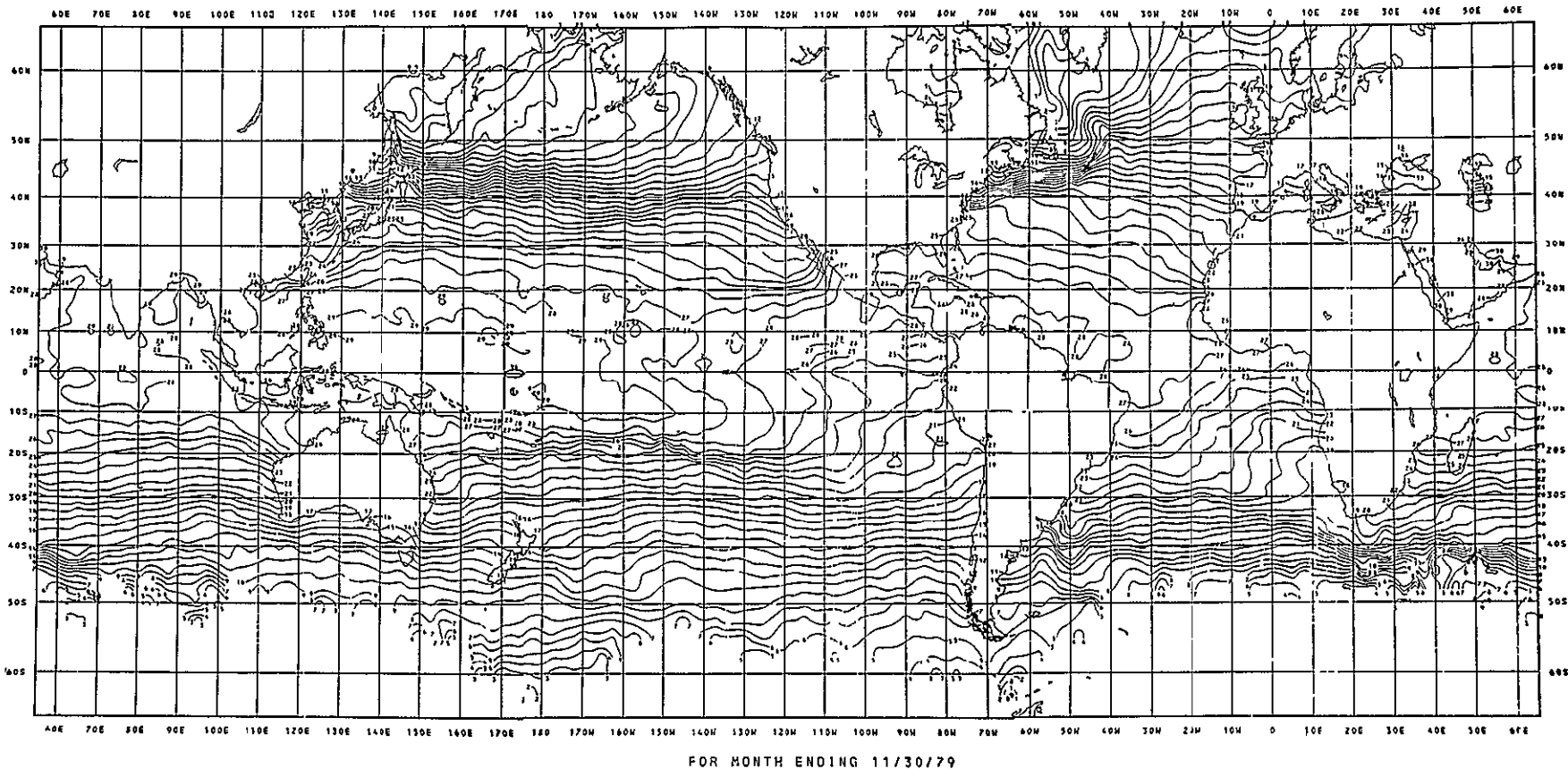
^aSatellite minus climatology monthly mean sea surface temperature difference, °C.

Table C-4. Global and 2.5 Zonal Mean Statistics for MCSST and Robinson-Bauer Climatology, March 1982^a (contd)

	LAT	GRID PTS	NO. OBS	OBS/PT	DELT-T	MEAN TMP	CLI TMP	RMS DIF
North	32.5	77	13976	181.5	-0.4	17.6	18.0	0.9
	35.0	83	12506	150.7	-0.5	16.0	16.5	0.8
	37.5	80	9783	122.3	-0.5	14.4	14.9	1.0
	40.0	77	9467	122.9	-0.2	12.3	12.6	0.9
	42.5	71	9056	127.5	-0.3	9.7	10.1	0.9
	45.0	68	7207	106.0	-0.4	7.4	7.8	0.8
	47.5	61	5961	97.7	-0.2	6.0	6.3	0.9
	50.0	54	5448	100.9	-0.1	5.7	5.8	0.6
	52.5	52	4335	83.4	-0.2	4.9	5.1	0.5
	55.0	49	3760	76.7	-0.2	4.1	4.4	0.7
	57.5	50	4066	21.3	-0.1	3.8	3.9	0.8
	60.0	46	3082	67.0	0.0	3.6	3.5	0.9
Global	999.0	4885.0	1029381.0	210.7	0.0	18.9	18.8	0.9

^aSatellite minus climatology monthly mean sea surface temperature difference, C.

MONTHLY MEAN SST

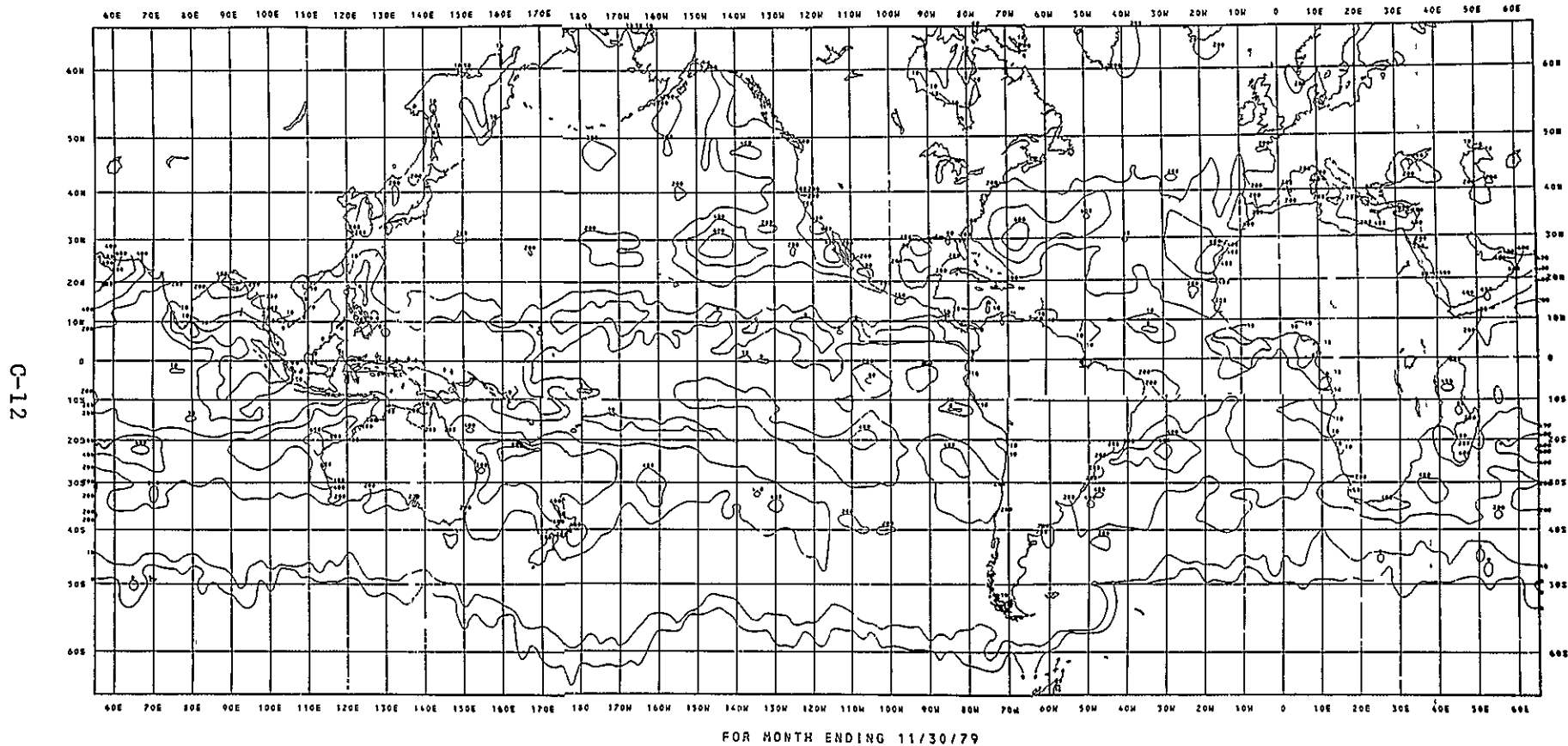


C-11

Figure C-1. GOSSTCOMP monthly mean global SST for November 1979

ORIGINAL PAGE IS
OF POOR QUALITY

NUMBER OF SATELLITE SST OBSERVATIONS



C-12

ORIGINAL PAGE IS
OF POOR QUALITY

Figure C-2. Number of satellite SST retrievals in 2.5° lat-lon bins for November 1979

SATELLITE MONTHLY MEAN ANOMALY

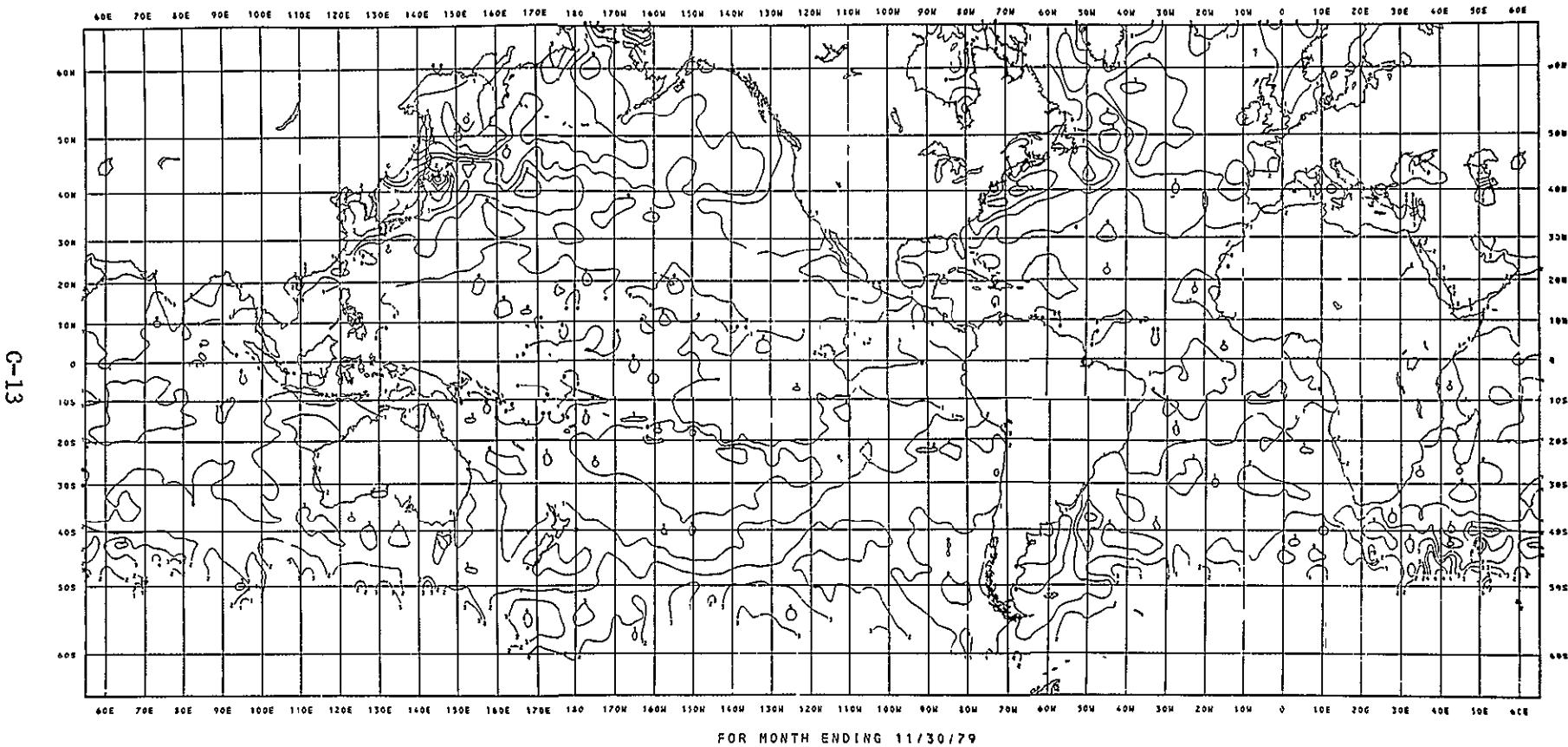


Figure C-3. Monthly mean SST anomaly (satellite minus NCAR climatology) for November 1979

ORIGINAL PAGE IS
OF POOR QUALITY

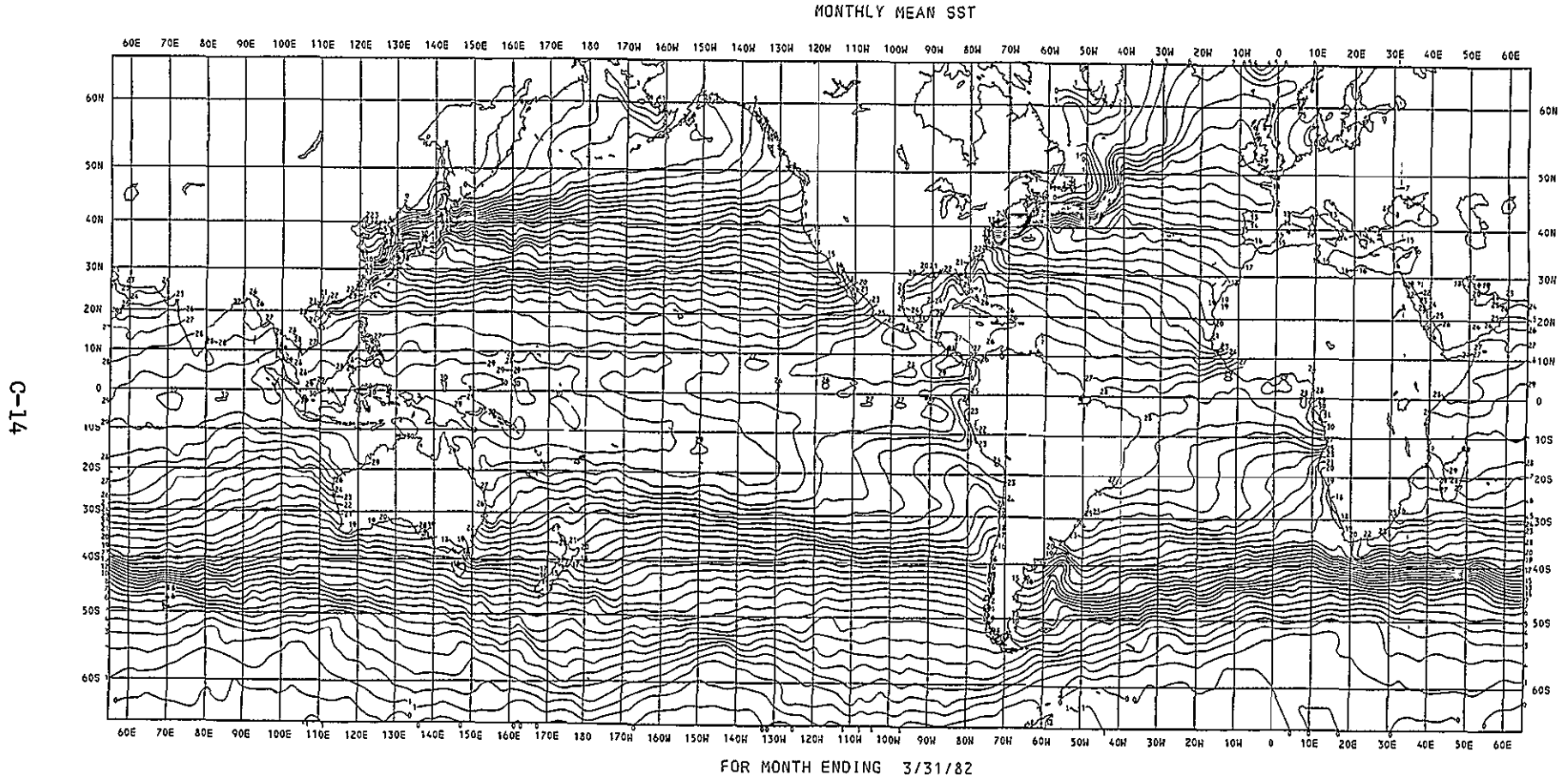


Figure C-4. MCSST monthly mean global SST for March 1982

NUMBER OF SATELLITE SST OBSERVATIONS

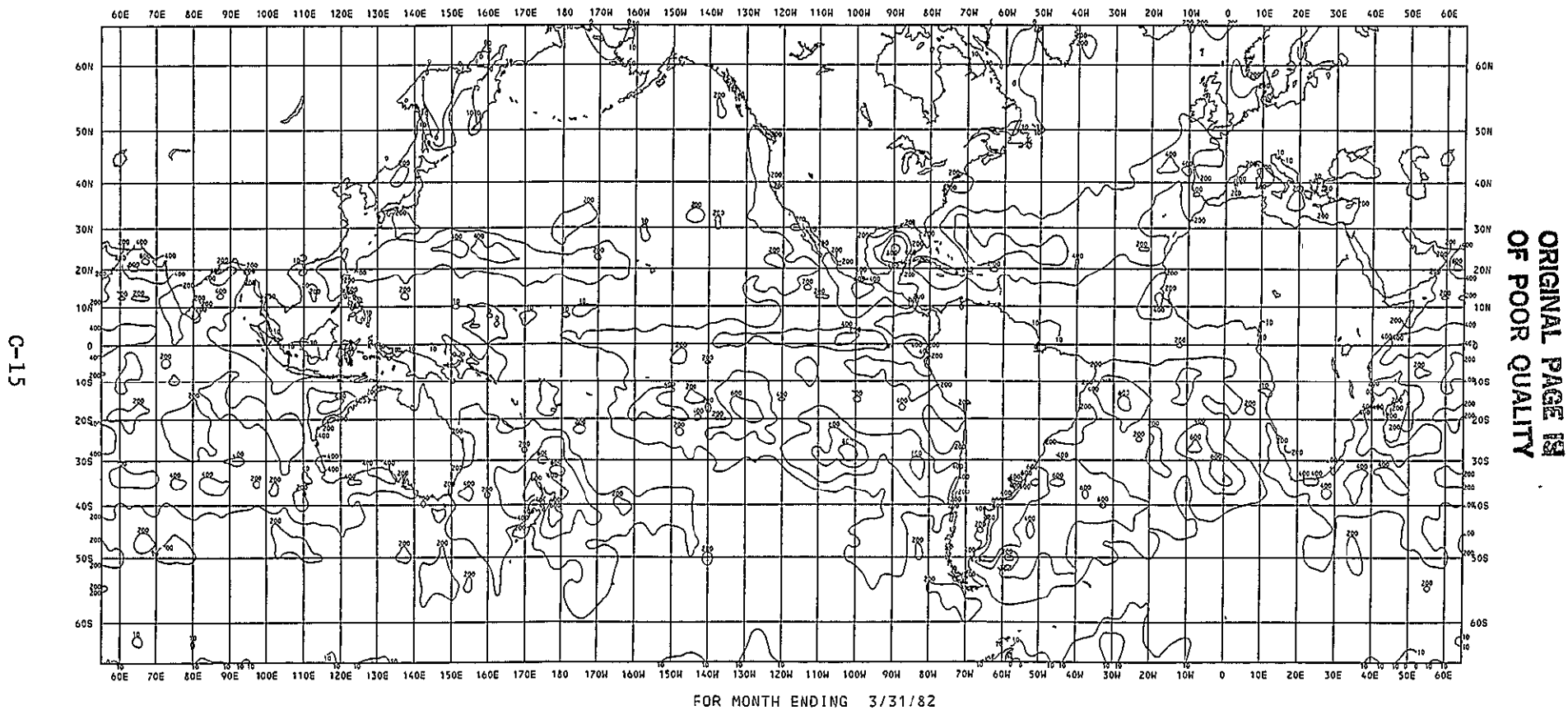


Figure C-5. Number of satellite SST retrievals in 2.5° lat-lon bins for March 1982

SATELLITE MONTHLY MEAN ANOMALY

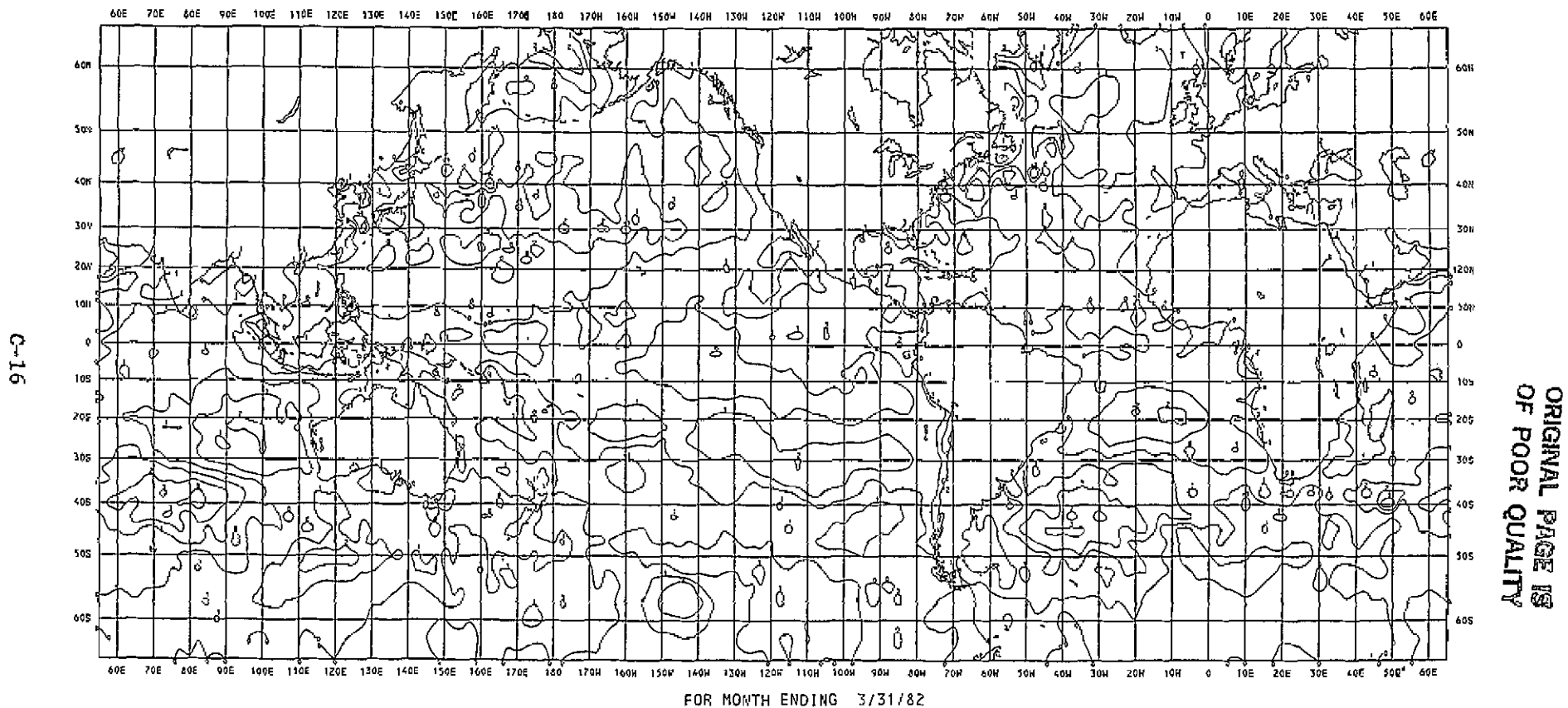


Figure C-6. Monthly mean SST anomaly (satellite minus Robinson-Bauer climatology) for March 1982

APPENDIX D

MEASUREMENT OF SEA SURFACE TEMPERATURE FROM HIRS2/MSU

MEASUREMENT OF SEA SURFACE TEMPERATURE FROM HIRS2/MSU

J. Susskind

The High-Resolution Infrared Sounder (HIRS), a 20-channel infrared sounder, and the Microwave Sounding Unit (MSU), a 4-channel microwave sounder, were first launched on the TIROS-N Satellite in November 1978 as an upgraded operational temperature sounding system. Essentially identical instruments have flown on NOAA-6 and NOAA-7 and are scheduled to fly on future operational satellites through the eighties. While HIRS2 and MSU were designed primarily for the purpose of measuring atmospheric temperature profiles, the observed radiances are also sensitive to other meteorological parameters such as sea surface temperature, ground temperature, cloud height and cloud amount, ice extent over ocean, snow cover over land, etc.

A physically based processing system for analysis of HIRS2/MSU data has been developed to determine the above atmospheric and surface parameters, which when substituted in the radiative transfer equation, match the satellite observations to a given noise level. All parameters are retrieved in a mutually interacting fashion. The infrared observations are significant primarily for determining the sea or land surface temperature, the mid-lower tropospheric temperature profile, and cloud fields. The microwave observations are significant primarily for determining the upper tropospheric and stratospheric temperature profile, the surface emissivity, from which can be inferred ice extent over ocean and snow cover over land, and most important of all, for enabling the infrared channels to be used in the presence of broken clouds.

A detailed description of the method is given in Reference 1. The sections from this reference that are most relevant to the retrieval of sea surface temperature are summarized in this report. These sections deal with the spatial processing of the data, the determination of surface temperature, and the treatment of data under partially cloudy conditions.

Figure D-1 shows the scan patterns of HIRS2 and MSU. In the processing system used in analysis of the data, one sounding, representative of an area of 125 x 125 km, was performed at a spacing of roughly 250 x 250 km. This resolution and spacing was chosen to be comparable to that used for operational temperature sounding by NOAA/NESS. Observations at the 125 x 125 km resolution were generated by averaging of the HIRS2 data as shown in the figure. First the HIRS spots are blocked into roughly 250 x 250 km areas in groups of 6 x 10, 6 x 8, 6 x 7, 6 x 5, or 6 x 3, depending on the location in the scan array. These blocks are further broken into quadrants, as indicated in the 6 x 10 array. In each quadrant, the spots were divided into two sets, one being the half containing the highest radiances for the 11 μ m window channel H8 on HIRS2. These spots are indicated as white in the figure. Radiances for all spots in a given set are averaged together for each channel. Each 125 x 125 km area is now characterized by two sets of HIRS2 radiances for each channel. These two sets will be referred to in the future as "two fields of view." The differences in the radiances in these fields of view will be utilized in the cloud correction algorithm to be described later, which estimates the effective clear column radiance that would have been observed in the 125 x 125 km area if it were cloud free. For each field of view, an effective satellite zenith angle is defined as the angle whose cosine is given by the average of the cosines of all the spot satellite zenith angles in the field of view.

The 125 x 125 km quadrant in which the sounding is performed was chosen as the one containing the warmest field of view as measured by the HIRS 11 μ m window channel. The latitude and longitude of the centroid of this quadrant is taken to be the location of the sounding that will be performed. The HIRS2 observations in this quadrant are also colocated with the MSU observations whose centroid is closest to that of the quadrant, and with initial estimates of temperature profile, humidity profile, and surface pressure obtained from interpolating a six-hour forecast generated by the GLAS GCM, to the appropriate location and time. For purposes of this workshop, the coverage of retrievals can be increased by sounding in two or more quadrants or in reducing the size of the sounding area from 250 x 250 km.

Given the observation in the two fields of view for the 125 x 125 km area, and initial guess temperature profile, humidity profile, and surface pressure, retrievals are performed in an iterative manner. The two fields of view are used to estimate the radiances, \tilde{R}_i , which would have been observed in channel i if no clouds were present. These estimated radiances are used in determining the surface temperature. Channels 18(4.0 μm) and 19(3.7 μm) are used on HIRS2 to determine the surface temperature. These channels are chosen rather than channel 8, the 11 μm channel, because observations in the short wavelength window channels are much less sensitive to humidity. Solar radiation reflected off the ground or clouds significantly affects observed radiances in the short wave window channels during the day, however.

The radiance for a given channel can be written as

$$R_i = \epsilon_i B_i(T_S) \tau_i(P_S) + R_{i,ATM} + \rho_i R_{i,SOLAR} \quad (1)$$

where ϵ_i is the emissivity of the ground, $B_i(T)$ is the Planck Black Body function for channel i at temperature T_i , T_S is the surface temperature, $\tau_i(P_S)$ is the atmospheric transmittance from the surface to the satellite for channel i , R_{ATM} is the contribution to the radiance originating from atmospheric emission, R_{SOLAR} is the solar radiation transmitted through the atmosphere and reflected to the satellite assuming unit reflectivity, and ρ_i is the actual reflectivity for channel i . At night, $R_{i,SOLAR}$ vanishes. $T_{S,i}$, the surface temperature estimated from channel i , is solved for according to

$$T_{S,i} = \frac{B_i^{-1} [\tilde{R}_i - R_{i,ATM}]}{\epsilon_i \tau_i} \quad (2)$$

where $R_{i,ATM}$ and τ_i are computed using the iterative temperature humidity profile and 0.96 is used for the emissivity of sea water at 3.7-4.0 μm . In general, $T_{S,18}$ and $T_{S,19}$ are found to agree with each other to 1°C, even under partially cloudy conditions. The surface temperature is taken as the average of the two estimates.

During the day, the effects of solar radiation on the 3.7 μm channels must be accounted for in obtaining accurate surface temperature retrievals from these channels. The solar radiation reflected off clouds in the field of view is assumed to be accounted for by the clear column radiance algorithm which provided \tilde{R}_i . If additional clouds are in the path of incident solar radiation with cloud fraction c , the solar radiation striking the ground will be attenuated by $(1-c)$. The solar radiation reflected off the clouds will not be seen by the instrument because of its narrow field of view. The net effect is to reduce the solar radiation by a factor of $(1-c)$.

One can attempt to account for reflected solar radiation directly by subtracting $\rho_i R_{i,\text{SOLAR}}$ from \tilde{R}_i and substituting the result into Equation (2). In the case of $c = 0$, $R_{i,\text{SOLAR}}$, the mean solar radiation across the channel traversing the path from the sun to the earth and back to the satellite, can be well estimated as $2.16\pi \times 10^{-5} B_i[5600 \text{ K}] \cos\theta_H \tau_i(P_s, \theta_{\text{EFF}})$ where θ_H is the solar zenith angle and the transmittance is computed at an effective zenith angle, θ_{EFF} , whose secant is given by the sum of the secants of the solar and the satellite zenith angles. The case of $c \neq 0$ is equivalent to an effective reflectivity $\bar{\rho} = \rho' (1-c)$.

This procedure is impractical because of the uncertainty in $\bar{\rho}_i$, even if $c = 0$. If the surface is Lambertian and the emissivity is known, ρ'_i , the directional reflectance, is equal to $(1 - \epsilon_i)/\pi$. Significant errors of up to a factor of two can be made in these estimations of ρ'_i , which may produce errors of up to 10°C in the retrieved surface temperature. These errors that arise from uncertainties in ϵ_i , however, do not appreciably affect the calculated thermal radiation. Rather than assume a value for ρ , T_s and $\bar{\rho}$ are solved for in an iterative manner, assuming only that $\bar{\rho}$ is the same for both 3.7 μm channels.

For 3.7 μm sounding channel i , we can write

$$\frac{\tilde{R}_i - R_{\text{ATM},i}}{\epsilon_i \tau_i(P_s)} = B_i(T_s) + d_i H_i = A_i \quad (3)$$

where $R_{ATM,i}$ is the atmospheric contribution to the calculated clear-column radiance, $d_i = \bar{\rho}/\epsilon_i$, and H_i is given by $H_i = R_{i,SOLAR}/\tau_i(P_s)$. The left-hand side of Equation (3), and consequently A_i , is known in a given iteration. Assuming $\bar{\rho}_i$ and ϵ_i are the same for both 3.7 μm channels, one obtains the equation

$$B_i(T_s) - aB_j(T_s) = A_i - aA_j = A \quad (4)$$

where $a = H_i/H_j$. This non-linear equation in one unknown, T_s , is solved iteratively according to

$$\frac{e^{-\bar{h\nu}/T_s^{M+1}}}{e^{-\bar{h\nu}/T_s^M}} = \frac{A}{B_i(T_s^M) - aB_j(T_s^M)} \quad (5)$$

where $\bar{\nu} = (\nu_i + \nu_j)/2$. This procedure converges rapidly. Monthly mean sea surface temperatures determined for January 1979 using this procedure gave day-night differences of ocean surface temperatures generally less than 0.5°C. This indicates that the solar correction algorithm works well even under cloudy conditions.

The cloud correction algorithm is one of the most important parts of the processing system. Unlike the approach in AVHRR, we do not look for, nor require, clear spots. Instead, we use observations in the two field of view associated with each 125 x 125 km area to estimate what the clear column radiances would have been if no clouds were present.

The radiance observed in an otherwise homogeneous field of view, containing partial homogeneous cloud cover α , is given, within a reasonable approximation by

$$R_i = \alpha R_{i,CLD} + (1 - \alpha) R_{i,CLR} \quad (6)$$

An estimate of the clear-column radiance, \tilde{R}_i , can be reconstructed from the observations in the two fields of view according to

$$\tilde{R}_i = R_{i1} + \eta[R_{i,1} - R_{i,2}] \quad (7)$$

where R_{ij} is the observation for channel i in the field of view j and η is given by $\alpha_1/(\alpha_2 - \alpha_1)$. The fields of view are numbered in the sense that $R_{8,1} > R_{8,2}$. Once η is determined, clear-column radiances can be reconstructed from the observations by using Equation (7). An estimate of η is obtained with each iteration.

It is seen from Equation (7) that large values of η will tend to amplify noise in the observations and are, therefore, undesirable. In the other extreme, $\eta = 0$ implies field of view 1 is clear and $\eta = -0.5$ is taken when it appears both fields of view are clear. As shown by Chahine (Ref. 2) and Halem et al., η can be determined from the infrared observations as part of an iterative scheme according to

$$\eta^N = \frac{R_7^N - R_{7,1}}{R_{7,1} - R_{7,2}} \quad (8)$$

where R_7^N is the computed clear-column radiance for the 15 μm surface channel, using the N^{th} iterative temperature profile. In this case, the scheme will converge provided only 4.3 μm infrared channels are used for temperature sounding in the lower troposphere. The rate of convergence increases with the difference between the surface temperature and the cloud-top temperature. Under some high-noise, low-contrast conditions, divergent solutions can occur in the sense that an overestimate of η^N will cause an overestimate of the reconstructed 4.3 μm clear-column radiances which, in turn, will yield an increased lower tropospheric temperature, produce an increased value of R_7^{N+1} , and lead to an increased η^{N+1} , etc.

When a lower tropospheric-sounding microwave channel is available, such as channel M2, a superior method for determining η can be used, making the estimate of η less sensitive to guess errors and alleviating the need for use of 15 μm channels, which are significantly affected by H_2O and O_3 absorption, in cloud filtering. η is determined as in Equation (8) but with the 4.3 μm surface channel 13 used instead of channel 7. The microwave channel is used to correct errors in R_{13}^N due to errors in the iterative temperature profile. The error in η^N determined from Equation (8) is a result of either use of an incorrect temperature profile to estimate the clear column radiance, computational uncertainties such as the effect of water vapor on the transmittance functions of channel 13, observational errors in $R_{13,i}$, or errors in the assumption of only one degree of non-homogeneity in the combined fields of view. The error in R_{13}^N due to a wrong temperature profile can be well accounted for by adjusting the computed brightness temperature (equivalent black body temperature) for channel M2 according to

$$T_{13} - T_{13}^N = T_{M2} - T_{M2}^N \quad (9)$$

where T_{M2} and T_{M2}^N are the observed and calculated microwave brightness temperatures, T_{13}^N is the calculated clear-column brightness temperature for channel 13, and T'_{13} is the corrected clear-column brightness temperature for channel 13. This correction is based on the approximation that a bias in the iterative temperature profile in the mid to lower troposphere will produce approximately the same error in computed brightness temperature in infrared and microwave channels sounding that portion of the atmosphere. The corrected clear-column radiance for channel 13 is then given by

$$R'_{13}{}^N = B_{13} [T'_{13}{}^N + T_{M2} - T_{M2}^N] \quad (10)$$

and η is now computed according to

$$\eta^N = (R'_{13}{}^N - R_{13,1}) / (R_{13,1} - R_{13,2}) \quad (11)$$

If the observations in the two fields of view are sufficiently close, most likely both fields of view are either clear or overcast. We discriminate these two cases by comparing T_{13} , the corrected clear column brightness temperature for channel 13, to $T_{13,1}$, observed brightness temperature for field of view 1. If $T_{13} - T_{13,1} > 8^{\circ}\text{C}$ and $\eta^N > 4$, the fields of view are considered to cloudy to do a retrieval. In the other limit, if $\eta^N \leq 0$ and $|T_{13,1} - T_{13,2}| \leq 1^{\circ}\text{C}$, η is taken as -0.5 , that is both fields of view are considered clear.

Retrievals of sea-surface temperature appear to have comparable accuracy under all conditions. It is clear from the previous discussions that potential hazards are clouds and reflected solar radiation, especially in conjunction with each other. Therefore, we will flag our retrievals from 1 through 4, where 1 is night clear, 2 is day clear, 3 is night cloudy, and 4 is day cloudy, in order of potential trouble. In addition, because of the averaging over a 125×125 km area, retrievals within 60 km of land may be contaminated by land temperatures.

REFERENCES

1. Susskind, J., Rosenfield, J., Reuter, D., and Chahine, M. T., The GLAS Physical Inversion Method for Analysis of HIRS/MSU Sounding Data. NASA Technical Memorandum 84936. Goddard Space Flight Center, Greenbelt, Maryland, 1982.
2. Chahine, M. T., Remote Soundings of Cloudy Atmospheres. I. The Single Cloud Layer, 1974.
3. Halem, M. and Susskind, J., The GISS VTPR Processing Manual. NASA Report X-130-77-53. Goddard Space Flight Center, Greenbelt, Maryland, 1977.

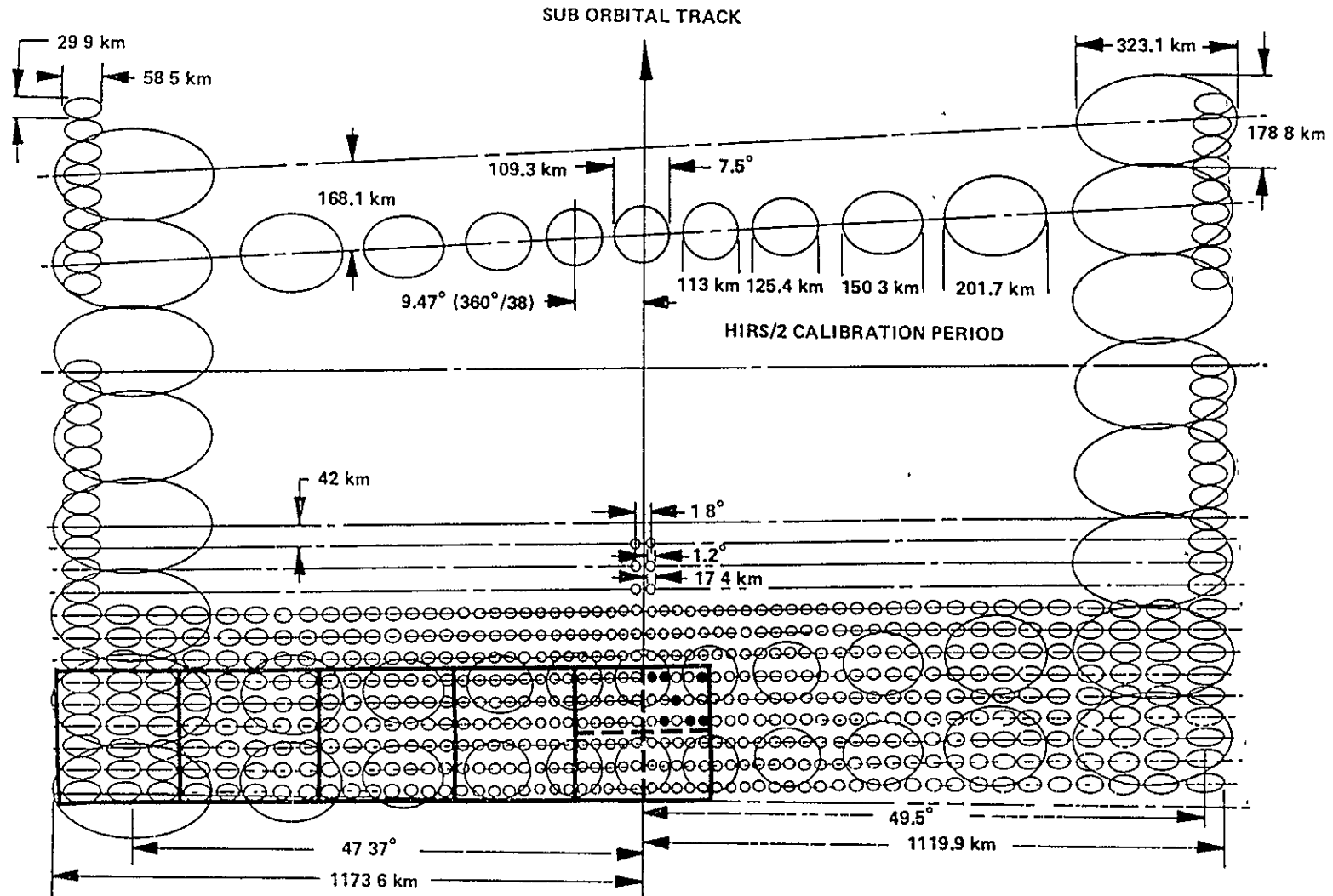


Figure D-1. Scan pattern for HIRS2 (small spots) and MSU (large spots). One retrieval is performed every 250 x 250 km (solid line box) area in one of the 125 x 125 km (dashed line box) quadrants. HIRS spots in each quadrant are averaged into 2 fields of view according to the warmest and coldest radiance from the 11 μm window channel. The closest MSU spot is assigned to the quadrant.

APPENDIX E

USE OF VAS MULTISPECTRAL DATA FOR SEA SURFACE
TEMPERATURE DETERMINATION

USE OF VAS MULTISPECTRAL DATA FOR SEA SURFACE
TEMPERATURE DETERMINATION

J. Bates

The Visible-Infrared Spin-Scan Radiometer Atmospheric Sounder (VAS) is a radiometer possessing eight visible channel detectors and six thermal detectors that sense infrared radiation in 12 spectral bands. A filter wheel in front of the detector package is used to achieve the spectral selection. The central wavelengths of the spectral bands lie between 3.9 and 15 microns (Ref. 1 and 2). Housed in the GOES satellite, VAS spins in a west to east direction at 100 rpm and achieves spatial coverage at resolutions of 1 km in the visible and 7 or 14 km in the infrared by stepping a scan mirror in a north to south direction.

Designed for multipurpose applications, the VAS can be operated in two different modes: (1) a multi-spectral imaging (MSI) mode, and (2) a dwell sounding (DS) mode. It is the MSI mode of operation that is used for sea surface temperature (SST) determination. Currently, a full-disk MSI image for SST determination is received every hour, 18 hours a day during weekdays. This MSI mode of operation for SST consists of data obtained from wavelengths centered at 3.9 microns (channel 12), 11.6 microns (channel 8), and 12.6 microns (channel 7) as well as visible data. In this mode, the data has a resolution of 14 km in the infrared and four kilometers in the visible. VAS infrared data are quantitized to a ten bit precision, visible data to a seven bit resolution.

The initial sounding retrieval system, developed by the NOAA/NESDIS Development Laboratory and Space Science and Engineering Center (SSEC) scientists at the University of Wisconsin, is man-machine interactive. An operator at a Man-computer Interactive Data Access System (McIDAS) terminal can view, on a television console, visible and infrared images obtained during the MSI period and select geographical positions of the image for processing SSTs.

Most of the data used in this study were acquired in real-time using the VAS-McIDAS link-up to ingest the data. Once the data are on the McIDAS system, geographical regions of interest are selected and saved for analysis later that same day. Both visible and infrared data are used.

The method of multispectral SST determination requires that only cloud-free fields of view be used. Thus, it is necessary to have rigid tests for whether the field of view of the observation is cloud free. The most rigid test for clouds over the oceans is a visible albedo test, since in cloud free areas remote from sunglint the albedo due to the reflectance from the oceans and atmosphere is generally less than 10 percent. Since the VAS operating schedule is geared to acquire the majority of data during the day, only data during the day, when the visible albedo test can be performed, are chosen for this study. Several cases using only infrared data during the night have been attempted and the results indicate that the cloud threshold tests based only on infrared data are inadequate.

Because the albedo of the ocean is generally much less than that of clouds, thresholds can be established that represent the expected bidirectional reflectance of the ocean and atmosphere in the absence of clouds. This threshold can be established by forming a histogram of visible reflectance value against number of times of occurrence. If there are a sufficient number of cloud-free samples, then a peak will form with a normal distribution at the low (dark) end of the scale. Then, any visible pixel whose reflectance value exceeds the one standard deviation value beyond the peak of this distribution is considered to be cloudy. The threshold is not constant but varies with solar zenith angle, satellite zenith angle, and azimuth of the viewed spot. It has been found that a fixed value of brightness is adequate when performing matchups with environmental buoys off the east coast and in the Gulf of Mexico. This bi-directional reflectance threshold test is generally sensitive to even small amounts of cloudiness but is subject to error for at least two reasons: (1) the reflectance threshold table may contain some residual cloud contamination; (2) the true cloud free reflectance varies with atmospheric state (aerosols) and sea state (wave conditions).

In an attempt to improve on the look-up table approach to determining a visible albedo threshold, a slightly different approach was used for performing regional analysis. A histogram of visible channel reflectances is constructed and a threshold value is calculated using the median of the low reflectance mode, and used for each corresponding new nine by nine infrared observation array. The new threshold is compared to a guess threshold based on the look-up table value for the particular satellite and solar angles of interest, and the lower of the two values is chosen as the threshold.

In addition to (or in the absence of) a visible albedo cloud threshold test, there are also several cloud threshold tests that can be performed using the infrared data alone. These infrared tests fall into two general categories, inter-channel comparisons and uniformity tests. The inter-channel comparisons are most important to VAS data processing. In the presence of transmissive clouds or small sub-resolution cloud elements, the measured upwelling radiance is a combination of the Planck radiance of the cold cloud and of the warm ocean surface. Because of the differential amount of water vapor absorption in each window region and because the Planck radiance is much more sensitive to temperature in the 3.9 micron window than in the 11.6 and 12.6 micron windows, the 3.9 micron temperature will be highly elevated relative to the 11.6 or 12.6 micron temperatures.

In the case of thick opaque clouds, the Planck radiance effect is insignificant. The optical properties of such clouds are, however, significantly different at 3.9 microns than at 11.6 and 12.6 microns. Theoretical studies have shown that the reflectivity of thick water droplet clouds is greater at 3.9 microns, with the difference increasing with decreasing water droplet size. This lowers the 3.9 micron temperature relative to the 11.6 and 12.6 micron temperatures much more than for cloud-free conditions. Thus, appropriate upper and lower bounds on the temperature differences between two infrared channels can serve as tests for cloud contamination.

Uniformity tests involve setting limits on the amount of temperature difference in any one channel between individual samples in a two by two infrared observation array. This test is based on the assumption that for

such small arrays, the SST is constant such that the largest acceptable difference in temperature within the array would be that due to instrument noise. While this test is used on AVHRR data, it does not work well with VAS data possibly due to the fact that the resolution of the VAS data is much more coarse and the instrument noise levels are somewhat higher than the AVHRR.

The regularly reporting NOAA fixed buoys used for matchups in this study measure SST at a depth of one meter. Observations from these buoys are available once every three hours and laboratory tests indicate that the buoys are capable of providing temperatures with one standard deviation of less than $\pm 0.2^{\circ}\text{C}$. Buoy observations of SST are much more reliable than merchant ship observations of SST because the buoys are subject to rigorous quality control. Studies of buoy versus ship observations of SST have shown that ship's observations are $0.2 \pm 1.5^{\circ}\text{C}$ greater than those of buoys.

In late March and early April 1982, El Chichon volcano in Mexico (17.33°N , 93.2°W) erupted and injected large amounts of aerosols into the stratosphere. By the end of April, the volcanic cloud had circled the earth and gradually spread latitudinally to cover the band 5°N to 30°N . The cloud has both increased the reflectance of visible solar radiation and the attenuation of infrared radiation from the surface. This suggests that some of the early match-ups with the most southerly of the buoys may be biased due to this aerosol. However, the small bias of the overall results indicates that aerosol contamination has probably not significantly affected the data analyzed so far.

VAS SST data used for matchups are obtained by averaging all cloud-free infrared observations within a three by three array centered at the buoy location. Only daytime data were used. The buoys report SSTs every three hours, so that the largest time difference between buoy and satellite observations is an hour and one half. During the period July 22 to October 13, 1982, the split window algorithm had a bias (i.e., mean satellite-buoy difference) of zero and a root mean square error (RMSE) of 1.15°C for 264 matches. The three-channel algorithm had a larger bias, -0.66°C , with a slightly smaller RMSE of 1.12°C for 224 matches. There

are fewer three-channel SST observations because for some periods only split window data were available. The low values of RMSE in both the two and three-channel algorithms are most encouraging. The low bias for the two-channel algorithm suggests that the original sample of ship data used to calculate the algorithm was quite representative. The RMSE for the three-channel algorithm is similar to that for the two-channel, but there is a significant bias, -0.66°C . This suggests that the three-channel algorithm, already with a slightly lower RMSE than the two-channel algorithm, may become more accurate by recalculating the coefficients of the algorithm to eliminate the bias.

Using these satellite-buoy matches to recalculate the two- and three-channel algorithms, it was found that the three-channel regression had a higher correlation coefficient (0.95 versus 0.83), a higher explained variance (0.90 versus 0.69), and a lower standard error (0.90 versus 1.12) than the two-channel regression. These results show that, in the absence of sunglint, the three-channel method is superior to the two-channel method.

REFERENCES

1. Smith, W. L., Suomi, V. E., Menzel, W. P., Woolf, H. M., Sromovsky, L. A., Revercomb, H. E., Hayden, C. M., Erickson, D. N., and Mosher, F. R., "First Sounding Results from VAS-D," Bulletin American Meteorological Society, 62, 1981, pp. 232-236.
2. Smith, W. L., and Woolf, H. M., "Algorithms Used To Retrieve Surface Skin Temperature and Vertical Temperature and Moisture Profiles from VISSR Atmospheric Sounder (VAS) Radiance Observations," Preprint volume: Fourth Conference on Atmospheric Radiation, June 16-18, 1981, Toronto, Ontario, Canada, American Meteorological Society, Boston, Massachusetts, 1982.

D13

N84 21968

APPENDIX F

PILOT OCEAN DATA SYSTEM
FILE FORMAT SPECIFICATIONS

PILOT OCEAN DATA SYSTEM (PODS)
FILE FORMAT SPECIFICATIONS

Table F-1. Sea Surface Temperature Workshop Tape File Format,
as received from investigator

*RECL=38

TAPE HEADER RECORD

<u>PARAMETER</u>	<u>START</u>	<u>FORMAT</u>
Investigator	1	A16
Platform, Sensor, Data Date	17	A22

TAPE DATA RECORD

<u>PARAMETER</u>	<u>BIAS</u>	<u>SCALE</u>	<u>UNITS</u>	<u>START</u>	<u>LENGTH</u>	<u>FORMAT</u>
Time Tag	0	1.000	YYMMDD	1	6	3I2
Time Tag	0	1.000	HHMMSS	7	6	3I2
Geodetic latitude	0	1.000	Degrees	13	7	F7.2
Longitude	0	1.000	Degrees	20	7	F7.2
SST	0	1.000	Deg-Cel	27	7	F7.2
Status Flag	0	1.000	Bits	34	7	F5.0

*RECL = Record length in bytes, where 1 byte = 8 bits

Table F-2. Sea Surface Temperature Workshop .Raw File Format,
original spot data

*RECL=12

.RAW HEADER RECORD 1

<u>PARAMETER</u>	<u>START</u>	<u>FORMAT</u>
Platform/sensor code	1	A2
Day/twilight/night code	3	A2
Data span code	5	A2
Data type (RAW)	7	A6

.RAW HEADER RECORD 2

<u>PARAMETER</u>	<u>START</u>	<u>FORMAT</u>
Comment	1	A12

.RAW DATA RECORD

<u>PARAMETER</u>	<u>BIAS</u>	<u>SCALE</u>	<u>UNITS</u>	<u>START</u>	<u>LENGTH</u>
Time tag	0	1.000	Seconds	1	4
Geodetic latitude	9000	0.010	Degrees	5	2
Longitude	0	0.010	Degrees	7	2
SST	1000	0.010	Deg-Cel	9	2
Status flag	0	1.000	Bits	11	2

*See Table F-1.

Table F-3. Sea Surface Temperature Workshop .Bin Format,
2 x 2 deg. binned data

*RECL=20

.BIN HEADER RECORD 1

<u>PARAMETER</u>	<u>START</u>	<u>FORMAT</u>
Platform/sensor code	1	A2
Day/twilight/night code	3	A2
Data span code	5	A2
Bin size (lat x long, deg.)	7	A4
Region	11	A6
(spare)	17	A4

.BIN HEADER RECORD 2

<u>PARAMETER</u>	<u>START</u>	<u>FORMAT</u>
Comment	1	A20

.BIN DATA RECORD

<u>PARAMETER</u>	<u>BIAS</u>	<u>SCALE</u>	<u>UNITS</u>	<u>START</u>	<u>LENGTH</u>
Time tag	0	1.000	Seconds	1	4
Geodetic latitude	9000	0.010	Degrees	5	2
Longitude	0	0.010	Degrees	7	2
Mean SST	1000	0.010	Deg-Cel	9	2
SST Std. dev.	0	0.010	Deg-Cel	11	2
Minimum SST	1000	0.010	Deg-Cel	13	2
Minimum SST	1000	0.010	Deg-Cel	15	2
Number of observations	0	1.000	Counts	17	4

*See Table F-1.

Table F-4. Sea Surface Temperature Workshop .DIF File Format,
difference 2 x 2 deg.

*RECL=34

.DIF HEADER RECORD 1

<u>PARAMETER</u>	<u>START</u>	<u>FORMAT</u>
Platform/sensor code A	1	A2
Day/twilight/night code A	3	A2
Data span code A	5	A2
Bin/grid size A	7	A4
Data type (DIF)	11	A6
(spare)	17	A18

.DIF HEADER RECORD 2

<u>PARAMETER</u>	<u>START</u>	<u>FORMAT</u>
Platform/sensor code B	1	A2
Day/twilight/night code B	3	A2
Data span code B	5	A2
Bin/grid size B	7	A4
Data type (DIF)	11	A6
(spare)	17	A18

.DIF DATA RECORD

<u>PARAMETER</u>	<u>BIAS</u>	<u>SCALE</u>	<u>UNITS</u>	<u>START</u>	<u>LENGTH</u>
Time (from input A)	0	1.0	Seconds	1	4
Geodetic latitude (from A)	9000	0.01	Degrees	5	2
Longitude (from A)	0	0.01	Degrees	7	2
Delta time (ABS (A-B))	0	1.0	Seconds	9	4
Delta SST (A-B)	15000	0.01	Deg-Cel	13	2
Std dev. SST (A)	0	0.01	Deg-Cel	15	2
Std. dev SST (B)	0	0.01	Deg-Cel	17	2
Minimum SST (A)	1000	0.01	Deg-Cel	19	2
Minimum SST (B)	1000	0.01	Deg-Cel	21	2
Maximum SST (A)	1000	0.01	Deg-Cel	23	2
Maximum SST (B)	1000	0.01	Deg-Cel	25	2
Number of obs. in A	0	1.0	Count	27	4
Number of obs. in B	0	1.0	Count	31	4

See Table F-1.

Table F-5. Sea Surface Temperature Workshop .MRG File Format,
spot-merged data

*RECL=26

.MRG HEADER RECORD 1

<u>PARAMETER</u>	<u>START</u>	<u>FORMAT</u>
Platform/sensor code A	1	A2
Data span code	3	A2
(spare)	5	A22

.MRG HEADER RECORD 2

<u>PARAMETER</u>	<u>START</u>	<u>FORMAT</u>
Platform/sensor code B	1	A2
Day/twilight/night code B	3	A2
(spare)	5	A22

.MRG DATA RECORD

<u>PARAMETER</u>	<u>BIAS</u>	<u>SCALE</u>	<u>UNITS</u>	<u>START</u>	<u>LENGTH</u>
Time (from input A)	0	1.0	Seconds	1	4
Geodetic latitude (from A)	9000	0.01	Degrees	5	2
Longitude (from A)	0	0.01	Degrees	7	2
SST (from A)	1000	0.01	Deg-Cel	9	2
Time (from input B)	0	1.0	Seconds	11	4
Geodetic latitude (from B)	9000	0.01	Degrees	15	2
Longitude (from B)	0	0.01	Degrees	17	2
SST (from B)	1000	0.01	Deg-Cel	19	2
Delta time (ABS (A-B))	0	1.0	Seconds	21	2
Distance between A and B	0	1.0	KM	23	2
Delta SST (A-B)	15000	0.01	Deg-Cel	25	2

*See Table F-1.

Table F-6. Sea Surface Temperature Workshop .S2M Format,
2 x 2 deg. binary matrix for Surface II

This file can be read directly by the Surface II RESTORE command:

```
RESTORE unit#,0,1
```

It is created by any of the GNVxxxS2M programs or by the Surface II command:

```
SAVE unit#
```

.S2M HEADER RECORD

<u>PARAMETER</u>	<u>START</u>	<u>LENGTH</u>
NCOLS - number of columns = 180	1	4
NROWS - number of rows = 90	5	4
IZERO - control code = 0	9	4

.S2M HEADER RECORD

<u>PARAMETER</u>	<u>START</u>	<u>LENGTH</u>
(SST(I,J),J=1,NCOLS)	1	180*4

Note: There are NROWS=90 data records in each .S2M file.

Table F-7. Sea Surface Temperature Workshop .MFM File Format,
spot-merged data

*RECL=85

.MFM DATA RECORD

<u>PARAMETER</u>	<u>BIAS</u>	<u>SCALE</u>	<u>UNITS</u>	<u>START</u>	<u>LENGTH</u>	<u>FORMAT</u>
(carriage control)	-	-	-	1	1	1X
Time (from input A)	0	1.0	Seconds	2	11	I11
Geodetic latitude (from A)	0	1.0	Degrees	13	7	F7.2
Longitude (from A)	0	1.0	Degrees	20	7	F7.2
SST (from A)	0	1.0	Deg-Cel	27	7	F7.2
Time (from input B)	0	1.0	Seconds	34	11	I11
Geodetic latitude (from B)	0	1.0	Degrees	45	7	F7.2
Longitude (from B)	0	1.0	Degrees	52	7	F7.2
SST (from B)	0	1.0	Deg-Cel	59	7	F7.2
Delta time (ABS (A-B))	0	1.0	Seconds	66	6	I6
Distance between A and B	0	1.0	KM	72	7	F7.2
Delta SST (A-B)	0	1.0	Deg-Cel	79	7	F7.2

Table F-8. Sea Surface Temperature Workshop .RFM File Format,
original spot data

*RECL=39

.RFM DATA RECORD

<u>PARAMETER</u>	<u>BIAS</u>	<u>SCALE</u>	<u>UNITS</u>	<u>START</u>	<u>LENGTH</u>	<u>FORMAT</u>
(carriage control)	-	-	-	1	1	1X
Time tag	0	1.000	Seconds	2	11	I11
Geodetic latitude	0	1.000	Degrees	13	7	F7.2
Longitude	0	1.000	Degrees	20	7	F7.2
SST	0	1.000	Deg-Cel	27	7	F7.2
Status flag	0	1.000	Bits	34	6	I6

*See Table F-1.

Table F-9. Sea Surface Temperature Workshop .GRD Format,
2 x 2 deg. gridded data

*RECL=12

.GRD HEADER RECORD 1

<u>PARAMETER</u>	<u>START</u>	<u>FORMAT</u>
Platform/sensor code	1	A2
Day/twilight/night code	3	A2
Data span code	5	A2
Data type	7	A6

.GRD HEADER RECORD 2

<u>PARAMETER</u>	<u>START</u>	<u>FORMAT</u>
Grid size	1	A6
Comment	7	A6

.GRD DATA RECORD

<u>PARAMETER</u>	<u>BIAS</u>	<u>SCALE</u>	<u>UNITS</u>	<u>START</u>	<u>LENGTH</u>
Time tag	0	1.000	Seconds	1	4
Geodetic latitude	9000	0.010	Degrees	5	2
Longitude	0	0.010	Degrees	7	2
SST	1000	0.010	Deg-Cel	9	2
(Spare)	0	1.000	Bits	11	2

*See Table F-1.

APPENDIX G

THREE-WAY PARTITIONING OF SEA SURFACE TEMPERATURE
MEASUREMENT ERROR

THREE-WAY PARTITIONING OF SEA SURFACE TEMPERATURE
MEASUREMENT ERROR

D. Chelton

Given any set of three 2° binned anomaly sea surface temperature (SST) data sets by three different sensors, estimates of the mean square error of each sensor estimate can be made using the method described in this appendix.

Define $T_k(n)$, $k = 1, 2, 3$ to be the anomaly SST value for sensor k at 2° lat-lon grid point number n . Use $\langle \rangle$ to denote the sample mean value computed over all N grid points n that are common to all three sensors. Compute the mean square difference between sensor 1 and sensor 2 SST anomalies by

$$D_{12} = \langle (T_1 - T_2)^2 \rangle = \frac{1}{N} \sum_{n=1}^N [T_1(n) - T_2(n)]^2.$$

T_1 and T_2 are sensor estimates of the true SST anomaly, which we will call T_t . Note that D_{12} can be written as

$$D_{12} = \langle (\epsilon_1 - \epsilon_2)^2 \rangle = \langle \epsilon_1^2 \rangle - 2\langle \epsilon_1 \epsilon_2 \rangle + \langle \epsilon_2^2 \rangle,$$

where $\epsilon_k = T_k - T_t$ is the error in SST measurement by sensor k . Assuming the SST measurement errors by sensors 1 and 2 to be uncorrelated (i.e., $\langle \epsilon_1 \epsilon_2 \rangle = 0$),

$$D_{12} = \langle \epsilon_1^2 \rangle + \langle \epsilon_2^2 \rangle. \quad (1)$$

This is a very strong assumption in some cases. For example, the AVHRR and VAS might be expected to err in the same sense for SST estimates over regions with partial cloud cover. Similarly, errors in SMMR SST are likely to be correlated among the various different methods of retrieving SST from SMMR brightness temperatures. However, over the entire earth and in monthly averages we can hope that the correlation between errors is small. If we assume this is the case, similar equations can be derived from the other two paired sensor combinations in the triplet:

$$D_{13} = \langle (T_1 - T_3)^2 \rangle = \langle \epsilon_1^2 \rangle + \langle \epsilon_3^2 \rangle \quad (2)$$

$$D_{23} = \langle (T_2 - T_3)^2 \rangle = \langle \epsilon_2^2 \rangle + \langle \epsilon_3^2 \rangle. \quad (3)$$

Equations (1), (2) and (3) form a set of three equations that can be easily solved for the three unknowns $\langle \epsilon_k^2 \rangle$, $k = 1, 2, 3$.

The above formalism can be performed on every possible triplet of sensors. A separate table of error estimates can then be constructed for each sensor k . Within each table, estimates of $\langle \epsilon_k^2 \rangle$ will be listed for every triplet formed by sensor k with all possible pairs of the other sensors. For example, if there are eight total sensors, there are a total of 21 possible combinations of triplets for each sensor. (In general, if there are M sensors, there are $(M^2 - 3M + 2)/2$ possible combinations of triplets.) All 21 individual estimates of $\langle \epsilon_k^2 \rangle$ will be listed in each table together with the overall average.

APPENDIX H

WORKSHOP-I PARTICIPANTS

WORKSHOP-I PARTICIPANTS

<u>Name</u>	<u>Affiliation</u>
Abbott, Mark	Scripps Institution of Oceanography, La Jolla, California
Bates, John	University of Wisconsin, Madison, Wisconsin
Bernstein, Robert L.	SeaSpace, San Diego, California
Brown, James	Jet Propulsion Laboratory, Pasadena, California
Chahine, Moustafa	Jet Propulsion Laboratory, Pasadena, California
Chelton, Dudley	Jet Propulsion Laboratory, Pasadena, California
Hagan, Denise	Jet Propulsion Laboratory, Pasadena, California
Hilland, Jeffrey E.	Jet Propulsion Laboratory, Pasadena, California
Kelly, Catherine	Scripps Institution of Oceanography, La Jolla, California
Liu, W. Timothy	Jet Propulsion Laboratory, Pasadena, California
McClain, E. Paul	NOAA/National Environmental Satellite, Data, and Information Service, Suitland, Maryland
Miller, Carol L.	Jet Propulsion Laboratory, Pasadena, California
Milman, Andrew S.	Systems and Applied Sciences Corporation, Hyattsville, Maryland
Njoku, Eni G.	Jet Propulsion Laboratory, Pasadena, California
Pazan, Steven	Jet Propulsion Laboratory, Pasadena, California
Prabhakara, Cuddappah	NASA/Goddard Space Flight Center, Greenbelt, Maryland
Susskind, Joel	NASA/Goddard Space Flight Center, Greenbelt, Maryland
Wilheit, Thomas T.	NASA/Goddard Space Flight Center, Greenbelt, Maryland